Synthesis, physicochemical and biological evaluation of N-dealkylated metabolites of antimalarial pyrido[1,2-*a*]benzimidazoles and related compounds containing a Mannich base side-chain

---

Dissertation presented for the degree of Master of Science in the Department of Chemistry, University of Cape Town

By

Richard Ferger

Supervisor: Professor Kelly Chibale

Department of Chemistry

University of Cape Town

Rondebosch, 7700

South Africa

December 2019

DECLARATION

I declare that ***Synthesis, physicochemical and biological evaluation of N-dealkylated metabolites of antimalarial pyrido[1,2-a]benzimidazoles and related compounds containing a Mannich base side-chain*** is my original work and has not been presented for the award of any degree at any university. I know the meaning of plagiarism and declare that all of the work in the dissertation, except for that which is properly acknowledged, is my own.

Signed by candidate

_____

Richard Ferger

ACKNOWLEDGEMENTS

The thesis work would not have been successfully completed without the guidance, support and outstanding mentorship of my supervisor Prof. Kelly Chibale. Thank you for enhancing my abilities in medicinal chemistry, for your time, and for being an incredible inspiration.

I acknowledge the contributions of Dr Godwin Dziwornu, his mentorship throughout the project, and his guidance and training in the laboratory. Furthermore, I would like to acknowledge Dr Lebu Taleli for his undying support during the writing process.

Special thanks to my previous mentor and friend Dickson Mambwe as well as Simone Renga for their support throughout my time in the laboratory and experience at the University of Cape Town. I appreciate the administrative support, helpful advice, and encouragement received from Elaine Rutherfoord-Jones, Saroja Naicker, and Deirdre Brooks.

Special thanks to Peter Roberts and Dr Neil Ravenscroft for acquiring some of my NMR data as well as to Amina Sayed for her meticulous attention to the maintenance of laboratory equipment, including the upkeep of the LC-MS apparatus.

I appreciate the support received from Dr Dale Taylor, Henrietta Attram, John Okombo, and Dr Mathew Njoroge for assistance and for conducting some of the biological assays. I would like to thank the University of Pretoria for the asexual parasite biological assays which they performed.

Many thanks to the fellow members of Kelly Chibale's research group for the support, ideas, and creating an enjoyable working environment. I appreciate the efforts of the Head of Department and both teaching and non-teaching staff of the Chemistry Department, UCT.

I extend my thanks to the South African Medical Research Council, South African National Research Foundation (NRF), and Department of Chemistry for their generous financial assistance, without which this work would not have been possible.

I thank my parents, Klaus and Theresa Ferger, for their love and support and for their contributions toward every aspect of my studies and early career. I would finally like to thank my partner, Demi Bucklow, for her undying support and love throughout my time at UCT and especially during the last two years.

CONFERENCES

American Society of Tropical Medicine and Hygiene 68th Annual Meeting

Gaylord National Resort and Convention Centre, National Harbor, Maryland

20-24 November 2019

Attended the 2019 ASTMH Annual Meeting where I presented a poster titled "*Synthesis and evaluation of metabolites of antimalarial pyrido[1,2-a]benzimidazoles and related compounds containing a Mannich base side-chain".*

H3D-MMV 10-year Celebration 2019 November

Hlanganani Junction, University of Cape Town, South Africa

24 May 2019

ABSTRACT

Malaria is one of the leading causes of deaths worldwide. Despite strategic implementations aimed at decreasing mortality and morbidity rates in recent decades, this plasmodial disease continues to impact public health and the economies of developing countries. Furthermore, the emergence of resistance toward current antimalarial treatments increases the necessity for the development of novel antimalarials.

The benzimidazole scaffold is an extensively researched privileged scaffold in medicinal chemistry because of its capacity to interact with numerous biological systems in various diseases, including malaria. Based on previous metabolite identification studies in liver microsomes, a new series of pyrido[1,2-*a*]benzimidazole (PBI) metabolites containing Mannich base side-chains were designed and synthesized. Their *in vitro* parasite (*Plasmodium falciparum*) growth and β-hematin formation inhibition activities, turbidimetric solubility, cytotoxicity, and microsomal metabolic stability in mouse liver microsomes were evaluated. To investigate structure activity relationships (SARs), the study was broadly diversified into two series (SAR-1 and SAR-2). Mannich base side-chains from SAR-1 were designed and synthesized as hypothesized *N*-dealkylated metabolites. In SAR-2, hypothesized N-dealkylated metabolites were compared with their respective parent compounds with a focus on modifications around the PBI core.

The most potent analogues exhibited sub-micromolar activity (50% inhibitory concentration (IC_{50}) < 1 μM) against the drug-sensitive NF54 strain of *Plasmodium falciparum.* Some compounds showed high activity against early- and late-stage gametocytes, the sexual stage transmissible forms of the parasite. Overall, compounds in this series were more active against early-stage gametocytes than late-stage gametocytes, thus indicating stage-specificity. All but three of the analogues synthesized were potent inhibitors of β-hematin formation. Most compounds showed no cytotoxicity against HepG2 and Chinese hamster ovarian (CHO) cells. Inclusion of Mannich base side-chains influenced the *in vitro* microsomal metabolic stability of compounds. As expected, N-dealkylated (desethyl) metabolites showed greater metabolic stability relative to their equivalent parent compounds.

TABLE OF CONTENTS

LIST OF ABBREVIATIONS

ACT	artemisinin combination therapy
ADMET	absorption, distribution, metabolism, excretion, and toxicity
AMU	atomic mass units
APCI	atmospheric pressure chemical ionization
AQ	amodiaquine
AQ-QI	amodiaquine quinoneimine
Ar	aromatic
CHO	Chinese hamster ovarian
CQ	chloroquine
DCM	dichloromethane
DEAQ	desethylamodiaquine
DMEM	Dulbecco's modified Eagle's medium
DMF	*N,N*-dimethylformamide
DMPK	drug metabolism and pharmacokinetics
DMSO	dimethyl sulfoxide
EF2	translation elongation factor 2
ESI	electrospray ionization
FBS	fetal bovine serum
FiH	first-in-human
FPIX	ferriprotoporphyrin IX
GPI	glycophosphatidylinositol
HLMs	human liver microsomes
HPLC	high-performance liquid chromatography
IC_{50}	50% inhibitory concentration
IPTp	intermittent preventative treatment in pregnant women
K1	chloroquine-resistant *P. falciparum*

LC-MS	liquid chromatography-mass spectrometry
MLMs	mouse liver microsomes
MMV	Medicines for Malaria Venture
MoA	mode of action
MS	mass spectrometry
MSP1	merozoite surface protein 1
MW	molecular weight
m/z	mass/charge ratio
NADPH	reduced nicotinamide adenine dinucleotide phosphate
NMR	nuclear magnetic resonance
NF54	chloroquine-sensitive strain of *P. falciparum*
PBI	pyrido(1,2-*a*)benzimidazole
Pf	*Plasmodium falciparum*
*pf*DHODH	*P. falciparum* dihydroorotate dehydrogenase
PK	pharmacokinetic
p.o.	per oral
$POCl_3$	phosphorous oxychloride
RBC	red blood cell
RLMs	rat liver microsomes
SAR	structure-activity relationship
SPR	structure-property relationship
TDR	Tropical Disease Research
THF	tetrahydrofuran
TLC	thin-layer chromatography
UV-VIS	ultraviolet-visible
VIS	volunteer infection studies
WHO	World Health Organisation

LIST OF FIGURES

LIST OF TABLES

LIST OF SCHEMES

CHAPTER 1: Introduction and literature review

1.1 Chapter overview

In this chapter, a brief overview of malaria and its treatment is provided. Malaria is highlighted with respect to disease and burden, the life-cycle of *Plasmodium falciparum,* current antimalarial chemotherapies, and the hemoglobin degradation pathway. The importance of drug properties with regard to absorption, distribution, metabolism, excretion, and toxicity (ADMET) is discussed with emphasis on metabolic bioactivation pathways. Background to the project is provided by highlighting the use of Mannich bases as antimalarials, as well as ongoing investigations into the potential of pyrido(1,2-*a*)benzimidazoles (PBIs) as antimalarials. To sum up the chapter, a research program is included, and study justifications, hypotheses, and study objectives are briefly mentioned.

1.2 Malaria

1.2.1 Malaria disease and burden

Malaria as a human parasitic disease represents one of the most significant burdens in terms of its impact on both economies and public health, especially in low-income countries.[1,2] Despite strategies implemented by the World Health Organisation (WHO) aiming to reduce mortality and morbidity rates in recent decades, 228 million malaria cases were recorded worldwide in 2018 (**Figure 1.1**).[1]

The malaria burden is heaviest in the WHO African region, with 213 million cases (93%) in 2018, followed by the WHO South-East Asia region (3.4%), and the Eastern Mediterranean region (2.1%).[1] *P. falciparum* is the pathogen responsible for disease associated with the highest rates of morbidity and mortality, although *Plasmodium vivax* is responsible for approximately 3.3% of all estimated cases, with 53% of these in the WHO South-East Asia region, and is the predominant parasite in the WHO region of the Americas (75%).[1] Despite the unprecedented progress made towards lowering these alarming statistics, recent findings showed an increase of approximately 4 million cases in 2016 compared to that in 2015 (**Figure 1.1**).[3]

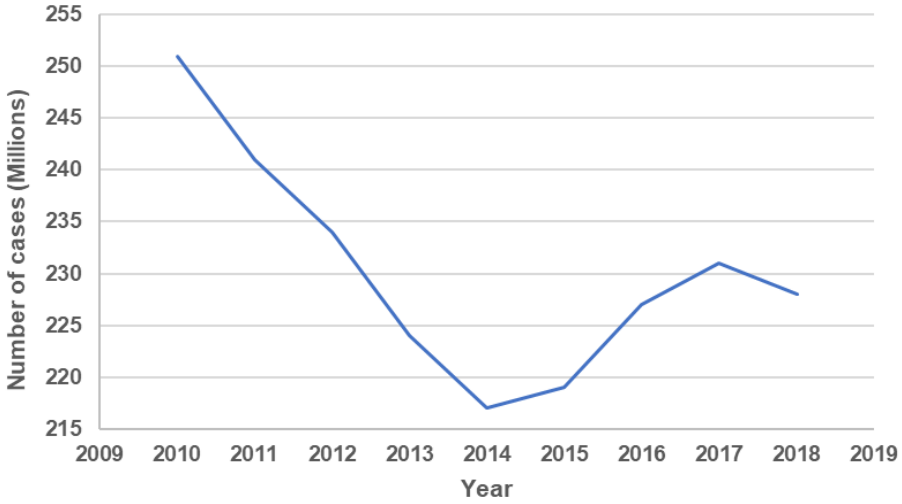

Figure 1.1: Mortality and incidence rates of malaria from 2010 to 2018 (World Health Organisation - World Malaria report 2019)

The number of malaria cases peaked in 2017 (231 million cases) and has since then decreased to approximately 228 million in 2018. Although these statistics attest to successful global efforts made to control the disease, they do remain alarmingly high, thus highlighting impediments to disease treatment including the development of insecticide resistance in malaria vectors[4] and reduced sensitivity to the first-line artemisinin combination therapy (ACT) regimen.[5] Furthermore, the only licensed vaccine (RTS,S) is hindered by limited efficacy and is currently being introduced only as a pilot scheme in a few regions in sub-Saharan Africa.[6] This situation urges the discovery of novel, safe, and effective therapeutic options to tackle this disease.[7]

1.2.2 *P. falciparum* life-cycle

Malaria is a parasitic disease that is transmitted via the bite of a female, *Plasmodium*-infected *Anopheles* mosquito.[8] Infection may be caused by five different species of the genus *Plasmodium*: *P. falciparum, P. vivax, P. ovale, P.knowlesi* and *P. malariae*. The most severe of these pathogens in terms of virulence and morbidity is *P. falciparum*,[9] although *P. vivax* also has a major impact on populations with regard to morbidity.[10] Understanding the life-cycle and transmission of *P. falciparum* may reveal the sites of action of potential drugs. The cycle has distinct stages that include both asexual and sexual reproduction in two hosts: *Anopheles* mosquitoes and humans (**Figure 1.2**).

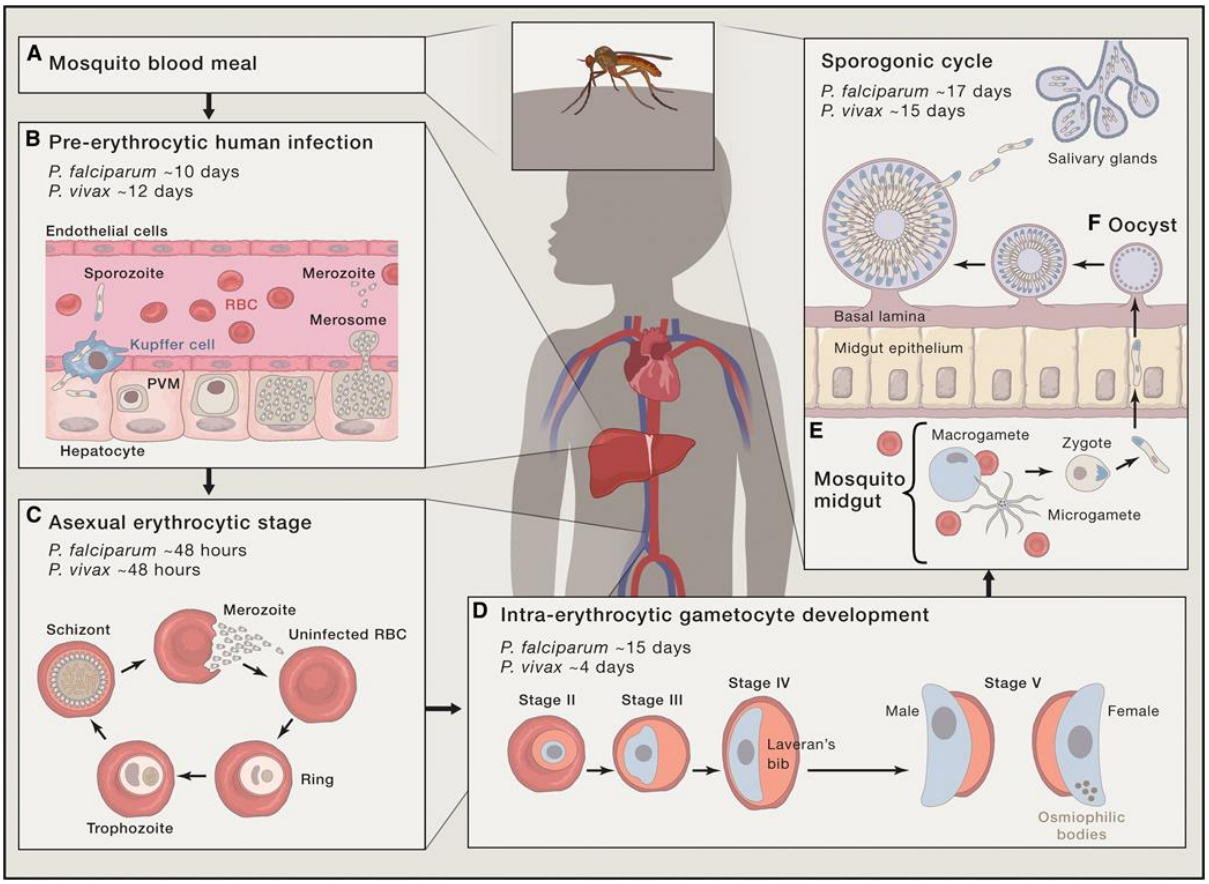

Figure 1.2: Life-cycle of the malaria parasite (Cowman, A; Healer, J; Marapana D et al. Malaria: Biology and Disease. Cell. 2016; 167(3):610-624)

The life-cycle of *P. falciparum* is a continuous loop that relies on numerous biological and cellular changes and regulation in both the *Anopheles* mosquito and human hosts. Briefly, during a blood meal, a parasite-infected mosquito injects sporozoites into the human host from its salivary glands (**Figure 1.2A**).[11] The motile sporozoites penetrate into small capillaries through the dermis of the human host, thus stimulating the host immune response.[12] Circulating sporozoites quickly access the liver by a process known as traversal.[13] Sporozoites are able to cross the sinusoidal barrier comprising fenestrated endothelial cells and are mopped up by Kupffer cells (macrophage-like immune cells) into the liver where the exo-erythrocytic or liver-stage cycle of growth occurs.[14,15] Importantly, sporozoites are injected into the dermis in “migratory mode” and convert to “invasive mode” upon interaction with hepatocytes.[13] Sporozoites penetrate hepatocytes and grow in size over a few days, developing into schizonts over the subsequent 2–10 days of the liver stage. Parasites remain within a

parasitophorous vacuole membrane into late liver-stage development (**Figure 1.2B**),[13] which culminates in the release of up to 40 000 merozoites per hepatocyte into the blood-stream by budding of parasite-filled merozoites[16,17] These merozoites are carried into general circulation and eventually break apart, releasing invasive merozoites that attach to and invade red blood cells (RBCs) to start the erythrocytic cycle of infection, also known as the blood-stage cycle.[15,18]

Erythrocyte invasion is a dynamic, multi-step process comprising pre-invasion, active invasion, and echinocytosis, and which is completed in 2 min.[19] Pre-invasion involves the initial interaction of merozoites with RBCs and little is understood about the molecular details of this step. Merozoite surface protein 1 (MSP1) is a major glycophosphatidylinositol (GPI)-associated protein on the merozoite surface that is involved in erythrocyte binding, although it is not absolutely required for invasion of RBCs.[20,21] Ultimately, pre-invasion involves robust interactions between merozoites and RBCs directed by a number of protein interactions and cellular signaling molecules resulting in parasite actomyosin motor-driven deformation of the host cell.[19]

Following deformation of the erythrocyte, the apical end of the merozoite orientates itself to lean against the RBC membrane.[22] A number of complex merozoite surface protein interactions are associated with an influx of Ca^{2+} into the host RBC.[19,23] Tight junctions formed between parasite-derived proteins cause the irreversible attachment of merozoites to erythrocytes. Lipid-rich rhoptry contents form the parasitophorous vacuole membrane while the merozoite is propelled into the RBC using the force generated by the parasite actomyosin motor.[24] After the active invasion phase, membranes at the posterior end of the merozoite fuse, thus sealing the parasite within the parasitophorous vacuole and erythrocyte, a process known as endocytosis. Echinocytosis follows, which causes RBC shrinkage and the formation of spiky protrusions.

Following RBC infection, cell division (schizogony) occurs over the next 48 h and results in the formation of 16–32 merozoites that migrate when developed. Merozoites immediately differentiate into erythrocytic trophozoites.[15] Trophozoites feed off the hemoglobin of invaded RBCs where mitotic growth causes the development of schizonts that continually divide by mitosis to form differentiated merozoites.[25] Approximately 48 h after intracellular growth, the host cell (RBC) membrane ruptures,

causing the release of merozoites that reattach and further invade healthy RBCs to continue the asexual blood cycle.[15] During schizogony, some merozoites within schizonts differentiate into male and female micro- and macro-gametocytes respectively, instead of the asexual trophozoites, upon entering a new RBC (**Figure 1.2C**).[17,26]

The transmission of malaria from humans to mosquitoes is dependent on development of the sexual stages and this has been recognized as a potential intervention point, either with the use of transmission-blocking drugs or vaccines.[27] Environmental stimuli, such as high parasitemia and exposure to drugs such as chloroquine (CQ), are associated with increased conversion to gametocyte production, indicating that parasites can sense their environment.[27, 28] The mosquito sexual stage of the parasitic life-cycle begins when a feeding female takes up circulating gametocytes in its blood meal (**Figure 1.2E**). In the midgut of the mosquito, RBCs lose their membranes and expose gametocytes, which become sexually stimulated. The male gametocyte undergoes nuclear division and flagellation to prepare for fertilization of the female gametocytes.[29] A diploid zygote is formed when a male gametocyte penetrates a female gametocyte. Further divisions allow for differentiation and growth of the zygote into elongated sporozoites.[30] Following sporozoite maturation, the capsule bursts open, thus releasing hundreds of sporozoites into the hemocoel of the mosquito. These eventually migrate to and penetrate the salivary gland of the mosquito.[30] When a mosquito in search of a blood meal penetrates the skin of a human, salivary fluid is released along with several hundred sporozoites, bringing the life-cycle of the mosquito back to its start.[30]

Transmission is limited by environmental factors (primarily temperature) affecting the ability of the mosquito to sustain parasite development. Transmission is also linked to the frequency of contact between infected mosquitos and humans, which is affected by mosquito density, location, and feeding habits. As exposure rises, transmission becomes more consistent year to year, and exposed individuals begin to develop a degree of immunity. In contrast, areas where the risk of infectious bites is low and unpredictable, malaria is said to be unstoppable.[27] Under such circumstances, patients of all ages are susceptible to infection, and infective episodes generally result in clinical disease.

1.2.3 Current antimalarial chemotherapies

Considerable progress has been made towards reducing the malaria burden through vector control, diagnostic-led case management, and chemoprevention.[31] Preventative strategies include the use of long-lasting insecticide-treated nets, indoor residual spray, and intermittent preventative therapy for pregnant women.[31] Over the last decade, technological progress in molecular platforms has stimulated tremendous advances in the research and development of novel drug candidates that may become viable alternatives to current clinically approved medicines. As malaria is an infectious disease, resistant parasite strains are continually emerging, requiring the constant development of new molecules. The last few years have seen a new generation of compounds with novel mechanisms of action entering clinical development.[31,32]

Malaria incidence rates have significantly reduced over the last 15 years, mainly via the protection of at-risk populations with insecticide-treated bed nets and spraying with insecticides and larvicides.[33] Perhaps the most exciting preventative strategy is the development of a malaria vaccine. The pre-erythrocytic vaccine RTS,S/AS01 offers the potential for a large-scale roll-out.[34] However, RTS,S/AS01 shows limited efficacy against severe cases of malaria (18–36%) with reported short-lasting immunity, and is thus not effective enough to drive eradication alone.[34] More vaccines are currently under evaluation, including an irradiated sporozoite vaccine that is approaching clinical phase III trials.[35] *P. falciparum*'s complex life-cycle presents an array of targets in the parasite developmental stages that may be inhibited using various drugs or drug combinations to treat malaria.[31] Burrows and colleagues recently profiled the ideal types of molecules (target candidates) and medicines (target product) for novel malaria therapy, thus helping to establish a crucial blueprint for malaria drug design by defining the minimum acceptable profiles for ideal candidate molecules and drugs.[31,36] Considering the various stages of *P. falciparum's* life-cycle, transmission blocking, efficacy, and exposure, target candidate profiles (TCPs) for new antimalarial drugs were defined.[31]

Current antimalarials may be grouped into several classes: 4-aminoquinolines, 8-aminoquinolines, arylamino alcohols, antifolates, artemisinins, antibiotics, and inhibitors of the bc1 complex in the parasite electron-transport chain. Artemisinin

combination therapy (ACT) is the current WHO-recommended treatment option for uncomplicated malaria.[37]

Artemisinins, including synthetic derivatives such as artesunate (**Figure 1.3** (**1**)), artemether (**2**), and dihydroartemisinin (**3**), act on both the early and late stages of the parasite's life-cycle within the human host.[38] ACT regimen is fast-acting and safe, and involves an artemisinin derivative combined with a long-acting partner antimalarial. Combination therapy aims to enhance the therapeutic effects of the treatment by lengthening drug exposure in a synergistic manner to delay the onset of resistance.[31] The antifolates sulfadoxine (**4**) and pyrimethamine (**5**) synergistically inhibit enzymes within the folate pathway and are currently recommended by the WHO as an intermittent preventative treatment in pregnant women (IPTp).[39]

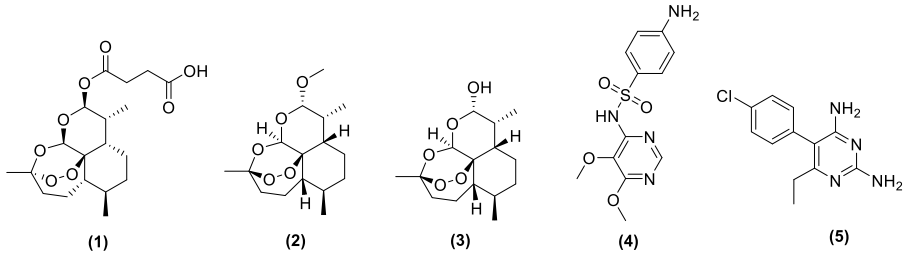

Figure 1.3: Current drugs used in artemisinin combination therapy (ACT) and intermittent preventive treatment in pregnant women (IPTp)
1, artesunate; **2**, artemether; **3**, dihydroartemisinin; **4**, sulfadoxine; **5**, pyrimethamine

Antibiotic antimalarials including doxycycline (**Figure 1.4** (**6**)) and clindamycin (**7**) inhibit protein synthesis. Their slow onset means they have therapeutic potential for combination with fast-acting artimisinins.[31] Quinine (**8**), mefloquine (**9**), lumefantrine (**10**), and halofantrine (**11**) are examples of aryl-amino alcohols. Both mefloquine (**9**) and lumefantrine (**10**) are used in combinations with artesunate (**1**) and artemether (**2**)**,** respectively, whilst halofantrine (**11**) is not widely used because of severe concerns relating to cardiotoxicity.[40] Atovaquone (**12**) is mostly used for chemoprevention in combination with proguanil (**13**), and for the treatment of uncomplicated malaria.[31]

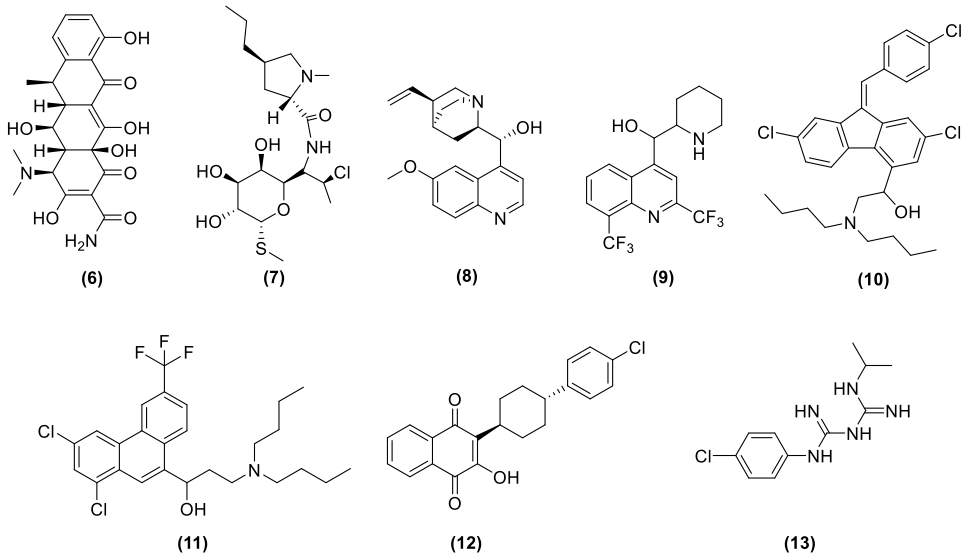

Figure 1.4: Chemical structures of currently prescribed antibiotics, aryl amino alcohols, and respiratory chain inhibitors
6, doxycycline; **7**, clindamycin; **8**, quinine; **9**, mefloquine; **10**, lumefantrine, **11**, halofantrine, **12**, Atovaquone and **13**, proguanil.

The only drug currently used for the treatment of infections with *P. vivax* and relapsing forms of malaria is the 8-aminoquinoline drug primaquine (**Figure 1.5** (**14**)).[41] Tafenoquine (**15**) is an analogue of **14** that has undergone phase II and phase III clinical evaluation and shows signs of increased potency and decreased toxicity compared to that of **14**.[42,43] CQ (**16**) is the most widely known of the 4-aminoquinoline class and is used to treat uncomplicated *P. vivax* malaria. Following widespread resistance to **16**, amodiaquine (**17**) was designed as an alternative, but presents limitations relating to agranulocytosis and hepatotoxicity. However, **17** is currently used in combination with **3** as part of the ACT-based treatment regimen. Piperaquine (**18**), another 4-aminoquinoline used in ACT treatment in combination with **3,** shows excellent tolerability and high malaria cure rates and has promising potential to prevent the relapse of *P. vivax*-associated infections.[44,45]

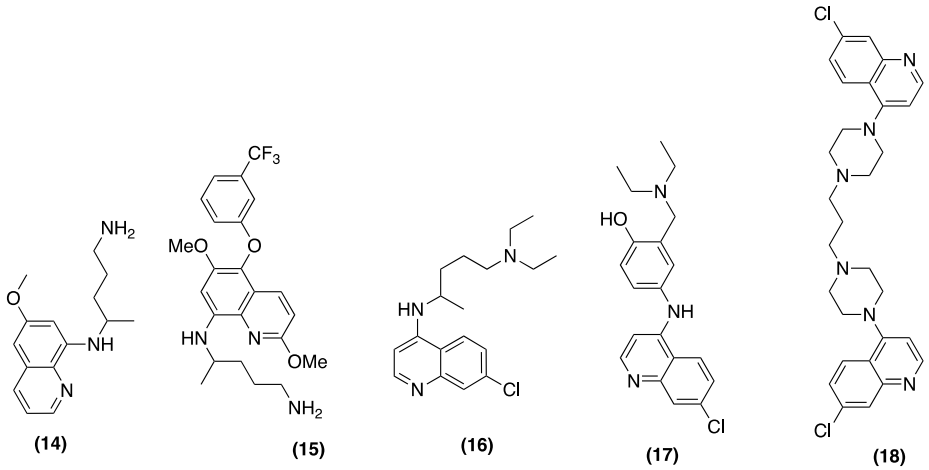

Figure 1.5: Chemical structures of various currently used antimalarials
14, primaquine; **15**, tafenoquine; **16**, chloroquine; **17**, amodiaquine; **18**, piperaquine

Although many uncomplicated malaria infections are successfully treated, the above mentioned chemotherapies have limitations.[3] Evidence of parasite tolerance towards ACT-based treatment heightens the urgency for novel antimalarial drug discovery and development. In order to fast track the eradication of malaria, Medicines for Malaria Venture (MMV) have an open portfolio of all the projects they support from research to product development. In this regard recent developments are summarized in **Table 1.1.**[31]

Table 1.1: Drug development stages and Medicines for Malaria Venture (MMV) open labeled portfolio

Research	Translational		Product Development	
Candidate Profiling	**Preclinical**	**Human Volunteers**	**Patient exploratory**	**Patient confirmatory**
• MMV1581373 (Novartis)	• MMV533 (Sanofi) • MMV370 MMV371 • MMV183 (TropIQ) • MMV646 (Jacobus) • INE693 (Novartis) • UCT943 (UCT)	• P218 (Janssen) • M5717 (Merck KGaA) • MMV253 (Zydus Cadila) • Antoguanil (Ipca)	• Ferroquine/ Artefenomel (Sanofi) • Ganaplacide/ Lumefantrine (Novartis) • Cipargamin (Novartis) • DSM265 (Takeda) • MMV048 (UCT)	• Dihydroartemisinin-piperaquine dispersible (Alfasigma) • Tafenoquine Paediatric (GSK) • Sulfadoxine-pyrimethamine (Universal Corporation) • Artemether-lumefantrine <5Kg (Novartis)

Target Candidate Profiles:

Asexual blood stages Prophylaxis Transmission reduction Relapse prevention

Target Product Profiles:

3-day cure, ACTs Uncomplicated malaria treatment for single-exposure radical cure and/or resistance management Severe malaria treatment / pre-referral intervention Intermittent / seasonal malaria chemoprevention Products targeting prevention of relapse for *P. vivax* Single-exposure chemoprotection

paediatric formulation

The importance of this portfolio is the transparent progression of compounds through the drug development pipeline. Currently there are several compounds undergoing lead optimization strategies (not shown), which is encouraging since there is currently only one compound in the candidate profiling stage of the pipeline, namely MMV1581373 which is currently undergoing profiling at Sanofi.

Furthermore, in order to support the malaria eradication campaign MMV has defined Target Candidate Profiles (TCPs) and Target Product Profiles (TPPs).[46] These TCPs highlight the important features of the individual compounds and give an indication of the effect of the compounds on various stages of the life cycle of *P. falciparum*. The TPPs are used to characterize compounds in the human volunteer stages of development according to the type of malaria which the compounds are likely to combat.

Briefly from **Table 1.1**, there are currently six preclinical candidates (MMV533, MMV370, MMV371, MMV183, MMV646 INE693 and UCT943) which are in the preclinical development phase all of which target the asexual blood stages. Additional to asexual blood stage activity MMV370 and MMV371 can be used for prophylaxis in order to prevent the disease. Furthermore, preclinical candidate MMV183 has the potential to reduce transmission of the disease.

There are currently four compounds in human volunteer trials namely P218 (**19**), M5717 (**20**), MMV253 (**21**) and Atoguanil which contains the active pharmaceutical ingredients atovaquone (**22**) and proguanil (**23**) shown in **Figure 1.6**. Compound **19** is a *P. falciparum* dihydrofolate reductase (DHFR) inhibitor with a clinically validated pathway and proof of pharmacology has been confirmed in volunteer infection studies (VIS). Although it has good tolerability and pharmacokinetics in humans, it is limited by a short human half-life.[47] Currently **19** is in VIS for prophylaxis which started in December 2018. Compound **20** is a *P. falciparum* translation elongation factor 2 (EF2) inhibitor which is a novel mechanism of action with comparable activity across all stages of the malaria parasite life-cycle. Currently **20** is undergoing a volunteer infection studies.[48] Compound **21** has an unknown mechanism of action, however it has a low resistance potential from *in vitro* studies. It was approved as a preclinical candidate in 2014 and first-in-human studies started in February 2019.[49] Atoguanil has the potential to provide a lower cost alternative, making such products more

accessible to people living in malaria endemic countries for prophylaxis and is currently under investigation by Ipca Laboratories.

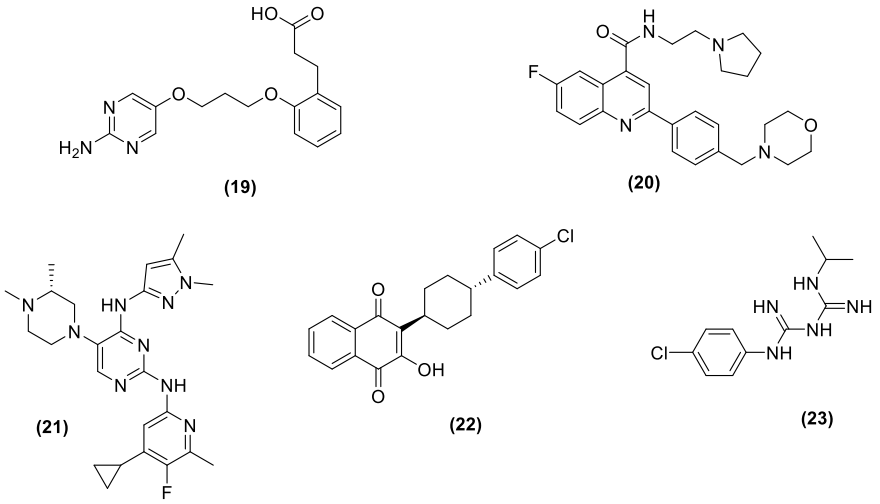

Figure 1.6: Chemical structures of compounds currently in the Human volunteer's stage of research **19**, P218; **20**, M5717; **21**, MMV253 and Atoguanil which is made up of **22**, atovaquone and **23**, proguanil

There are currently six treatments in the patient exploratory phase of development namely; Ferroquine/Artefenomel (**24**), Ganaplacide/Lumefantrine (**25**), Cipargamin (**26**), DSM265 (**27**) and MMV048 (**28**) shown in **Figure 1.7**. The Ferroquine/ Artefenomel (**24**) treatment makes use of Ferroquine which inhibits heme detoxification combined with the synthetic trioxolane mode of action of Artefenomel. The combination of these two drugs allows for long duration of plasma exposure (Ferroquine) with the fast killing of parasites as well as the possibility of transmission blocking.[48] This combination treatment is currently undergoing phase IIb clinical studies. The combination therapy involving Ganaplacide and Lumefantrine (**25**) has the potential for prophylaxis and the treatment for uncomplicated malaria. Furthermore, Ganaplacide has a novel mechanism of action which shows activity to resistant strains of *P. falciparum*, with the rapid killing of parasites.[50] This combination therapy is currently undergoing a phase IIb combination study. Cipargamin (**26**) aims to treat both uncomplicated cases of malaria as well as severe malaria with a novel mode of action by inhibiting the PfATP4 pathway of *P. falciparum*. **26** shows rapid killing of parasites and has the potential for transmission-blocking. **26** does however need further safety profiling and is therefore undergoing a phase II malaria patient study which started in February 2019 as well as Parenteral Glucagon-like peptide

(GLP) safety study which is currently in progress.[51] DSM265 (**27**) is a Plasmodial dihydroorotate dehydrogenase inhibitor which is a novel mode of action. There is however a potential for resistance because it targets a single enzyme only.[52] Currently **27** has undergone phase IIa studies and controlled human malaria infection studies in combination with Artefenomel.[53,54] UCT identified the aminopyridine **28** and revealed its novel mode of action which is by inhibiting the *P. falciparum* phosphatidylinositol 4-kinase (PfPI4K) enzyme. Encouragingly, there is a long half-life found in humans as well as the potential for transmission blocking. There are however safety concerns in pregnant women which is a challenge which needs to be addressed. **28** is currently undergoing phase IIa studies in Ethiopia.[31]

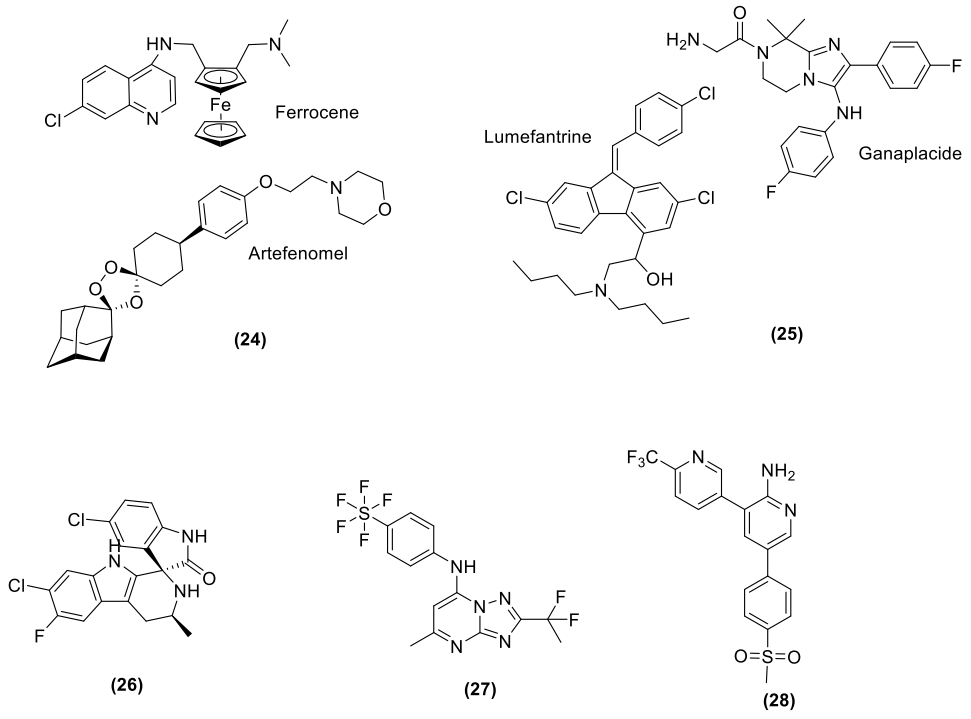

Figure 1.7: Chemical structures of compounds currently in the patient exploratory stage of development; **24**, Ferroquine/Artefenomel; **25**, Ganaplacide/Lumefantrine; **26**, Cipargamin; **27**, DSM265 and **28**, MMV048.

There are currently four treatment candidates in the patient confirmatory phase of development, namely; (**29**) Dihydroartemisinin-piperaquine dispersible, (**30**) Tafenoquine Paediatric, (**31**) Sulfadoxine-pyrimethamine and (**32**) Artemether-lumefantrine shown in **Figure 1.8**. The combination therapy of Dihydroartemisinin-piperaquine (**29**) aims to make use of a pharmacokinetic bridging strategy to establish a paediatric dose on an already used ACT treatment regime in adults.[55] **29** is

anticipated to have comparatively long post-treatment protection. There are however confirmed piperaquine resistance cases and there is a potential for cardiac monitoring restrictions.[56,57] **29** has undergone pharmacokinetic studies in children and a dossier is under development for submission to the European Medicines Agency. Tafenoquine paediatric (**15**) makes use of the already approved antimalarial Tafenoquine and using a pharmacokinetic bridging strategy to establish a paediatric dose. The efficacy in adults is already established and a single-dose treatment in children who cannot take the adult tablet is being developed.[58] There are however challenges associated with glucose-6-phosphate dehydrogenase (G6PD) deficient patients which requires quantitative testing for G6PD deficiency in patients.[59] Sulfadoxine-pyrimethamine (**30**) combination aims to cure intermittent and seasonal malaria by means of chemoprevention. Although the treatment is currently being used in adults in combination with amodiaquine, a treatment regime is being developed for sulfadoxine and pyrimethamine without any additional antimalarial compounds. Artemether-lumefantrine (**31**) is an already approved combination therapy which is undergoing pharmacokinetic studies to tailor a dose for children that weigh less than 5 kg.

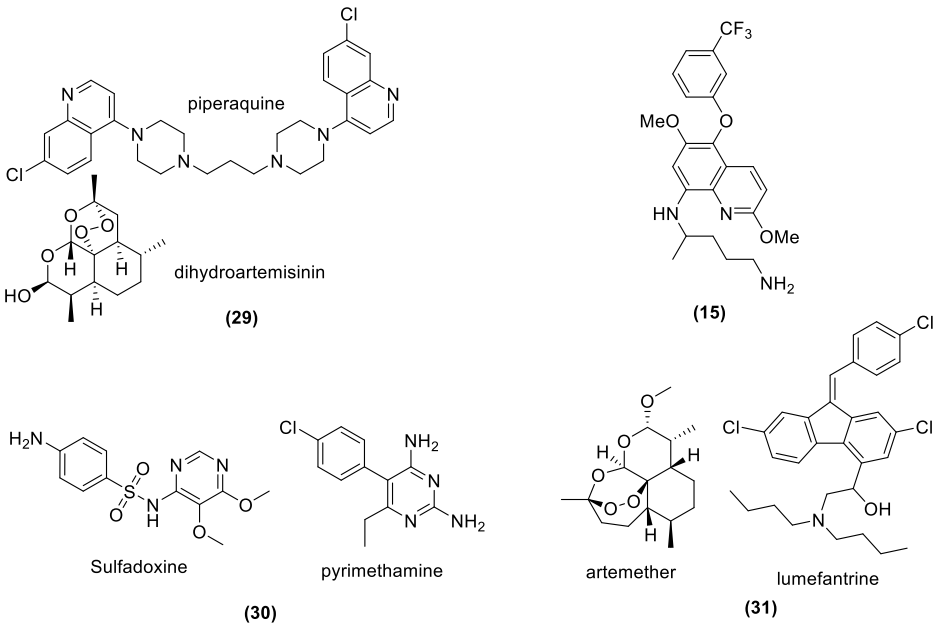

Figure 1.8: Chemical structures of compounds currently in the patient confirmatory stage of development; **29**, Dihydroartemisinin-piperaquine dispersible; **15**, Tafenoquine Paediatric; **30**, Sulfadoxine-pyrimethamine; **31**, Artemether-lumefantrine <5Kg.

The malaria drug development process highlights the need for a full understanding of drug and safety profiles to predict therapeutic effects expected in humans. By

understanding drugs that have been rejected in the late stages of development, possible liabilities that may be associated with new drug candidates based on chemotypes, specific MoAs, and modes of resistance can be flagged. One way to achieve this is by understanding the MoAs of established drugs as a starting point for the development of new drug candidates. Structural similarities with existing drug candidates displaying established MoAs could indicate that a particular scaffold may impact a specific pathway because of its similarity to other drug candidates. One such pathway is the hemoglobin degradation pathway, which is present in *Plasmodium spp.* and has been targeted by other prescribed antimalarials.[60]

1.2.4 Hemoglobin degradation

Hemoglobin degradation and formation is a part of the *P. falciparum* life-cycle that is an established target of certain antimalarial drugs such as CQ and AQ.[61,62] The formation of hemozoin from toxic heme is a unique process that has been adopted by *Plasmodium spp.* for survival. As is outlined in **Figure 1.9,** *P. falciparum* relies on human hemoglobin for growth and division.[60] Hemoglobin is catabolized into hemozoin and free amino acids for protein synthesis.

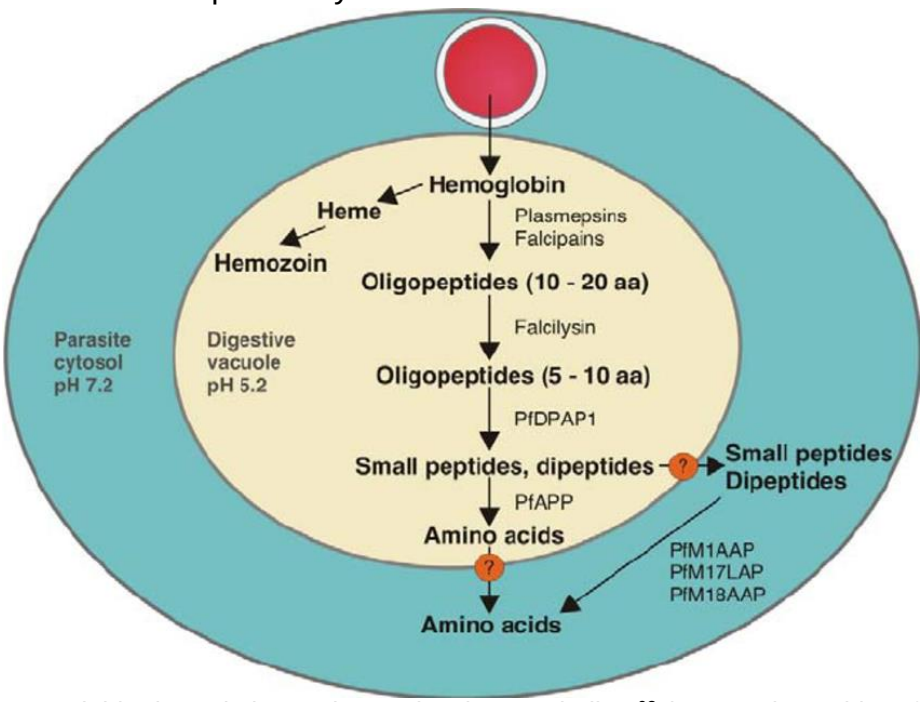

Figure 1.9: Hemoglobin degradation pathway showing catabolism[63] (aa – amino acids; PfDPAP1 – *P. falciparum* Dipeptidyl Aminopeptidases 1; PfAPP – *P. falciparum* aminopeptidase P; PfM1AAP - *P. falciparum* M1 alanyl aminopeptidase, PfM17LAP – *P. falciparum* M17 leucine aminopeptidase and PfM18AAP – *P. falciparum* M18 aspartyl aminopeptidase).

Heme (or hematin, **Figure 1.10**) that is released during hemoglobin catabolism is toxic to vacuolar proteases and parasite membranes.[62] Parasites have developed a non-enzymatic strategy to detoxify free heme by converting it into an insoluble polymer called hemozoin, which aggregates in the digestive vacuole.[64] Several antimalarial drugs are known to inhibit hemozoin formation by complexing with ferriprotoporphyrin IX (FPIX), thereby preventing polymerization to form hemozoin.[62] Drugs that inhibit the formation of hemozoin include the 4-aminoquinolines CQ (**16**) and AQ.[62,65] It was recently hypothesized that PBIs may adopt flat conformations to allow for π-π stacking interactions with FPIX, thus inhibiting hemozoin formation and killing the parasite as shown recently.[66]

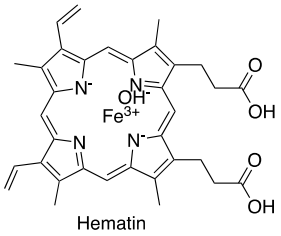

Hematin

Figure 1.10: The structure of hematin, a toxic molecule to *P. falciparum* that is detoxified by the parasite by converting to hemozoin

1.3 ADME profiling in drug discovery and development

Pharmacokinetics (PK) defines the processes that a drug undergoes after oral administration, and may be referred to as drug metabolism and pharmacokinetics (DMPK).[67] After oral administration, the therapeutic effects of a drug may only be realized if the compound can successfully dissolve, cross the biological membranes of the gastrointestinal tract and surrounding tissues, and enter systemic circulation. This is vital for effective therapeutic control as target organs must be reached for maximum effect.[68] The most common reason for the failure of orally administered drugs is low intestinal absorption and/or rapid clearance, drug-drug interactions, and the presence of reactive metabolites causing undesirably low and/or variable bioavailability.[69] Understanding the DMPK properties of molecules is important in rational drug discovery as these predict human drug PK and metabolism, and help to reduce the number of unsuitable compounds being filtered out early in the drug development process.[70] DMPK is determined and expressed by chemically modifiable factors that influence the ADME of drugs.[71] A rational approach to drug discovery encompasses a balance between strategies in chemistry, pharmacology, and drug PK.[71]

1.4 Bioactivation and metabolism in drug discovery

Understanding bioactivation through drug metabolism is important as it is often suspected to be the event initiating drug toxicity. Metabolism is often an important contributor to drug clearance via the excretion of metabolized drugs.[72] Drug metabolism also underlies drug-drug interactions, detoxification and excretion of toxic agents, drug activation or targeting, and has the potential to generate oxidative stress by producing reactive electrophiles or radical products.[73] The two most common enzyme systems involved in bioactivation are the cytochrome P 450 (CYP450) and peroxidase enzyme systems.[73] A third mechanism for the formation of chemically reactive species is the glucuronyl transferase enzyme system, which has been extensively reviewed with regard to carboxylic acids.[74]

The CYP450 catalytic cycle is a monooxygenous heme-containing enzyme system that directly binds to the substrate. Following substrate binding, two single-electron reductions of the substrate by CYP450 itself and NAPDH occurs. However, this mechanism is not concerted and therefore depends on the substrate's reduction potential. One-electron reductions could therefore occur at the substrate rather than the oxygen level, thereby allowing free-radical formation.[73]

Peroxidases are involved in bioactivation in non-hepatic tissue in contrast with the full-body distribution associated with the CYP450 enzyme system.[75] Peroxidases usually act with electron-rich functional groups such as aromatic π systems, and this enzyme system differs from CYP450 in that the heme is attached to an apoprotein. Furthermore, the nature of the axial ligand is different.[76] Peroxidase bioactivation results more frequently in radical formation without oxygen rebound.[73] Peroxidases are associated with neutrophils, which are of interest as neutrophil infiltration occurs during the inflammatory response and is associated with many disease states. When infiltration into the liver occurs, the potential for peroxidase reactions to generate radical metabolites increases and drug metabolism in healthy and sick patients may therefore vary.[73]

Glucuronyl transferases affect the transfer of glucuronic acid to mostly nucleophilic functional groups.[77] Mechanisms by which these acyl glucuronides react have been extensively studied.[78] Glucuronides are often stable enough to be characterized and challenges concerning bioactivation are thus easily overcome in drug design.[79]

Functional group bioactivation pathways have also been extensively reviewed.[80] Such potential issues can be easily avoided, although this may not always be practical as a wide range of functional groups present bioactivation liabilities.[73]

1.5 Project background

1.5.1 Amodiaquine (AQ)

AQ is a 4-aminoquinoline, Mannich base-containing CQ derivative that has been used as an antimalarial for more than 50 years in Africa and Asia.[81] Compared to CQ, and other 4-aminoquinoline compounds, AQ showed greater efficacy and was better tolerated in outpatients with uncomplicated malaria.[82] However, AQ was withdrawn from several countries or prohibited from use as a single administration because of severe toxicity relating to agranulocytosis and hepatotoxicity.[3,83] Rapid bioactivation to form protein-reactive metabolites is thought to play a critical role in such toxicity.[84]

After oral administration, AQ is rapidly metabolized to form the major metabolite N-desethylamodiaquine (DEAQ), which shows 100–240-fold higher internal exposure than AQ *in vivo*.[85] Other metabolites include N-bis-desethylamodiaquine (*bis*-DEAQ) and 2-hydroxyl-desmethylamodiaquine.[86] DEAQ is rapidly formed and has a longer *in vitro* half-life than AQ so pharmacological studies for AQ may ultimately be influenced by DEAQ formation, even though the potency of AQ is 3-fold higher than that of DEAQ.[86] Bioactivation of AQ to its metabolites occurs both *in vitro* and *in vivo*,[86] and oxidative bioactivation is achieved via dehydrogenation of the 4-aminophenol moiety by CYP450 to obtain reactive AQ quinoneimine (AQ-QI; **Figure 1.11**). Cytotoxicity to neutrophils and hepatocytes is dependent on bioactivation to AQ-QI by cytochrome myeloperoxidase and CYP450s, respectively.[87] Similarly, bioactivation of the major metabolite DEAQ via CYPs (**Figure 1.11**) also forms reactive quinoneimine. Hepatotoxicity may be explained by covalent binding of both AQ and DEAQ quinoneimines.[86]

Genetic and non-genetic factors such as the expression of CYPs described in **Figure 1.11** also influence AQ-induced toxicity, as the expression of these isozymes influences bioactivation kinetics.[86] Considering the liabilities associated with quinoneimine formed during AQ bioactivation, a literature search was conducted to

identify strategies that may be used to mitigate the risk associated with quinoneimine formation.

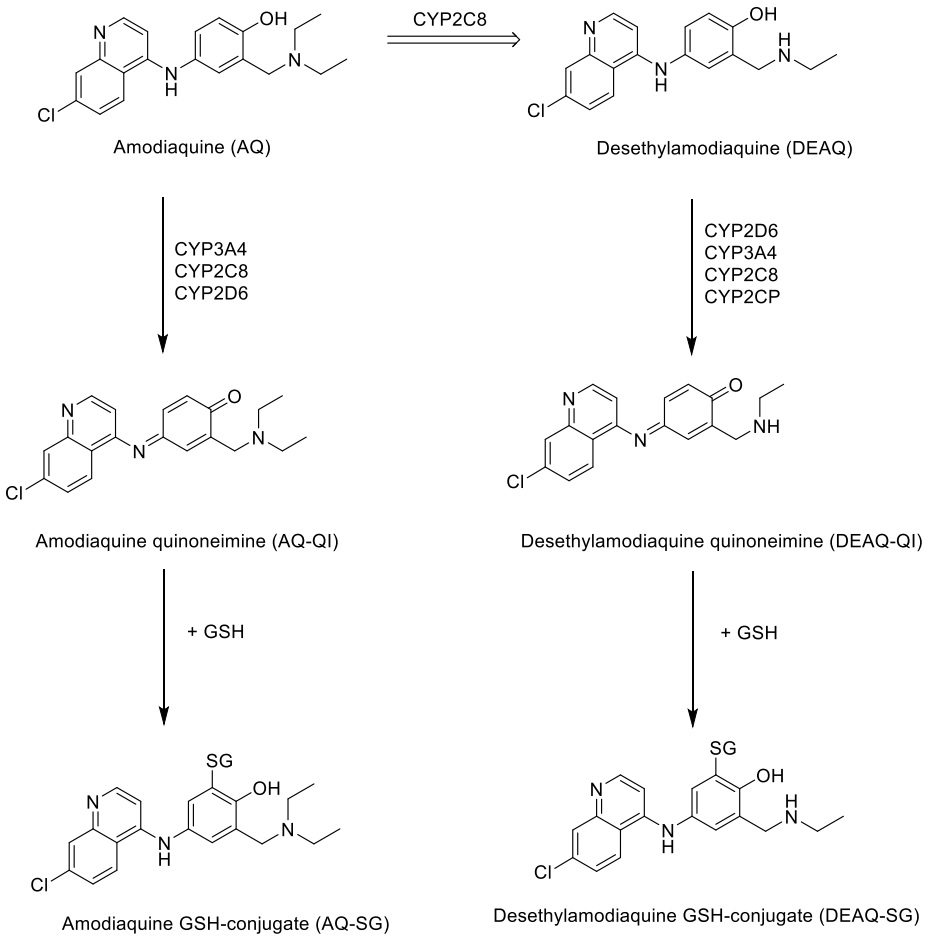

Figure 1.11: Bioactivation of amodiaquine and N-desethylamodiaquine by human cytochrome P450 enzymes[86]

1.5.2 Strategies to mitigate rapid bioactivation

The metabolic studies outlined previously showed that the rapid metabolism of AQ contributed importantly to its hepatotoxicity. It is therefore important to mitigate the rapid bioactivation and metabolism of this molecule to improve its PK properties and overall potency. Researchers have employed the following tactics to achieve this:[80]

- Eliminating the suspect functional group
- Inhibiting potential metabolism (e.g., by site fluorination)

- Lowering the potential for metabolism via steric hindrance or reducing oxidation potentials
- Incorporating metabolic soft spots away from the suspect group

However, this may not always be practical as the functional groups contributing toward metabolism may also be responsible for the compound's biological activity and a balance between PK parameters and the biological activity should therefore be achieved.

1.5.3 Pharmacological activity of PBI-Mannich base compounds

The benzimidazole scaffold is privileged in medicinal chemistry because of its capacity to interact with numerous biological systems.[88] The antibacterial, antifungal, antiviral, and antitumor activities of PBIs have been extensively researched.[89] In light of the spread of drug-resistant parasites, researchers from Tropical Disease Research (TDR) in collaboration with Tibotec screened a small library of 2000 non-proprietary compounds donated by Specs against protozoa *in vitro*. This led to the identification of a PBI coded TDR15087 (**Figure 1.12**), which showed moderate activity against GHA and W2 strains of *P. falciparum* (IC_{50} = 0.17–0.37 μM).[90] This is significant since no prior published work suggested that PBIs displayed antimalarial activity. This prompted a medium throughput screening of 535 commercially available analogues which were selected on the basis of providing structural diversity around the PBI core. This led to the identification of 49 compounds with IC_{50} < 0.1 μg/mL; notably included the *N*-benzylpiperazinyl derivatives TDR35885 and TDR44047 seen in **Figure 1.12.**

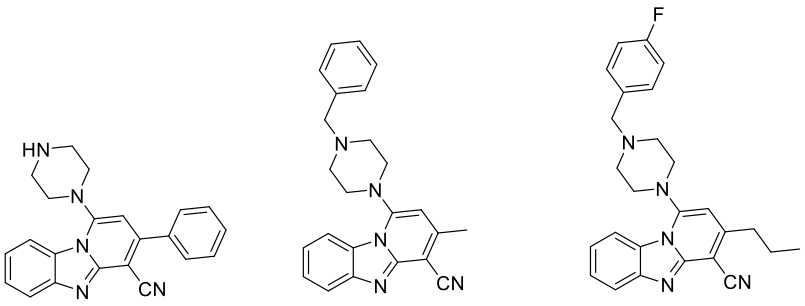

Figure 1.12: Pyrido(1,2-*a*)benzimidazole screening hits with potent activity toward *P. falciparum.*

However, the original hit compounds (**Figure 1.12**) all proved inactive in a *P. berghei* mouse model which prompted Ndakala and co-workers to further investigate the structure-activity relationship (SAR) of PBIs in an extensive study. Further development and SAR exploration of PBIs by Ndakala and co-workers led to the identification of pyrido(1,2-*a*)benzimidazoles that combine good *in vitro* activity against *P. falciparum* with oral efficacy in the *P. berghei* mouse model. *In vivo* and *in vitro* activities were strongly influenced by metabolic stability, and therefore microsomal stability studies were performed to guide researchers in overcoming metabolic liabilities.[66] Several PBI analogues were synthesized by Ndakala et al.[66] and showed *in vitro* antiplasmodium activities comparable to CQ (IC_{50} = 0.17–0.20 μM). In general, lipophilicity influences *in vitro* activity and selectivity, although structural features of the side-chains also play a role.[66] The *in vivo* activity of compounds that were most active *in vitro* was assessed and the mean survival time of *P. berghei* infected mice increased significantly compared to that after CQ treatment.[66] *In vitro* metabolic stability studies showed moderate to high rates of metabolic degradation, with the exception of a few compounds showing moderate metabolic degradation. Deamination, N-dealkylation, and ring cleavage was suggested to be responsible for this rapid metabolic degradation.[66] The lead compound **A** (**Figure 1.13**) showed high antiplasmodium activity *in vitro* (IC_{50} in *P. falciparum* (*Pf*) NF54 = 0.11 μM; IC_{50} in *Pf*K1 = 0.12 μM) as well as promising antimalarial oral efficacy *in vivo* (96% at 4 × 25 mg/kg per oral (p.o.)) in a *P. berghei* rodent model. However, PK studies indicated low solubility and saturation in absorption at low oral doses.[66]

Further SAR studies conducted by Singh and co-workers based on the lead compound **A** (**Figure 1.13**) led to the identification of potent, metabolically stable compounds with improved *in vivo* oral efficacy in the *P. berghei* mouse model and additional activity against parasite liver and gametocyte stages, making them potential candidates for preclinical development.[7] Among the most active compounds *in vitro*, **B** and **C** showed significantly better *in vivo* activity in the mouse than the original lead compound **A**.[7]

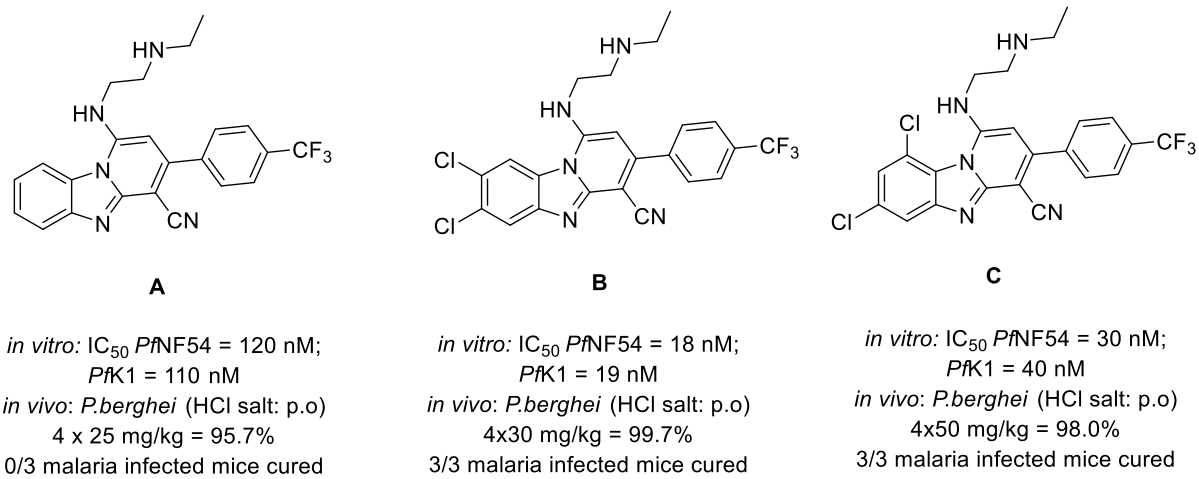

Figure 1.13: Original lead PBI compound **A** and subsequently identified lead compounds **B** and **C,** by SAR expansion showing activity against chloroquine-sensitive (NF54) and chloroquine/multidrug-resistant (K1) Plasmodium *falciparum* strains as well as the *in vivo* mouse model efficacy studies**.** [7,66] IC_{50}, 50% inhibitory concentration; *Pf*, *Plasmodium falciparum*; *P. berghei*, *Plasmodium berghei*; p.o., per oral

The most active compounds also showed good activity against gametocytes, indicative of potential as dual-acting antimalarials. Other analogues have shown activity against the liver stage of P. berghei. There is no conclusive evidence for their mode of action, although inhibition of Hemozoin formation is identified as a potential contributing factor. Mechanistic studies performed on PBIs have focused on the potential for inhibition of hemozoin formation, based on the hypothesis that the flat conformation of PBIs would allow for π-π stacking with FPIX, thus leading to hemozoin formation inhibition and parasite death.[7,66] Among the diverse mode of actions (MoAs) reported for PBIs is the inhibition of the pore-forming protein perforin in mammalian cells by 1-amino-2,4-dicyanopyrido[1,2-*a*]benzimidazoles. This is of interest as the *P. falciparum* proteome contains perforin-like proteins, which are involved in permeabilizing the erythrocyte membrane during egress of gametocytes and merozoites which is a potential target for parasite elimination.[91] Because of the antimalarial activities described, PBIs have been extensively investigated.[7,66]

1.6 Aims and objectives

1.6.1 Objective

a) Design and synthesize potential N-dealkylation metabolites of parent antimalarial PBIs containing Mannich base side-chains.

1.6.2 Specific aims

i) Synthesize and characterize potential N-dealkylation metabolites of antimalarial PBIs and related compounds with Mannich base side-chains.
ii) Profile synthesized compounds with respect to physico-chemical properties, antiplasmodium activity, cytotoxicity and microsomal metabolic stability.
iii) Derive antiplasmodium SAR profiles.
iv) Conduct mechanistic investigations with respect to β-hematin inhibition.

CHAPTER 2: Design, synthesis, and characterization of pyrido(1,2-*a*)benzimidazoles

2.1 Chapter summary

In this chapter, the design, synthesis, and spectroscopic characterization of pyrido(1,2-*a*)benzimidazole-based compounds containing a phenolic Mannich base side-chain are discussed. This is preceded by a brief overview of prior work conducted by our research group at the University of Cape Town (UCT).

2.2 Introduction and preliminary work

Previous work on PBIs as antimalarial agents is well documented.[92,7] A brief summary of the medicinal chemistry efforts made by the Chibale research group on the development of PBIs serves as a preface for this work. These analogues generally comprise a PBI core linked to a phenolic Mannich base side-chain via *N*-arylation (**Table 2.1**). Medicinal chemistry efforts led to the identification of compound **KP84**, a potent inhibitor of the growth of the chloroquine (CQ)-sensitive (NF54) and –multidrug-resistant (K1) *Plasmodium falciparum* strains. Varying the position of the Mannich base substituent on the aromatic ring (**Ar**) and the substituents at the **R** and **X**-positions of the pyridine and benzimidazole benzene rings influenced the antiplasmodium activity, cytotoxicity, and metabolic stability. Results for **KP84**, along with other selected Mannich-base PBI analogues, are summarized in **Table 2.1**.[92]

Table 2.1: Phenolic Mannich base-containing pyrido(1,2-*a*)benzimidazoles evaluated by the Chibale research group

Code	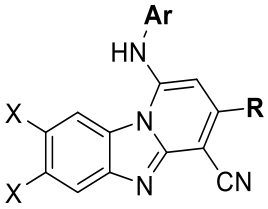			*In vitro* antiplasmodium activity		Cytotoxicity	Stability in MLMs	*In vivo* antimalarial activity	
	Ar	R	X	NF54 IC_{50} (μM)	K1 IC_{50} (μM)	CHO IC_{50} (μM)	%Remaining at 30 min	%Reduction in parasitaemia (4×50 mg/kg)	Mean Survival days
KP84	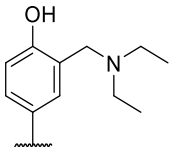	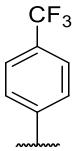	H	0.11	0.18	189	35 ± 3	95	16
KP94	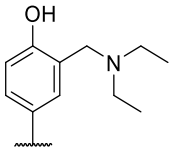		H	0.89	1.0	23.6	15 ± 3	<40	4
KP87	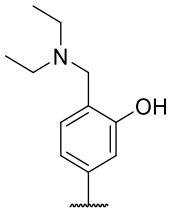		H	4.0	3.81	173	<10	-	-
KP98	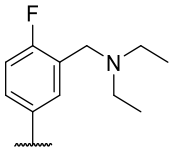		H	5.14	4.66	142	<10	-	-
LB88	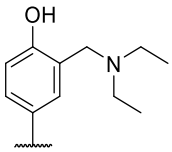	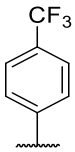	F	0.07	0.07	>100	30 ± 9.4	-	-

CHO, Chinese hamster ovarian cells; MLM, mouse liver microsomes.[92]

All compounds were evaluated for *in vitro* antiplasmodium activity against the NF54 and K1 strains. Antiplasmodium activity (IC_{50}) ranged from 0.07 to 5.14 μM. Compound KP84 showed sub-micromolar *in vitro* activity against the K1 and NF54 strains (NF54 IC_{50} = 0.11 μM, K1 IC_{50} = 0.18 μM). The replacement of the R-substituent in **KP94** from the para-trifluoromethyl phenyl (4-CF_3Ph) substituent to trifluoromethyl (CF_3) whilst maintaining the aromatic Mannich base resulted in a slight

loss of activity (NF54 IC_{50} = 0.89 µM, K1 IC_{50} = 1.0 µM). Interchanging the hydroxyl and Mannich base side group (**KP87**) or substituting the 4-hydroxyl with fluorine (**KP98**) was significantly detrimental to activity. However, an introduction of fluorine atoms at the X-positions on the left-hand side (LHS) of the PBI molecule while maintaining the para-trifluoromethyl phenyl (4-CF_3Ph) substitution appeared to afford the most active compounds (represented by **LB88**).

Furthermore, two compounds were prioritised for *in vivo* studies namely **KP84** and **KP94**. **KP84** exhibited high *in vitro* potency and resulted in *in vivo* parasitemia reduction of 94.5% at a dose of 4 × 50 mg/kg in mice, with a mean survival period of 16 days post treatment. Replacement of the para-trifluoromethyl phenyl (4-CF_3Ph) substituent with trifluoromethyl (CF_3) whilst maintaining the aromatic Mannich base resulted in a loss of activity in the case of **KP94** with less than 40% reduction in parasitemia at the same dose. The *in vivo* efficacy of these phenolic Mannich-based derivatives may be ascribed to their active metabolites.[92,66] It is this hypothesis that the compounds may be producing active metabolites which prompted metabolic stability studies and subsequent metabolite identification studies.

Rapid metabolism of the parent compounds was observed *in vitro* for all analogues and <40% parent compound remained after 30 min when the compounds were incubated with liver microsomes. This was characterized by short degradation half-lives, suggesting the compounds are significantly susceptible to hepatic metabolism regardless of the modifications on the Mannich base side group. Furthermore, Disubstitution with fluorine at the X-positions did not improve metabolic stability. Based on previous knowledge of the antimalarial amodiaquine (AQ) and its route of metabolism it was hypothesised that similar desethyl metabolites may be contributing to the activity of the parent compounds of these Mannich base containing PBIs.[93] There was no metabolism observed in the presence of NADPH which implies that the observed biotransformations is primarily a function of the p450 enzyme-mediated phase 1 metabolism with *N*-deethylation seemingly the predominant route of metabolism.[92] To investigate reactive metabolite formation compounds were screened by LC-MS/MS in rat liver microsomes. The main biotransformation following incubation at 37 ˚C with human and/or mouse liver microsomes in the presence of phosphate buffer and NADPH as cofactor are highlighted in **Figure 2.1**. Using glutathione (GSH)

as a trapping agent GSH-drug adducts were detected in samples for **KP84**, **KP94** and **LB88** but were not detected in **KP87** or **KP98** shown in **Figure 2.1**.

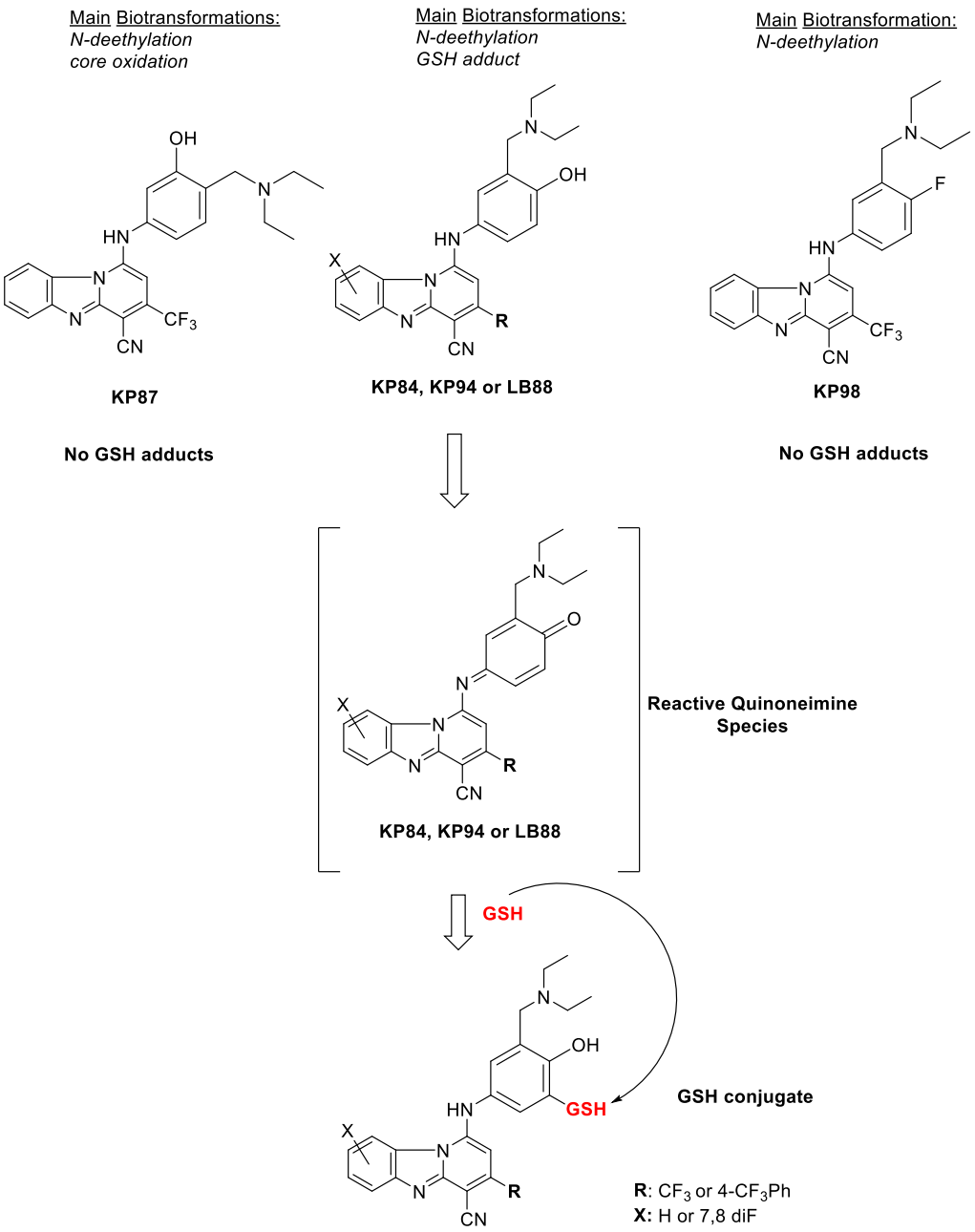

Figure 2.1: Proposed bioactivation of KP84, KP94, and LB88 and their putative conjugation with reduced GSH compared with the non adduct-forming KP87 and KP98

Microsomal metabolic stability and metabolite identification studies performed suggested that the *N*-deethylated metabolite persists in systemic circulation long enough to suppress parasitemia, even after concentration of the parent compound decreased below the therapeutic threshold.[92] Furthermore, formation of a

quinoneimine through a bioactivation pathway was confirmed via glutathione (GSH)-trapping studies performed with compounds **KP84**, **KP94,** and **LB88** (**Figure 2.1**).[92] Additional metabolic pathways such as oxidative quinoneimine formation result in the formation of highly reactive metabolites that are linked to toxic side-effects *in vivo*.[73]

In order to avoid potential issues with quinoneimine formation, Mannich base regio-isomer was developed for **KP87** which resulted in *N*-deethylation and core oxidation as the main biotransformations, without the formation of GSH adducts which implies that the reactive quinoneimine does not form. Similarly, **KP98** did not form any GSH conjugates and the main biotransformation is *N*-deethylation. However, these modifications were detrimental to *in vitro* antiplasmodium activity compared with that of **KP84**, **KP94** and **LB88**.

These findings compelled us to further explore the multi-parameter SARs and structure-property relationships (SPRs) of PBIs. The phenolic Mannich base PBI **KP84** was therefore used as a model hit compound. In this work, the **R**-position was either fixed to the trifluoromethyl group (as in **KP94**, **KP87** and **KP98**) or to a methyl group. The group's extensive experience on the synthesis of various PBI analogues thus informed the choice of scaffold and synthetic methods used in this work.

Without providing a detailed account of the literature, this introduction reflects and builds on aspects of antiplasmodium activity and the merits of phenolic Mannich base-containing PBIs. Synthesis has been divided into construction of the PBI core, preparation of phenolic Mannich base side-chains, and finally the coupling reaction between the PBI core and Mannich base side-chains to afford target compounds. Of note is the SAR studies, which have been split into **SAR-1** and **SAR-2** in this dissertation. In **SAR-1,** the parent compounds and their *N*-dealkylated counterparts were investigated. In this study, the parent compounds contain an *N*,*N*-diethylated terminal amine and their corresponding *N*-deethylated analogues are considered primary metabolites *in vivo*.[92] **SAR-2** was systematically mapped onto **SAR-1** with structural modifications around the PBI core. SAR studies on the phenolic Mannich base-containing PBIs are discussed in detail hereafter.

2.3 Design rationale and SAR development for new Mannich base PBIs

One of the critical challenges in designing phenolic Mannich base PBI analogues was addressing microsomal stability. With this information, two points of SAR were investigated (**Figure 2.2**): (i) **SAR-1**, replacing the **Ar** fragment of **KP84** with various structurally diverse phenolic Mannich base side-chains (with the exception of one analogue which possesses a only a phenolic group) guided by the commercial availability of substituted aminophenols. and (ii) **SAR-2**, introduction of substituents in the PBI core.

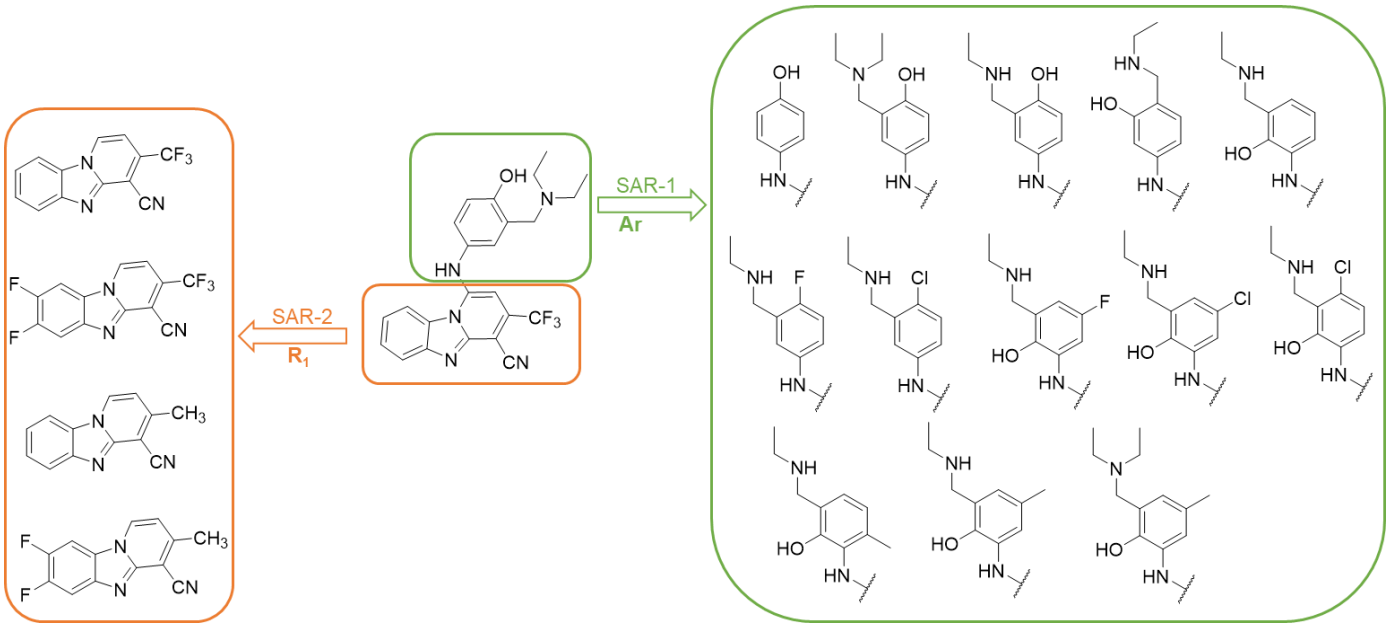

Figure 2.2: Structure activity relationship design of SAR-1 and SAR-2

It should be noted that **SAR-2** was designed as an extension of **SAR-1** and that *N*-dealkylated analogues selected comprised of the Mannich base fragments that gave the most active compounds from **SAR-1**. Selected parent compounds and presumed N-dealkylated metabolites were synthesized and structural modifications made around the PBI core.

2.4 Synthesis and characterization of Mannich base PBIs

The overall procedure for the synthesis of all target compounds in both **SAR-1** and **SAR-2** is shown in **Scheme 2.1.**

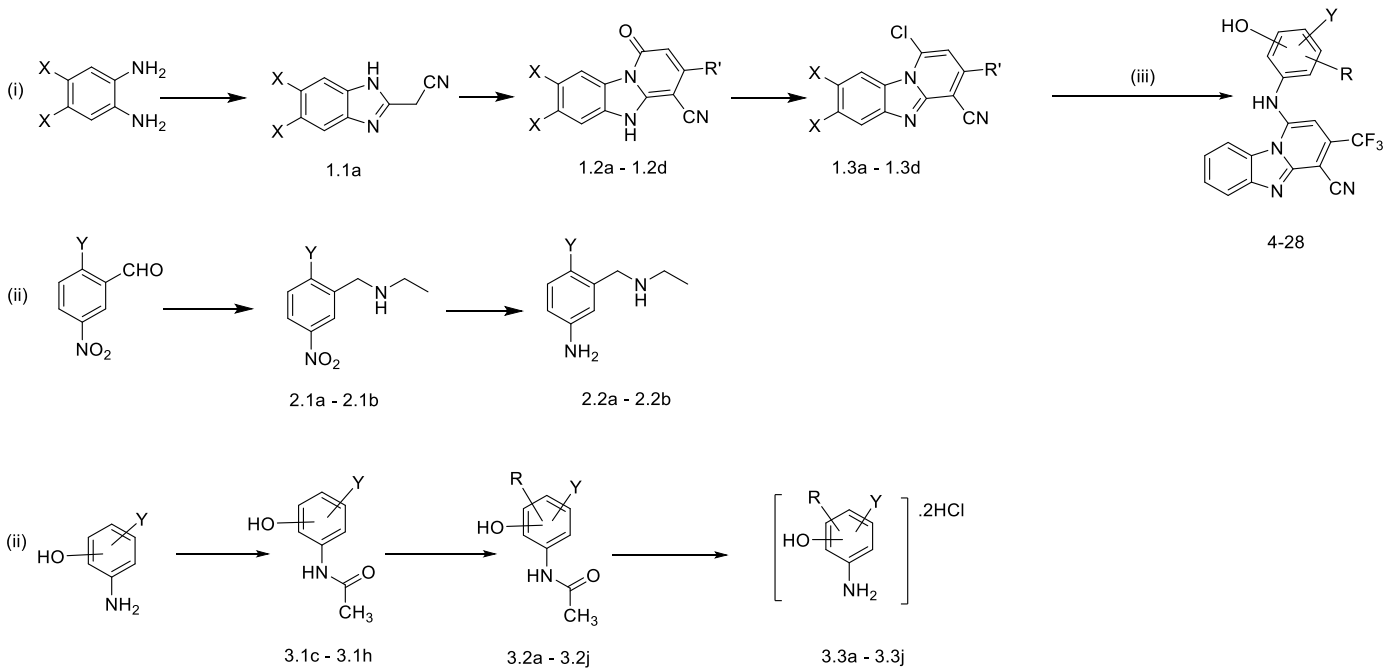

Scheme 2.1: General synthetic protocol for target compounds **4–28**, according to the following steps: (i) synthesis of the pyrido(1,2-*a*)benzimidazole (PBI) core (**1.1–1.3**), (ii) synthesis of free phenolic Mannich base side-chain (**2.1–2.2** and **3.1–3.3**), and (iii) final coupling reaction b

Briefly, substituents mentioned at positions **R'** (CF_3 or CH_3) and **X** (H or F) were introduced during synthesis of the PBI core. Phenolic Mannich base side-chains were synthesized using the two synthetic pathways previously highlighted. Specifically, synthesis of 1,4-halogenated anilines (**2.2a** and **2.2b**) began with commercially available 3-nitrobenzaldehydes. The *N*-dealkylated side-chain was introduced via reductive amination while subsequent reduction of the nitro group furnished the respective aniline necessary for the final coupling reaction. Synthesis of the second phenolic Mannich base side-chain began by protecting substituted aminophenols via an acetylation reaction. Acetylation of the amine is necessary to attenuate its reactivity so that polysubstitution products are avoided during electrophilic aromatic substitution. The **R**-substituent was introduced in a Mannich reaction as either the *N*-dealkylated (proposed metabolite) or diethyl (parent) side-chain specific to the desired phenolic Mannich base intermediates. Finally, deprotection of the aniline nitrogen was

necessary for the final coupling reaction. The final targeted compounds were obtained via a coupling reaction with the appropriate phenolic Mannich base side-chain-containing phenol and PBI core to afford compounds **4-28**.

2.4.1 Synthesis and characterization of the PBI core

The synthesis and characterization of PBI intermediates are shown in **Scheme 2.2**.

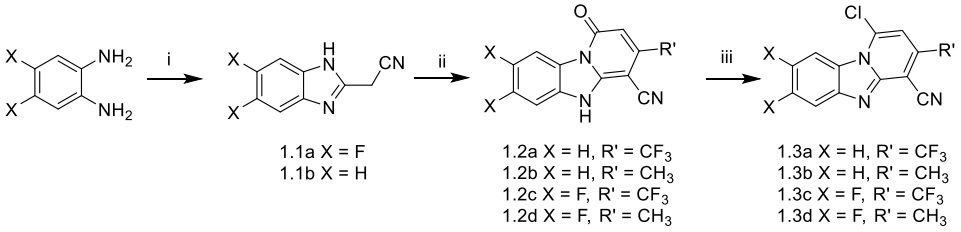

.

Scheme 2.2: General procedure for the synthesis of the PBI core
Reagents and conditions: (i) ethyl-cyanoacetate, dimethylformamide (DMF), 100 °C, 7 h, microwave radiation (MW); (ii) di-keto ester with appropriate R' group, NH_4OAc, 150 °C, 12 h; (iii) $POCl_3$, 120 °C, 12–15 h

In order for the final coupling reaction to occur between the appropriate Mannich base side-chain-containing phenol and the PBI core, a chlorinated PBI intermediate (**1.3a–d**) was synthesized (**Scheme 2.2**). A commercially available unsubstituted benzimidazole acetonitrile was used to synthesize unsubstituted keto-PBI intermediates (**1.2a** and **1.2b**, where **X** = H) whereas synthesis of difluorinated keto-PBI intermediates was achieved using commercially available 4,5-difluorobenzene-1,2-diamine. Briefly, the difluorinated benzimidazole acetonitrile (**1.1a**) was synthesized using 4,5-difluorobenzene-1,2-diamine via cyclization with ethyl cyanoacetate. Keto-PBIs (**1.2a–1.2d**) were achieved via cyclization of commercially available benzimidazole acetonitrile or intermediate **1.1a**. Deoxy-chlorination of intermediates **1.2a–1.2d** was achieved using phosphorous oxychloride ($POCl_3$) to obtain compounds **1.3a–1.3d.** The synthesis and characterization of the PBI core intermediates are detailed here. Details of selected key reaction steps leading to the formation of critical PBI intermediates and the proton nuclear magnetic resonance (^{1}H-NMR) spectroscopic analyses of representative compounds are described here.

Preparation of benzimidazole acetonitrile 1.1a

As previously mentioned, it was necessary to prepare the difluorinated benzimidazole acetonitrile (**1.1a**) as it was not available commercially unlike the unsubstituted benzimidazole acetonitrile. The cyclization reaction used is shown below in **Scheme 2.3**.

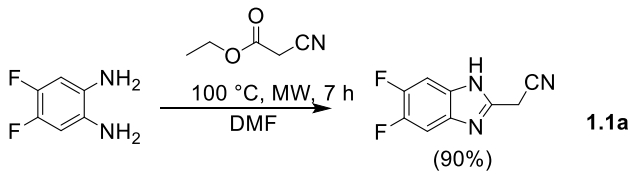

Scheme 2.3: Reaction conditions for the preparation of difluorinated benzimidazole acetonitrile intermediate **1.1a**

The synthesis of 2-(5,6-difluoro-1H-benzo[d]imidazol-2-yl)acetonitrile (**1.1a**) was achieved via cyclization of commercially available 4,5-difluorobenzene-1,2-diamine and ethyl cyanoacetate in *N*,*N*-dimethyl formamide (DMF). The mixture was irradiated under microwave conditions at 100 °C for 7 h for formation of the desired product. A proposed mechanism for the formation of **1.1a** is shown below **(Scheme 2.4).**

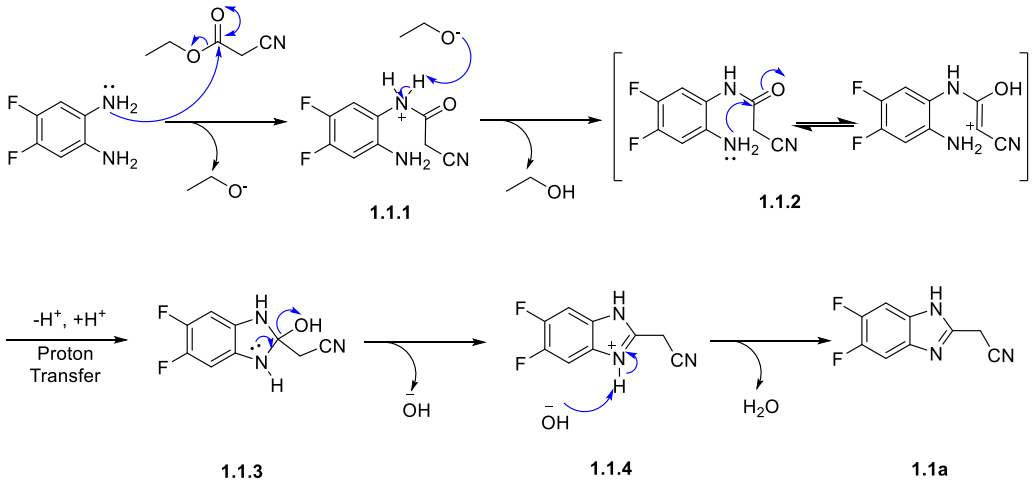

Scheme 2.4: Proposed mechanism of the formation of 2-(1H-benzo[d]imidazole-2-yl)acetonitrile **1.1a**

The formation of **1.1a** began with nucleophilic addition of the amino group to the electrophilic carbonyl carbon of ethyl cyanoacetate (**1.1.1, Scheme 2.4**). The ethoxide leaving group formed subsequently deprotonated the hydrogen of the positively charged nitrogen ion intermediate, resulting in the formation of the amide **1.1.2**. As

shown (**1.1.2, Scheme 2.4**), potential exists for amide iminol tautomerism, however formation of the product that would result in the addition step at the carbon adjacent to the hydroxyl substituent (shown using ***, 1.1.2**, **Scheme 2.4**) was not observed. The intramolecular nucleophilic addition at the amide carbonyl leads to ring closure, and subsequent iminol formation and dehydration resulted in the formation of 2-(5,6-difluoro-1H-benzo[d]imidazol-2-yl)acetonitrile (**1.1a**). To confirm the success of the cyclization reaction, ^{1}H-NMR analysis of **1.1a** was performed (**Figure 2.3**).

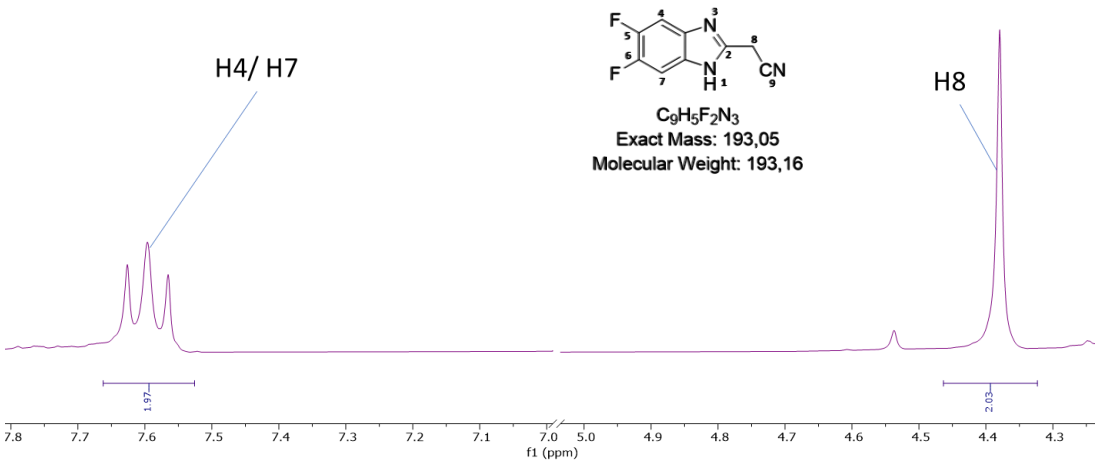

Figure 2.3: ^{1}H-NMR (DMSO-d_6, 400 MHz) spectrum of **1.1a**

The difluorinated benzimidazole diagnostic peaks for **1.1a** showed characteristic splitting patterns and *J* coupling constants. A doublet of doublets integrating for two protons at δ 7.59 ppm, which looks like a triplet, was observed for protons **H4** and **H7**. The splitting pattern was attributed to ortho and meta coupling to the fluorine atoms at positions **C5** and **C6** with respect to protons **H4** and **H7.** Considering the symmetry of the molecule, the chemical environment surrounding **H4** and **H7** is identical due to tautomerism of the NH hydrogen with the other nitrogen. The remaining singlet at δ 4.38 ppm integrates for 2 protons, confirming successful cyclization, and was assigned to **H8**.

Mass analysis of compound **1.1a** was performed using ESI in the positive mode (ESI^{+}). The parent peak revealed an *m*/z of 194.1 $[M+H]^{+}$, which was corroborated with the

calculated mass for $C_9H_5F_2N_3$ (193.05)**.** Having successfully obtained intermediate **1.1a,** a second cyclization reaction was performed to obtain keto-PBIs **1.2a–1.2d** from **1.1a** or the commercially available benzimidazole acetonitrile.

Synthesis of keto-PBI intermediates

The general cyclization procedure used to afford keto-PBI intermediates is shown in **Scheme 2.5**.

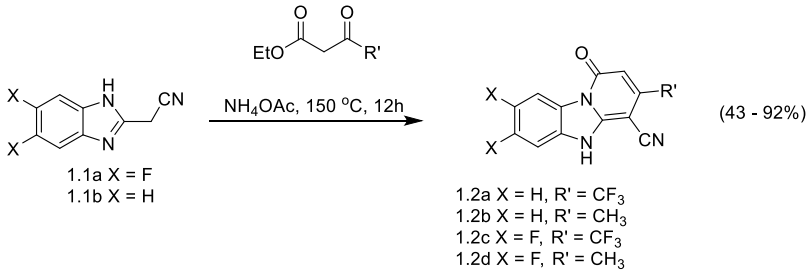

Scheme 2.5: General cyclization procedure used to afford keto-PBI intermediates **1.2a–1.2d**

Synthesis of keto-PBI intermediates **1.2a–1.2d** was achieved via cyclization with either **1.1a** or commercially available 2-benzimidazole acetonitrile (**1.1b**) and the appropriate diketo-ester in the presence of NH_4OAc at 150 °C for 12 h. The formation of the keto-PBI intermediate **1.2b** via cyclization of 2-benzimidazole acetonitrile with ethyl 3-oxobutanoate is outlined in **Scheme 2.6**.

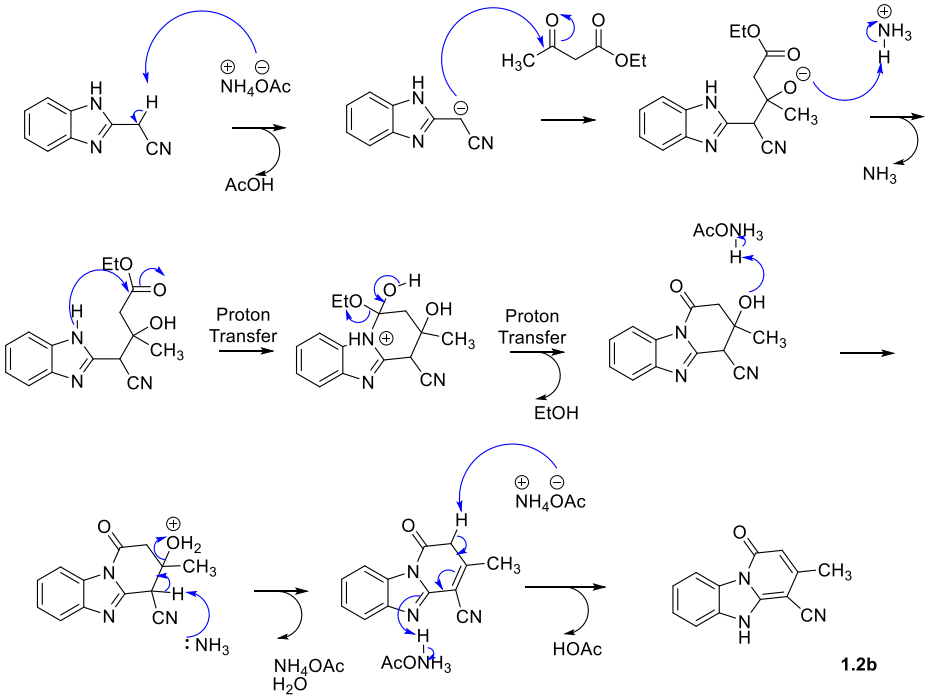

Scheme 2.6: Proposed method of cyclization to keto-intermediate **1.2b** from 2-benzimidazole acetonitrile with ethyl 3-oxobutanoate

The reaction proceeds via deprotonation of the α-proton to the CN group by the basic ($^{-}$OAc) to form a carbanion. The carbanion attacks the carbonyl centre of 3-oxobutanoate, and this is followed by protonation of the oxygen anion to a hydroxyl group by NH_4OAc. A second addition reaction occurs at the carbonyl centre of ethyl 3-oxobutanoate by the nucleophilic nitrogen of the benzimidazole acetonitrile. This subsequently causes an intramolecular proton transfer. Internal cyclization is achieved by elimination of ethanol as a result of the proton transfer during formation of the keto-PBI intermediate.

A second protonation of the OH group mediated by NH_4OAc, which converts the hydroxy to a better leaving group occurs. Proton abstraction from the α-hydrogen to the carbonyl group is facilitated by NH_4OAc to afford **1.2b**. In order to confirm the success of the cyclization reaction, ^{1}H-NMR analysis of **1.2b** was performed (**Figure 2.4**). The diagnostic peaks include the absence of an aromatic proton signal corresponding to the **C4** position due to the CH_2 protons similar to those in intermediate 1.1a. Furthermore, the singlet at δ 5.55 ppm integrating for a single proton corresponding to **H2** supported the formation of a new aromatic ring. Cyclization of the benzimidazole scaffold to a PBI resulted in a loss of symmetry in the molecule and was evident with respect to the aromatic protons **H7–H10**. The rest of the aromatic signals were observed as a doublet (J = 8.0 Hz) and a triplet (J = 7.6 Hz), each integrating for one proton. **H10** was assigned to a doublet at δ 8.49 ppm because of its high down-field chemical shift relating to the lack of electron density attributed to the tertiary amide of the imidazole. The **H7** proton was assigned to a doublet at δ 7.48 ppm. Finally, two remaining aromatic signals were observed as triplets at δ 7.33 ppm (J = 7.6 Hz) and at δ 7.12 ppm (J = 7.6 Hz), corresponding to **H9** and **H8,** respectively. An additional singlet corresponding to the methyl peak at δ 2.31 ppm integrating for three protons also confirmed the presence of **H13**. The ^{1}H-NMR data were backed-up by the ^{13}C-NMR results for **1.2b** (**Figure 2.5**).

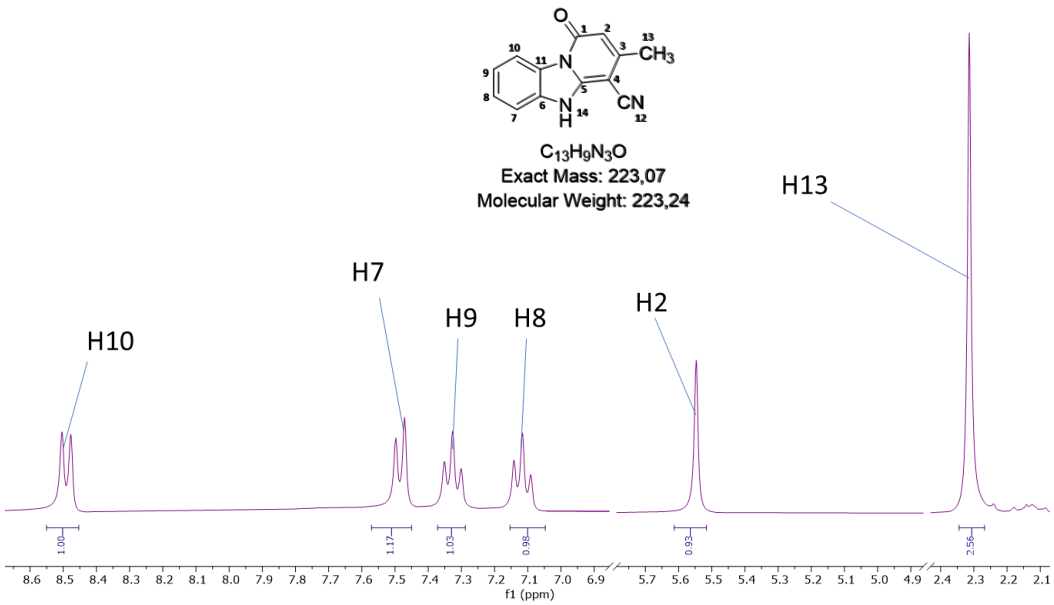

Figure 2.4: ^{1}H-NMR (DMSO-d_6, 400 MHz) spectrum of **1.2b**

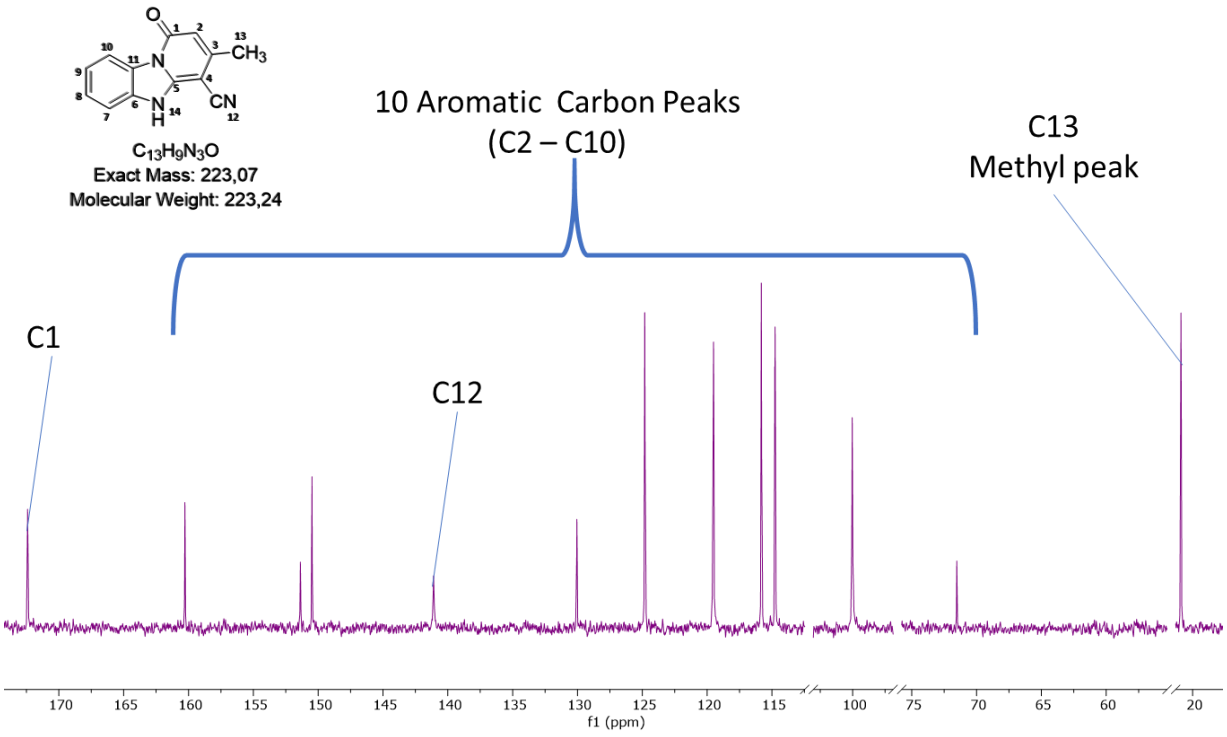

Figure 2.5: ^{13}C-NMR (DMSO-d_6, 151 MHz) spectrum of **1.2b**

The ^{13}C-NMR spectrum for **1.2b** is shown in **Figure 2.5** and peaks were assigned using diagnostic peaks identified in the ^{13}C-NMR spectrum. These diagnostic features include the appearance of two carbon signals attributed to the carbonyl peak corresponding to **C1** at δ 172.41 ppm and the methyl peak at δ 20.90 ppm corresponding to **C13**. The remaining peaks were assigned to 10 aromatic carbons corresponding to **C2–C10** as well as the CN peak at δ 141.10 corresponding to **C12,** further supporting the success of the cyclization reaction to form **1.2b**. The LC-MS (ESI$^+$) analysis of compound **1.2b** indicated a chemical purity of 94% (254 nm) and retention time of 2.36 min. The parent peak showed an *m*/z value of 224.2 $[M+H]^+$, which was found to corroborate the calculated mass for $C_{13}H_9N_3O$ (223.07).

Having successfully synthesized keto-PBI intermediates (**1.2a–1.2d**), chlorinated PBIs necessary for the final *N*-arylation coupling reaction were prepared via deoxy-chlorination using $POCl_3$ **(Scheme 2.7)**.

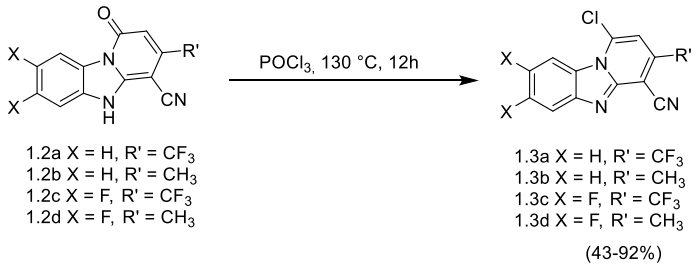

Scheme 2.7: General procedure for the deoxy-chlorination reaction used to afford chlorinated PBIs **1.3a–1.3d**

The synthesis of chlorinated PBIs **1.3a–1.3d** (**Scheme 2.7**) was achieved by treating **1.2a–1.2d** with $POCl_3$ at 130 °C for 12 h. The proposed reaction mechanism and characterization of chlorination is exemplified using compound **1.3b** (**Scheme 2.8**).

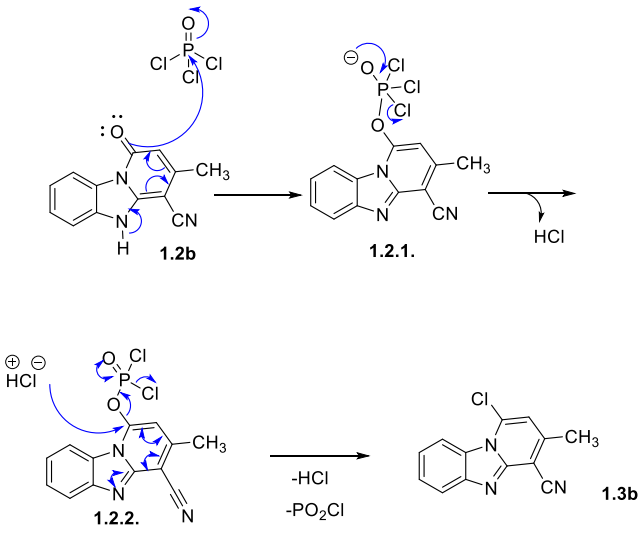

Scheme 2.8: Proposed method of deoxy-chlorination to form chloro-intermediate PBI **1.3b**

Formation of the chlorinated PBI intermediate **1.3b** using $POCl_3$ is shown in **Scheme 2.8**. The reaction is driven by the nucleophilic addition of electrons from the keto-oxygen to the phosphorous centre which forms an irreversible O-P bond by addition-elimination to $POCl_3$, which results in free Cl^- release in solution (**Scheme 2.8: 1.2.1)**. The chloride anion attacks the electrophilic carbon of the phosphonate ester in an aromatic nucleophilic substitution reaction to afford compound **1.3b** with release of PO_2Cl and Cl^-, which further drives the reaction.

The ^{1}H-NMR spectrum for keto-PBI intermediate **1.2b** overlaid with that of chlorinated PBI intermediate **1.3b** is shown in **Figure 2.6**.

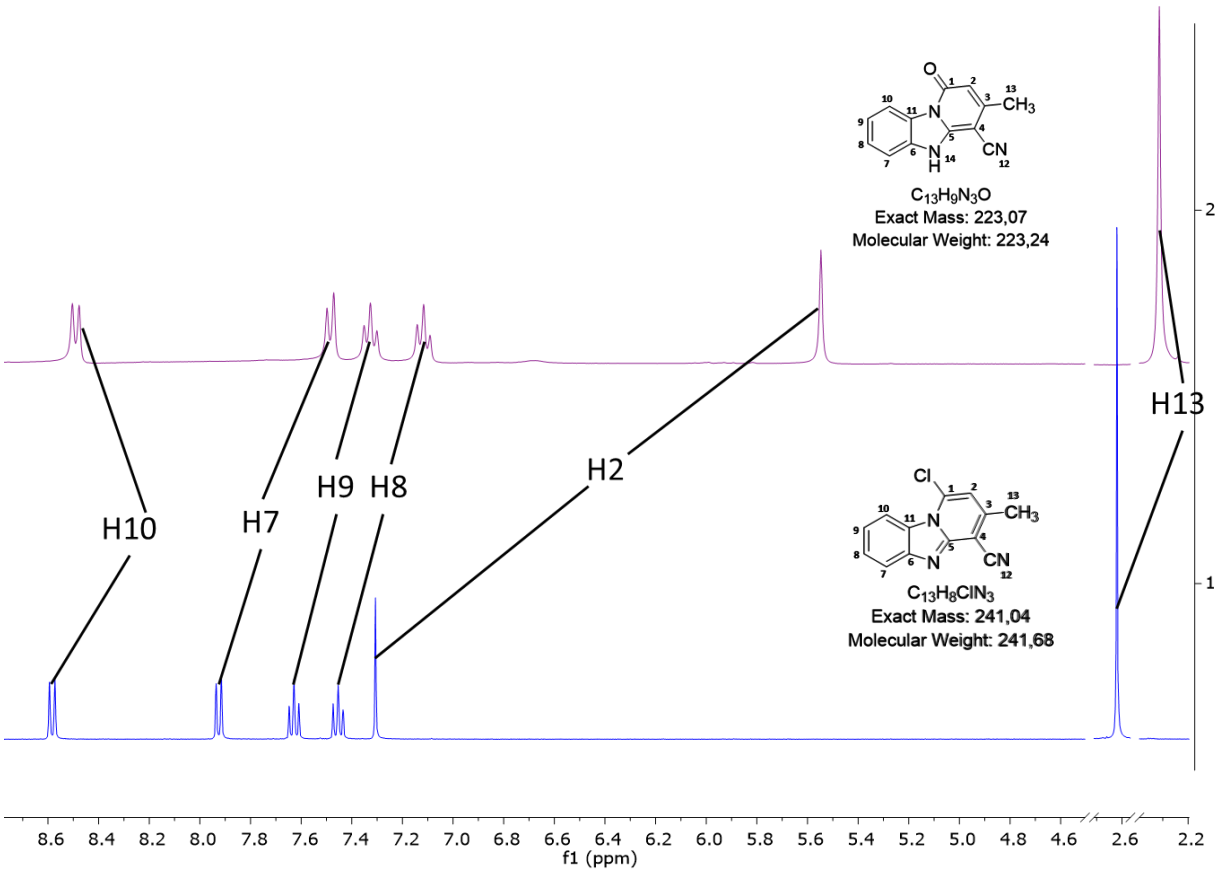

Figure 2.6: ^{1}H-NMR (DMSO-d_6, 400 MHz) spectrum of **1.2b** (top) and **1.3b** (bottom), stacked to show corresponding PBI intermediate peaks

^{1}H-NMR patterns indicating successful chlorination were readily observed in the downfield shift of **H2** to a higher frequency compared to that in **1.2b** (**Figure 2.6**), which was observed as a singlet integrating for one proton at δ 7.31 ppm. The remaining aromatic peaks identified for **1.2b** are observed in the ^{1}H-NMR spectrum for **1.3b** (**Figure 2.6**).

The ^{13}C-NMR spectrum for **1.3b** (**Figure 2.7**) further validates the success of the deoxy-chlorination reaction. Formation of **1.3b** was confirmed by the absence of a carbonyl signal in the region of 150–180 ppm. Furthermore, there are 12 carbon peaks in the aromatic region corresponding to **C1-C12** and a peak at 20.68 ppm corresponding to the methyl carbon **C13**, which are the peaks expected for intermediate **1.3b**.

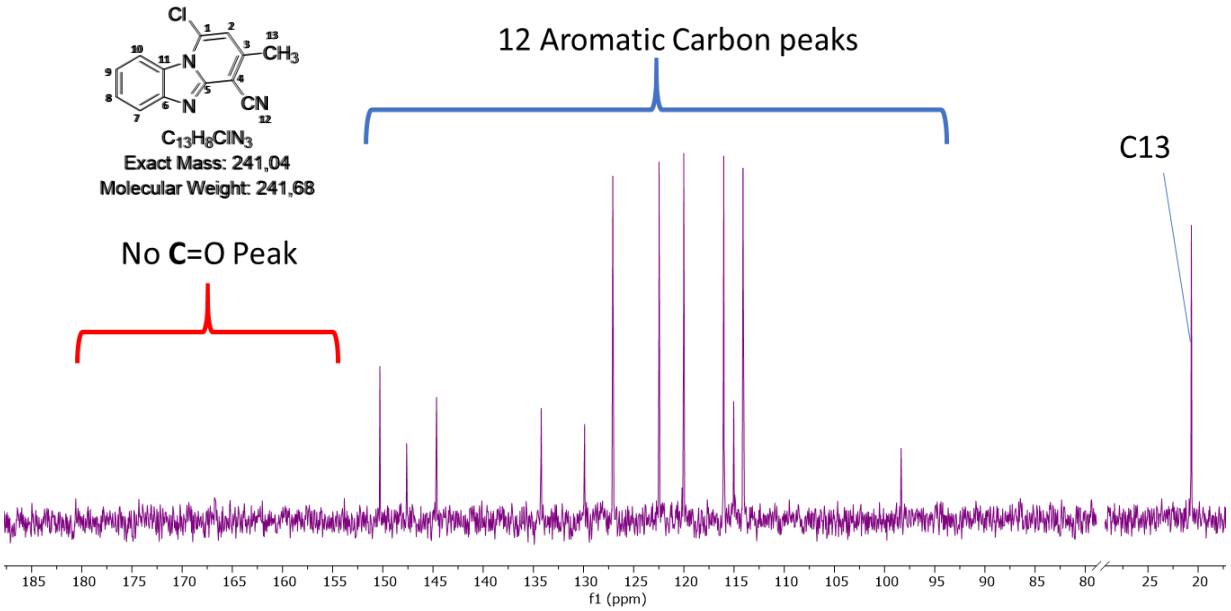

Figure 2.7: ^{13}C-NMR (DMSO-d_6, 151 MHz) spectrum of **1.3b**

Mass analysis was done using ESI$^+$. The parent peak indicated an *m*/z of 242.7 $[M+H]^+$, which was found to corroborate the calculated mass for $C_{13}H_8ClN_3$ (241.68)**.** Having successfully synthesized chlorinated PBIs (**1.3a–1.3d**), these intermediates were used in subsequent coupling reactions with synthesized Mannich base side-chain-containing phenols.

2.4.2 Synthesis of phenolic Mannich base side-chains

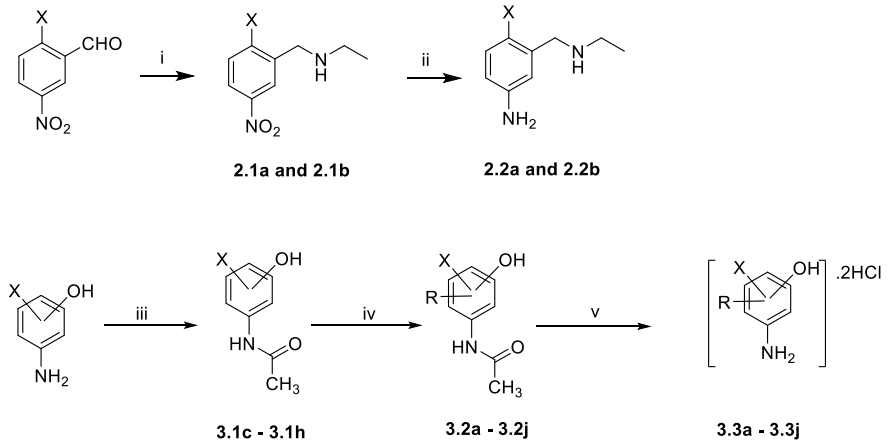

Scheme 2.9: General synthetic route for the production of Mannich base side-chains

Mannich base intermediates were synthesized using two distinct pathways (**Scheme 2.9**): (i) 3-nitrobenzaldehydes were subjected to reductive amination in the presence

of ethylamine to afford intermediates 2.1a and 2.1b, and (ii) use of amine-protected aminophenols with acetic anhydride to form acetamides **3.1c–3.1h**. A Mannich reaction was then used to form substituents designated as **R**-groups in **3.2a–3.2j**. Deprotection of acetamides was achieved using 6 M aqueous hydrogen chloride solution in to afford intermediates **3.3a–3.3j** as HCl salts. The detailed synthesis and characterization of Mannich base side-chains as well as key intermediates along with ^{1}H-NMR spectroscopy analyses of representative compounds are described below.

Reductive amination reaction

Reductive amination was used to introduce the appropriate **R** substituent for intermediates **2.1a** and **2.1b** (**Scheme 2.10**) and was performed using the commercially available nitrobenzaldehydes 2-fluoro-5-nitrobenzaldehyde and 2-chloro-5-nitrobenzaldehyde to obtain amino-alkylated intermediates **2.1a** and **2.1b,** respectively. .

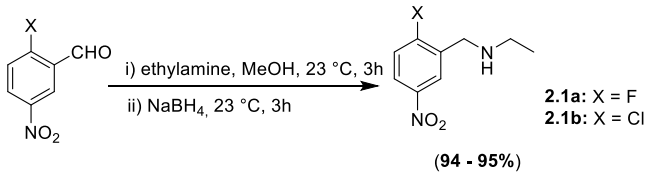

Scheme 2.10: General procedure for the reductive amination reaction used to afford amino-alkylated intermediates **2.1a-2.1b**

The proposed reaction mechanism for the reductive amination of compound **2.1b** is shown in **Scheme 2.11**.[94] The reaction begins with the nucleophilic attack of the primary amine at the electrophilic carbonyl carbon in a protic solvent to form a tetrahedral transition-state intermediate. The protic solvent acts as a proton source and stabilizes the tetrahedral transition state. Nucleophilic addition of the amine group in the first step results in hydroxyl formation and subsequent proton transfer enables an iminol-dehydration process. This results in the loss of a water molecule and formation of the imine intermediate. The imine nitrogen coordinates to a vacant boron orbital and this coordination subsequently encourages the release of a hydride ion from sodium borohydride in a concerted transition state. The hydride adds to the electrophilic carbon of the imine intermediate whilst the pi-electrons of the imine bond

add to the vacant boron orbital forming a N-B bond. The N-B bond is broken due to protonation by methanol which causes the subsequent release of BH_3 and the desired intermediate **2.1b**. The success of the reductive amination reaction for compound **2.1b** was checked by ^{1}H-NMR (**Figure 2.8**).

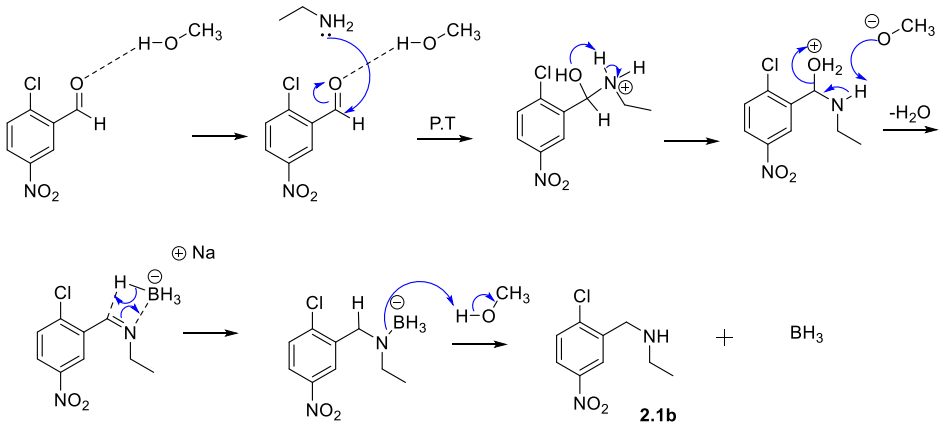

Scheme 2.11: Proposed mechanism for the reductive amination reaction used to afford **2.1b**

An illustrative example for all reductive amination reactions is shown in the ^{1}H-NMR spectrum for compound **2.1b** (**Figure 2.8**). Diagnostic peaks for successful reductive amination were new proton peaks corresponding to the ethylamine substituent and methylene carbon spacer. Ethylamine peaks (**H7, N-H, H8**, and **H9**) are shown as a broad **N-H** singlet at δ 4.81 ppm integrating for a single proton, another singlet integrating for two protons at δ 3.94 ppm corresponding to **H7**, a quartet at δ 2.72 ppm (J = 7.2 Hz) integrating for two protons corresponding to **H8,** and a triplet integrating for three protons at δ 1.19 ppm (J = 7.2 Hz) corresponding to **H9**. The aromatic region peaks displayed a doublet at δ 8.38 ppm (J = 2.8 Hz), showing meta coupling between **H6** and **H2** protons. A doublet of doublets integrating for one proton at δ 8.11 ppm was assigned to **H6** because of **H5** ortho (J = 8.7 Hz) and **H2** meta coupling (J = 2.8 Hz) constants. **H5** was represented by a doublet at δ 7.63 ppm (J = 8.8 Hz) integrating for a single proton. To further support these assignments, ^{13}C-NMR was performed for **2.1b** (**Figure 2.9**).

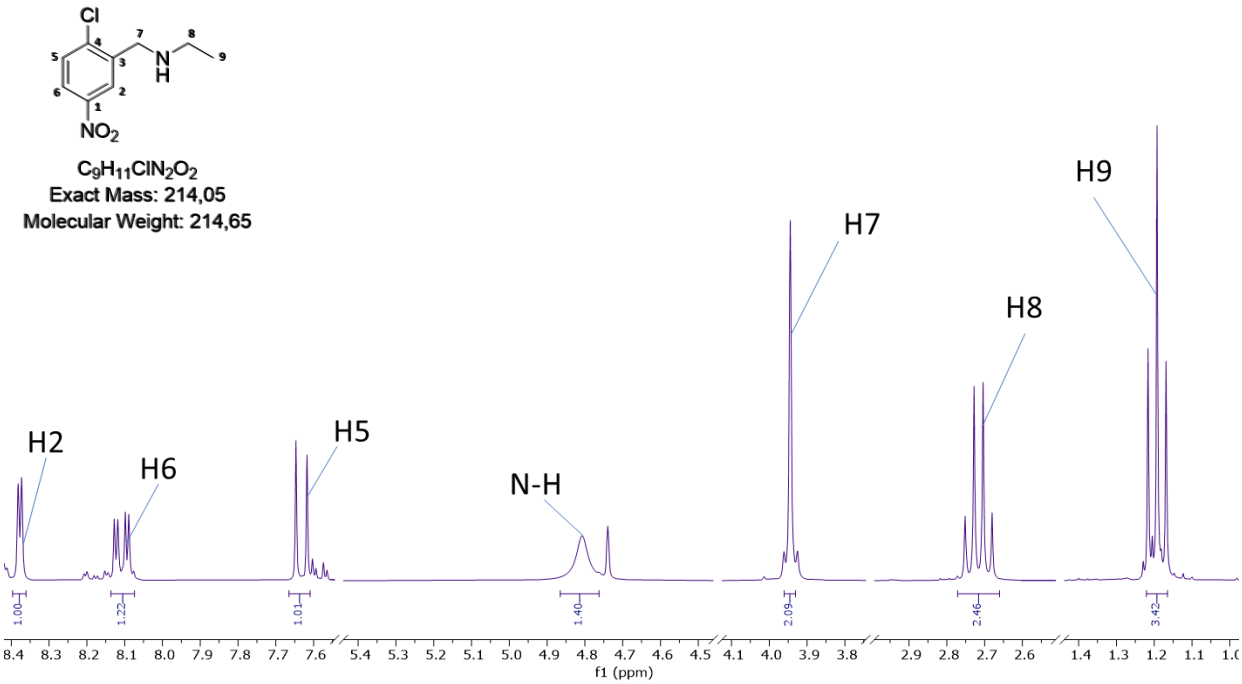

Figure 2.8: ^{1}H-NMR (MeOD-d_4, 400 MHz) spectrum of **2.1b**

The ^{13}C-NMR spectrum for compound **2.1b** is shown in **Figure 2.9**. Diagnostic signals of **2.1b** confirming successful completion of the reductive amination reaction include the appearance of three new signals in the aliphatic region corresponding to **C7–C9**. These peaks are attributed to the ethylamine chain and methylene linker, thus confirming the successful transformation expected in the reductive amination reaction. Furthermore, six aromatic peaks corresponding to **C1–C6** of the substituted benzene ring were observed.

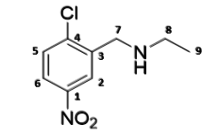

$C_9H_{11}ClN_2O_2$
Exact Mass: 214,05
Molecular Weight: 214,65

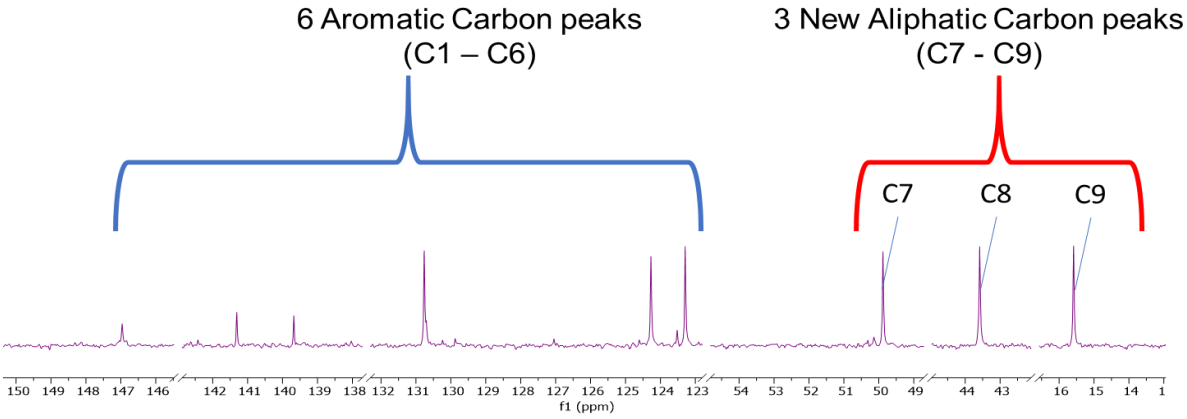

Figure 2.9: ^{13}C-NMR (MeOD-d_4, 151 MHz) spectrum of **2.1b**

Mass analysis of compound **2.1b** was performed using ESI^+. The parent peak indicated an *m*/z of 215.3 $[M+H]^+$, which was obtained to corroborate the calculated mass for $C_9H_{11}ClN_2O_2$ (214.05). Having successfully synthesized the amino-alkylated nitrobenzene intermediates **2.1a** and **2.1b**, these were subjected to tin(II) chloride reduction to reduce the nitro group to a primary amine. This is necessary for the final coupling reaction between the Mannich base inputs and chlorinated PBI intermediates **1.3a–1.3d** as final coupling relies on the presence of a nucleophilic primary amine.

Tin(II) chloride nitro reduction to primary amine

Reduction of the nitro group in compounds **2.1a** and **2.1b** to the primary amine was achieved using Sn(II)Cl in tetrahydrofuran (THF) in the presence of 1 M HCl aqueous solution (**Scheme 2.12**). To confirm the success of the reduction reaction, ^{1}H-NMR spectra were recorded for each compound and **2.2b** will be used as a representative compound for discussion.

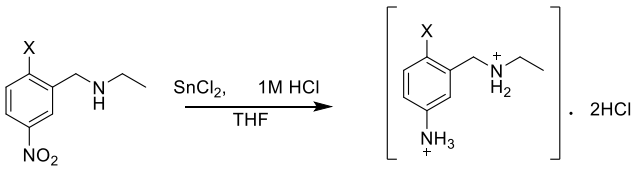

2.1a, X = F
2.1b, X = Cl

2.2a, X = F
2.2b, X = Cl

(91 - 95%)

Scheme 2.12: General procedure for tin(II) chloride reduction from a nitro to a primary amine to afford **2.2a** and **2.2b**

The ^{1}H-NMR spectrum of compound **2.2b** is shown in **Figure 2.10**. One distinct change following the transformation of **2.1b** to **2.2b** was a upfield chemical shift in aromatic protons, which occurred as a result of the presence of the electron-donating NH_2 substituent compared to the electron-withdrawing nitro group in **2.1b**. Protons situated ortho to the NH_2 substituent show a downfield shift compared to **2.1b**, as exemplified by **H2** and **H6** appearing as a doublet at δ 6.75 (J = 2.8 Hz) and a doublet of doublets at δ 6.62 (J = 8.5, 2.8 Hz), each integrating for a single proton. **H5** showed almost no downfield shift as a doublet integrating for a single proton at δ 7.09 (J = 8.4 Hz) compared to that in **2.1b,** which is expected for meta substituents to electron-donating groups. The remaining peaks included a singlet integrating for two protons at δ 3.75 ppm corresponding to **H7**, a quartet integrating for two protons at δ 2.66 ppm (J = 7.2 Hz) corresponding to **H8**, and a triplet integrating for three protons at δ 1.15 ppm (J = 7.1 Hz) corresponding to **H9**. It is also important to note the water peak observed in the solvent, which resulted in the exchange of NH_2 protons.

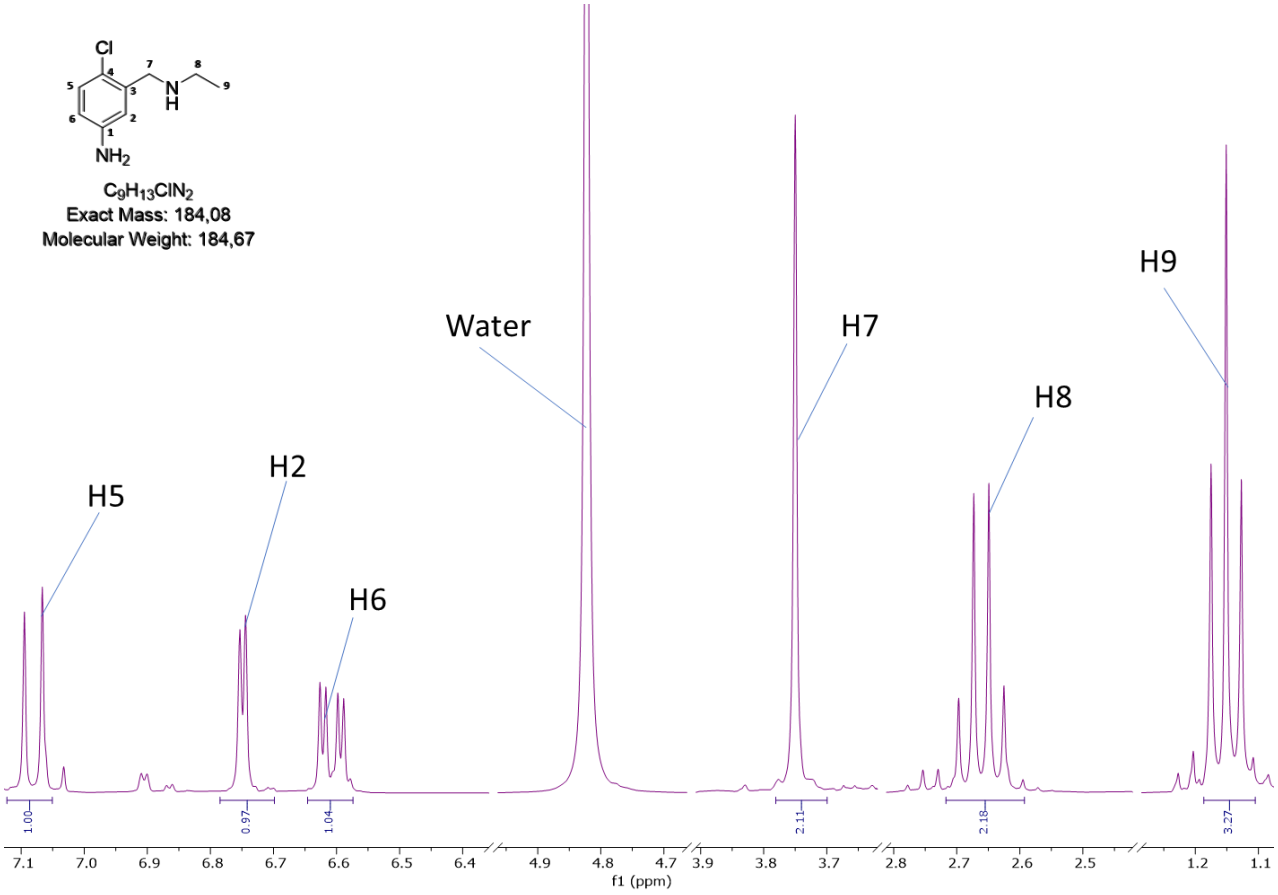

Figure 2.10: ^{1}H-NMR (DMSO-d_6, 400 MHz) spectrum of **2.2b**

Mass analysis for compound **2.2b** was performed using ESI^+ and the parent peak indicated an *m*/z of 185.1 $[M+H]^+$, which was obtained to corroborate the calculated mass for $C_9H_{13}ClN_2$ (184.08)**.**

Having successfully obtained the halogenated Mannich base intermediates **2.2a** and **2.2b,** the last remaining step to produce the final compounds was a final coupling reaction with chlorinated PBI intermediate **1.3a**. The second route for synthesizing Mannich base side-chain inputs involved a Mannich reaction following an acetylation protection reaction and finally a deacetylation reaction. Details of these reactions follow here.

Formation of acetamides from aminophenol intermediates

Acetylation using acetic anhydride was performed to protect the free amine of aminophenols to obtain intermediates **3.1c**–**3.1h** (**Scheme 2.13**). The compounds were isolated in high yields and progressed without further purification.

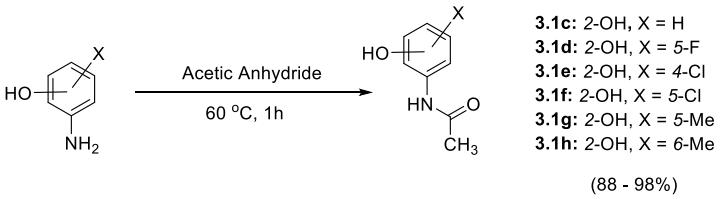

Scheme 2.13: General procedure for the formation of acetamide intermediates **3.1c–3.1h** from commercially available aminophenols

Intermediate compound **3.1e** will be used as an illustrative example (**Figure 2.11**) for the acetylation reaction. Diagnostic features of the ^{1}H-NMR spectrum of **3.1e** include a signal arising from introduction of a methyl group. The methyl peak was assigned as a singlet at δ 2.18 ppm, which integrates for three protons and corresponds to **H8**. The remaining peaks are a doublet integrating for a single proton at δ 7.66 ppm (J = 8.6 Hz) corresponding to **H6**, a doublet at δ 6.87 ppm (J = 2.3 Hz) integrating for a single proton corresponding to **H3,** and the final peak appearing at δ 6.81 ppm as a doublet of doublets (J = 8.6, 2.3 Hz) integrating for a single proton corresponding to **H5**.

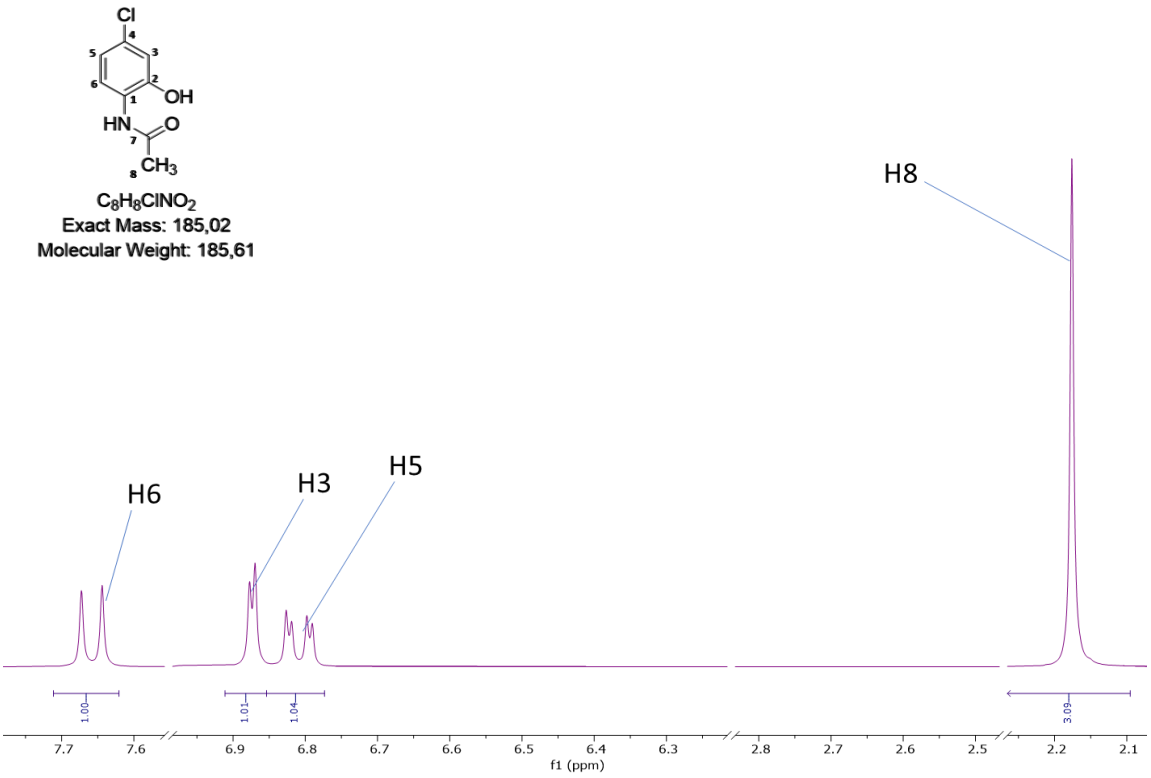

Figure 2.11: ^{1}H-NMR (DMSO-d_6, 400 MHz) spectrum of **3.1e**

Diagnostic features of the ^{13}C-NMR spectrum for **3.1e** (**Figure 2.12**) include the appearance of two new carbon signals corresponding to a carbonyl carbon and a methyl group. These peaks were assigned at δ 24.09 ppm, corresponding to **C8,** and the carbonyl carbon peak at δ 169.41 ppm corresponding to **C7**. The remaining signals for six aromatic carbons are also shown below.

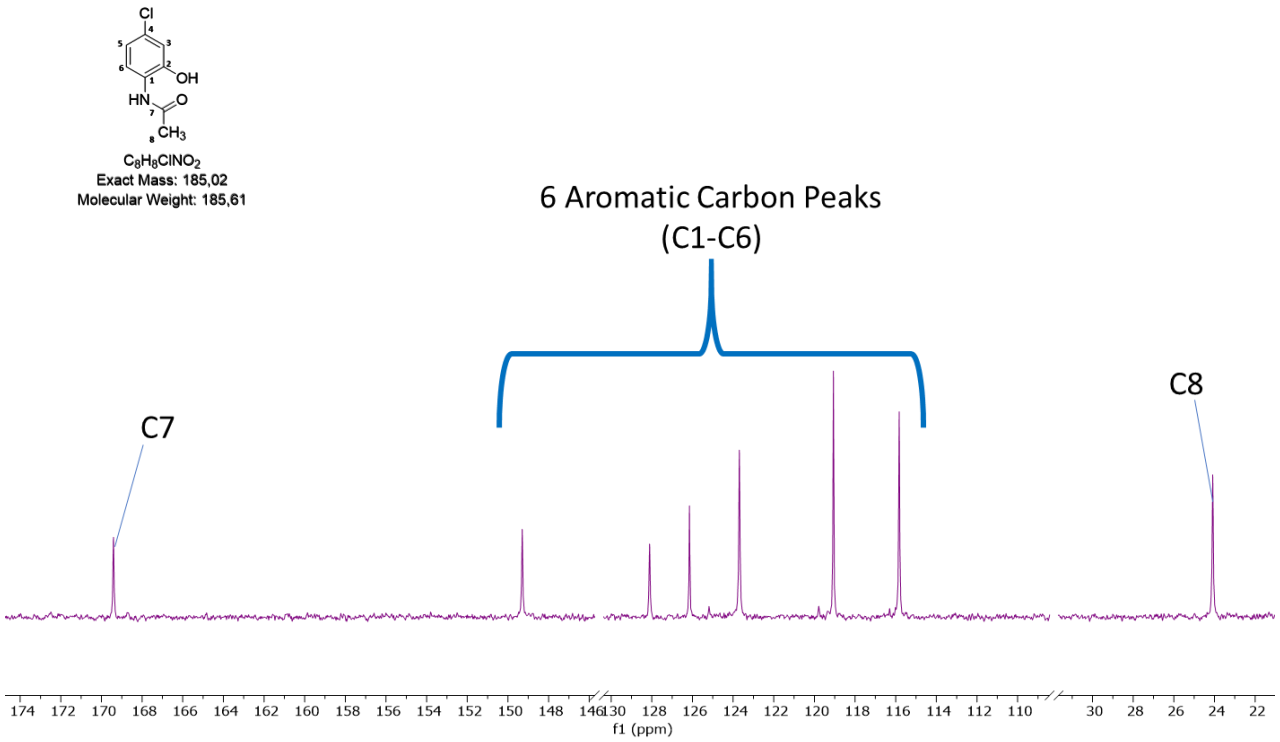

Figure 2.12: ^{13}C-NMR (DMSO-d_6, 151 MHz) spectrum of **3.1e**

Mass analysis for compound **3.1e** was performed using ESI$^+$. The parent peak indicated an *m*/z of 186.2 $[M+H]^+$, which was obtained to corroborate the calculated mass for $C_8H_8ClNO_2$ (185.02)**.**

Having successfully obtained acetamides **3.1c–3.1h**, the Mannich reaction was performed. Details of the Mannich reaction follow.

Mannich reaction to afford amino-alkylated intermediates

The general procedure used to synthesize amino-alkylated Mannich base intermediates **3.2a–3.2j** is shown in **Scheme 2.14.** Synthesis began using synthesized acetamides **3.1c–3.1h** or commercially available acetamides. The Mannich reaction was performed using formaldehyde and ethylamine or diethylamine depending on the desired amino-alkyl substituent (**R**-group). Yields of isolated intermediates **3.2a–3.2j**

ranged from low to high. The lower yields obtained resulted from nucleophilic promiscuity, which is a mechanistic liability of the Mannich reaction. The electrophilic aromatic substitution step (**Scheme 2.15**) proceeds both at the ortho and para positions relative to the hydroxy substituent of the protected aminophenol. For intermediates in which the para position bears a substituent, higher yields were observed. Intermediate **3.2f** is used as an illustrative example for the Mannich reaction in **Scheme 2.15**.

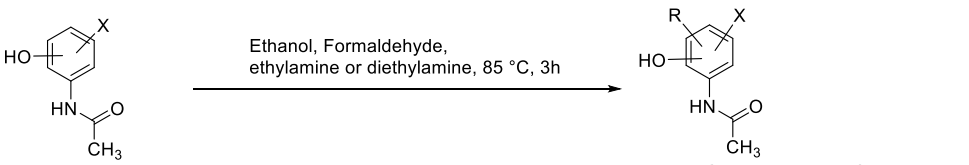

3.1c: 2-OH, X = H
3.1d: 2-OH, X = 5-F
3.1e: 2-OH, X = 4-Cl
3.1f: 2-OH, X = 5-Cl
3.1g: 2-OH, X = 5-Me
3.1h: 2-OH, X = 6-Me

3.2a: 4-OH, X = H, R = 3-CH_2NHEt
3.2b: 3-OH, X = H, R = 4-CH_2NHEt
3.2c: 2-OH, X = H, R = 3-CH_2NHEt
3.2d: 2-OH, X = 5-F, R = 3-CH_2NHEt
3.2e: 2-OH, X = 4-Cl, R = 3-CH_2NHEt
3.2f: 2-OH, X = 5-Cl, R = 3-CH_2NHEt
3.2g: 2-OH, X = 5-Me, R = 3-CH_2NHEt
3.2h: 2-OH, X = 6-Me, R = 3-CH_2NHEt
3.2i: 4-OH, X = H, R = 3-$CH_2N(Et)_2$
3.2j: 2-OH, X = 5-Me, R = 3-$CH_2N(Et)_2$
(8 - 83%)

Scheme 2.14**:** General procedure for the Mannich reaction used to synthesise amino-alkylated intermediates **3.2a-3.2j**

The proposed mechanism of the Mannich reaction used to convert compound **3.1f** to the amino-alkylated intermediate **3.2f** is represented in **Scheme 2.15**. This reaction relies on formation of the carbocation intermediate via nucleophilic addition of the ethylamine nitrogen at the electrophilic carbonyl of formaldehyde. The carbocation is quenched by the electrophilic aromatic substitution reaction which proceeds via Wheland intermediate, followed by re-aromatization of the molecule to afford **3.2f**. To confirm the success of the Mannich reaction, ^{1}H-NMR analysis of **3.2f** was performed (**Figure 2.13**).

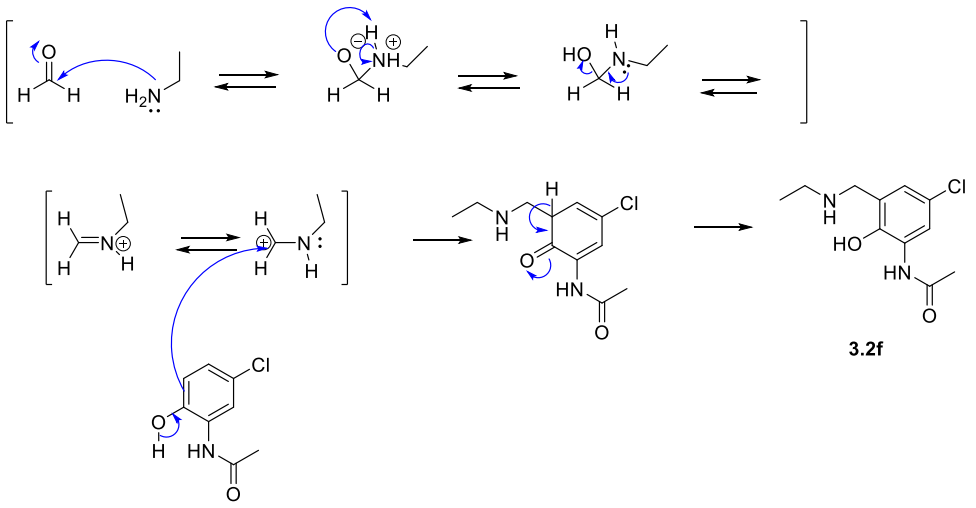

Scheme 2.15: Proposed mechanism of the Mannich reaction used to afford compound **3.2f**

The diagnostic shifts indicating the successful transformation of **3.1f** to intermediate **3.2f** include signals arising from addition of the ethylamine protons and methylene linker. These peaks are clearly seen in **Figure 2.13** and were assigned as a singlet at δ 3.91 ppm integrating for two protons corresponding to the methylene linker **H7**. The remaining diagnostic ethylamine peaks appear as a quartet at δ 2.60 ppm (*J* = 7.2 Hz) integrating for two protons corresponding to **H8,** and a triplet at δ 1.08 ppm (*J* = 7.3 Hz) integrating for 3 protons corresponding to **H9**. Another diagnostic feature is the loss of an aromatic proton at the **C3** position of **3.1f**. There are two aromatic signals which appear as two doublets at δ 7.94 ppm (*J* = 2.7 Hz) and δ 6.81 ppm (*J* = 2.7 Hz), both integrating for single protons corresponding to **H6** and **H4** respectively. The final peak for this intermediate is the appearance of a singlet at δ 2.10 ppm, integrating for three protons corresponding to the C(O)C**H**$_3$ peak of **H11**. To further confirm the success of the Mannich reaction, ^{13}C-NMR analysis was performed for **3.2f** as shown in **Figure 2.14**

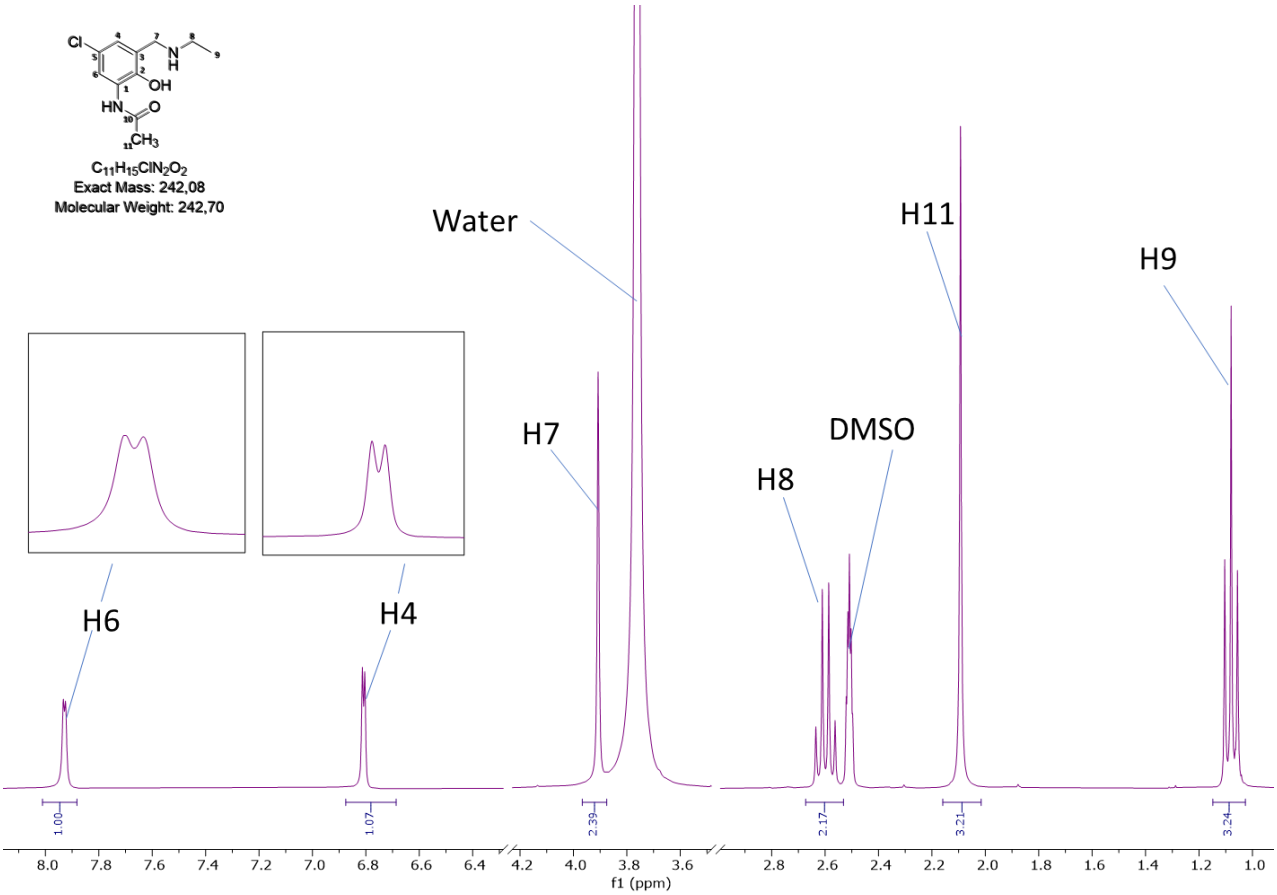

Figure 2.13: ^{1}H-NMR (DMSO-d_6, 400 MHz) spectrum of **3.2f**

Diagnostic features of the ^{13}C-NMR spectrum include the appearance of three new carbon signals corresponding to the ethylamine chain and methylene linker. These peaks are clearly seen at δ 14.35 ppm corresponding to **C9,** δ 42.32 ppm corresponding to **C8**, and δ 50.88 ppm corresponding to **C7**. The remaining peaks corresponding to **C10** and **C11** are shown in **Figure 2.14** as well as the remaining six aromatic carbons.

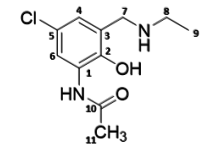

$C_{11}H_{15}ClN_2O_2$
Exact Mass: 242,08
Molecular Weight: 242,70

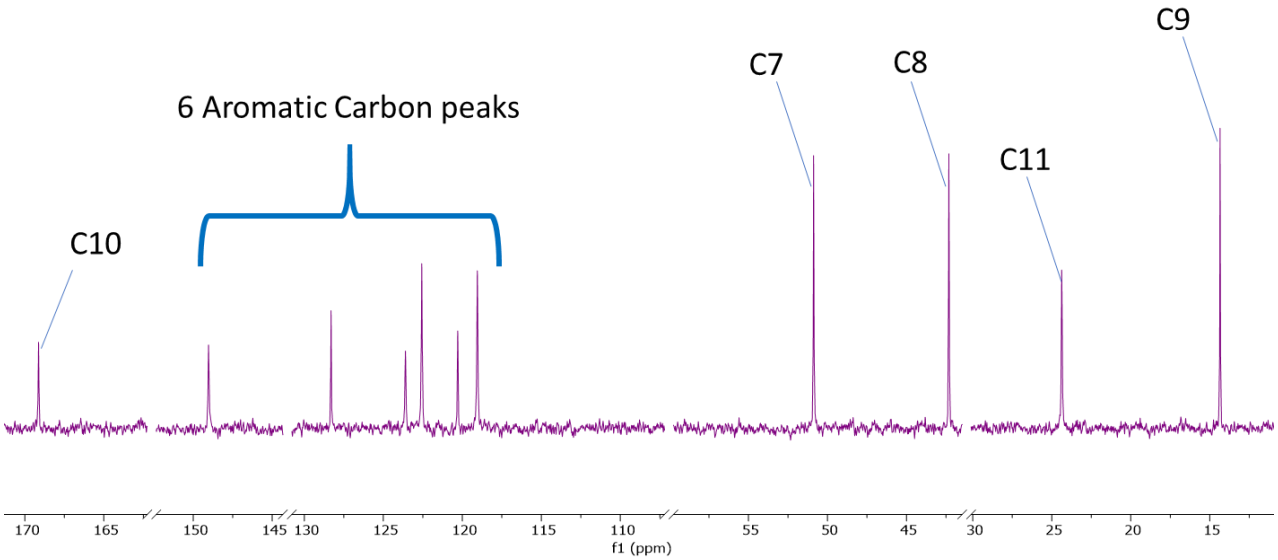

Figure 2.14**:** ^{13}C-NMR (DMSO-d_6, 151 MHz) spectrum of **3.2f**

Mass analysis of compound **3.2f** was performed using ESI^+ and the parent peak indicated an *m*/z of 243.0 $[M+H]^+$, which was obtained to corroborate the calculated mass for $C_{11}H_{15}ClN_2O_2$ (242.08)**.**

Having successfully obtained protected amino-alkylated acetamides **3.2a–3.2j**, hydrolysis of the acetamide was performed under acidic conditions to obtain the deprotected Mannich base inputs necessary for the final coupling reaction.

Hydrolysis of acetamides under acidic conditions

Acetamide intermediates (**3.2a–3.2j**) were hydrolysed using 6 M aqueous hydrogen chloride solution at 100 °C to **3.3a–3.3j** (**Scheme 2.16**). The compounds were isolated in low to high yields as dark oils. Compound **3.3i** is shown below as an example for characterization following the transformation achieved via hydrolysis (**Figure 2.15**).

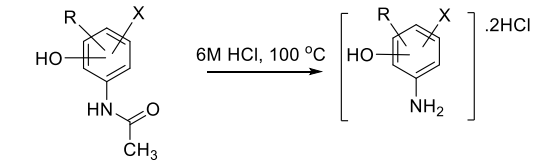

3.2a: 4-OH, X = H, R = 3-CH_2NHEt
3.2b: 3-OH, X = H, R = 4-CH_2NHEt
3.2c: 2-OH, X = H, R = 3-CH_2NHEt
3.2d: 2-OH, X = 5-F, R = 3-CH_2NHEt
3.2e: 2-OH, X = 4-Cl, R = 3-CH_2NHEt
3.2f: 2-OH, X = 5-Cl, R = 3-CH_2NHEt
3.2g: 2-OH, X = 5-Me, R = 3-CH_2NHEt
3.2h: 2-OH, X = 6-Me, R = 3-CH_2NHEt
3.2i: 4-OH, X = H, R = 3-$CH_2N(Et)_2$
3.2j: 2-OH, X = 5-Me, R = 3-$CH_2N(Et)_2$

3.3a: 4-OH, X = H, R = 3-CH_2NHEt
3.3b: 3-OH, X = H, R = 4-CH_2NHEt
3.3c: 2-OH, X = H, R = 3-CH_2NHEt
3.3d: 2-OH, X = 5-F, R = 3-CH_2NHEt
3.3e: 2-OH, X = 4-Cl, R = 3-CH_2NHEt
3.3f: 2-OH, X = 5-Cl, R = 3-CH_2NHEt
3.3g: 2-OH, X = 5-Me, R = 3-CH_2NHEt
3.3h: 2-OH, X = 6-Me, R = 3-CH_2NHEt
3.3i: 4-OH, X = H, R = 3-$CH_2N(Et)_2$
3.3j: 2-OH, X = 5-Me, R = 3-$CH_2N(Et)_2$

(20 - 96%)

Scheme 2.16: General procedure for the hydrolysis of acetamides under acidic conditions to afford HCl Mannich base salts **3.3a–3.3j**

The ^{1}H-NMR spectrum of the deprotected Mannich base input **3.3i** is shown in **Figure 2.15**. Features confirming the deacetylation reaction include the disappearance of the C(O)C**H**$_3$ peak at approximately δ 2 ppm. The aromatic protons for **3.3i** each integrate for one proton and are assigned as a doublet at δ 7.56 ppm (*J* = 2.6 Hz) corresponding to **H2**, a doublet of doublets at δ 7.34 ppm (*J* = 8.7, 2.6 Hz) corresponding to **H6,** and a doublet at δ 7.16 ppm (*J* = 8.7 Hz) corresponding to **H5**. As **3.3i** was isolated as a 2•HCl salt, it is expected that **3.3i** is protonated at the tertiary and primary amine functionalities as these are the two most basic sites of the molecule. This was confirmed by the splitting observed for **H7,** which is a doublet integrating for two protons at δ 4.22 ppm (*J* = 4.6 Hz). Furthermore, splitting of the expected quartet in **H8** to a doublet of quartets at δ 3.07 ppm (*J* = 13.9, 7.0 Hz) integrating for four protons further confirms protonation of the tertiary amine. The final peak is that of **H9,** which appears as a triplet at δ 1.27 ppm (*J* = 7.2 Hz) integrating for six protons.

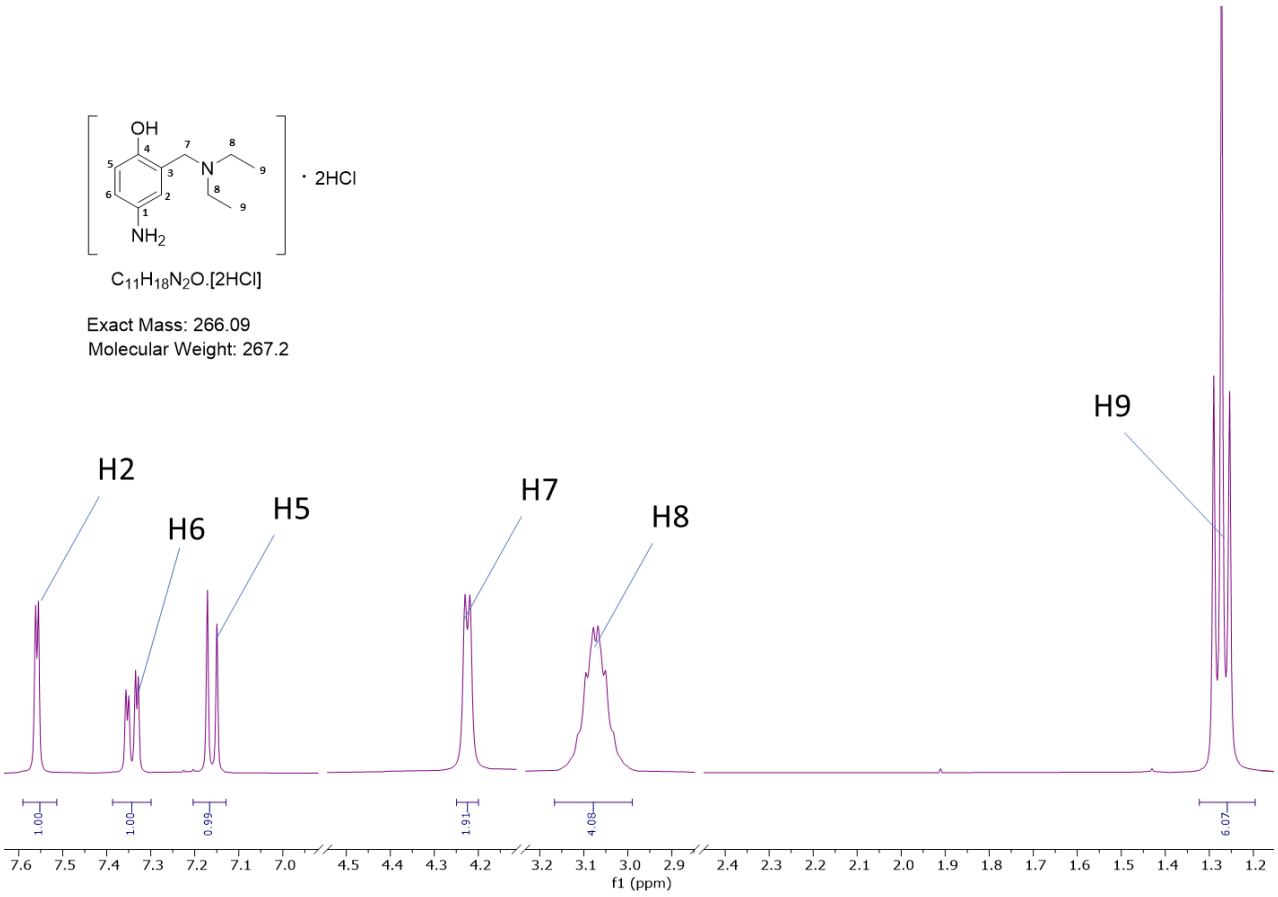

Figure 2.15: ^{1}H-NMR (DMSO-d_6, 400 MHz) spectrum of **3.3i**

The ^{13}C-NMR spectrum for **3.3i** is shown in **Figure 2.16**. Diagnostic features include the disappearance of two carbon signals attributed to the acetyl protecting group found in **3.2i,** which are expected to appear at δ 20–25 ppm for the CH_3 peak and δ 165–175 ppm for the carbonyl peak. The remaining peaks are the six aromatic carbon peaks corresponding to **C1-C6**, a peak at δ 49.64 ppm corresponding to **C7**, and two peaks integrating for 2 C at δ 45.67 and δ 7.11 ppm and corresponding to **C8** and **C9,** respectively.

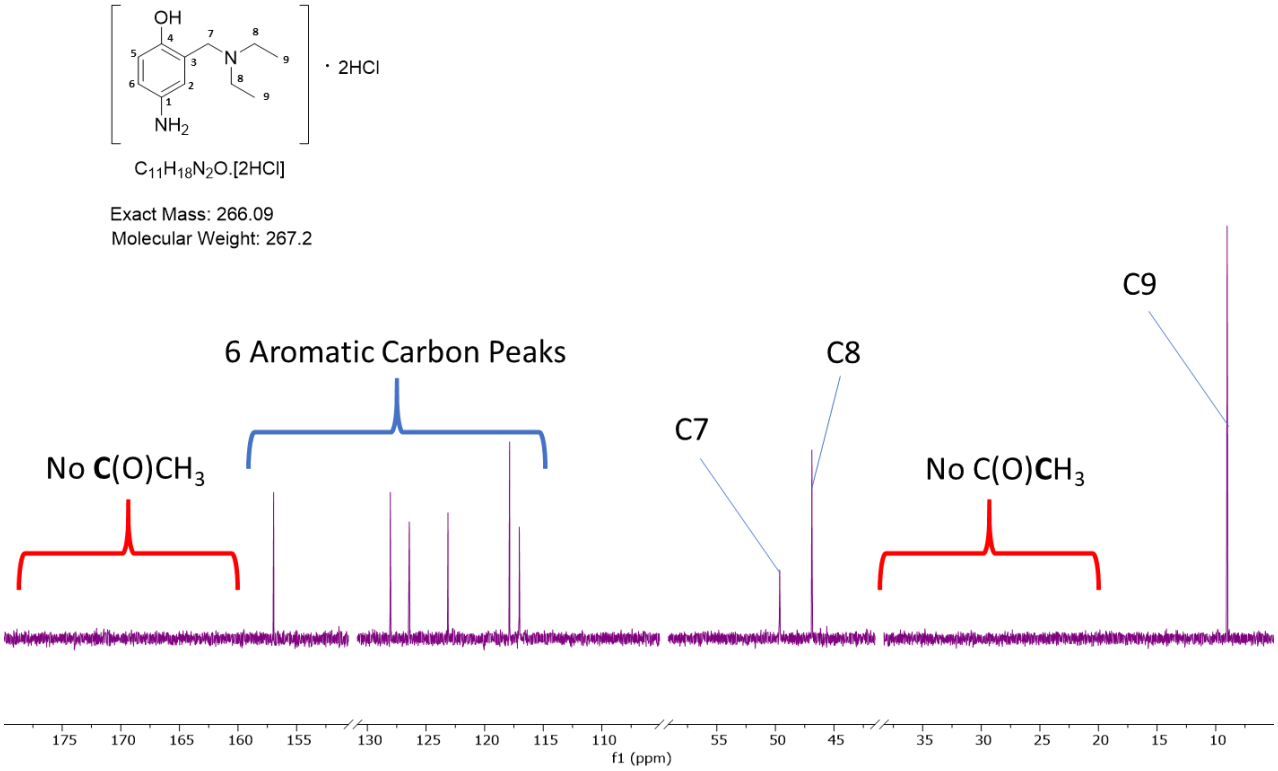

Figure 2.16: ^{13}C-NMR (DMSO-d_6, 151 MHz) spectrum of **3.3i**

Mass analysis of compound **3.3i** was performed using ESI^+. The parent peak indicated an *m*/z of 209.2 $[M+H]^+$, which was obtained to corroborate the calculated mass for $C_{11}H_{18}N_2O$ (208.16) as the chloride counter-ions are not observed in LC-MS**.**

Having successfully synthesized Mannich base inputs as 2•HCl salts (**3.3a–3.3j**), these were subjected to a final coupling reaction with the appropriate chlorinated PBI intermediates (**1.3a–1.3d**) to obtain the desired final compounds.

2.4.3 Synthesis of target compounds

Synthesis of all final target compounds was achieved via a coupling reaction in which the appropriate chlorinated PBI intermediate (**1.3a–1.3d**) underwent a nucleophilic aromatic substitution reaction by the free primary amine of the Mannich base fragment (MBF) (**2.2a–2.2b** and **3.3a–3.3j**; **Scheme 2.17**).

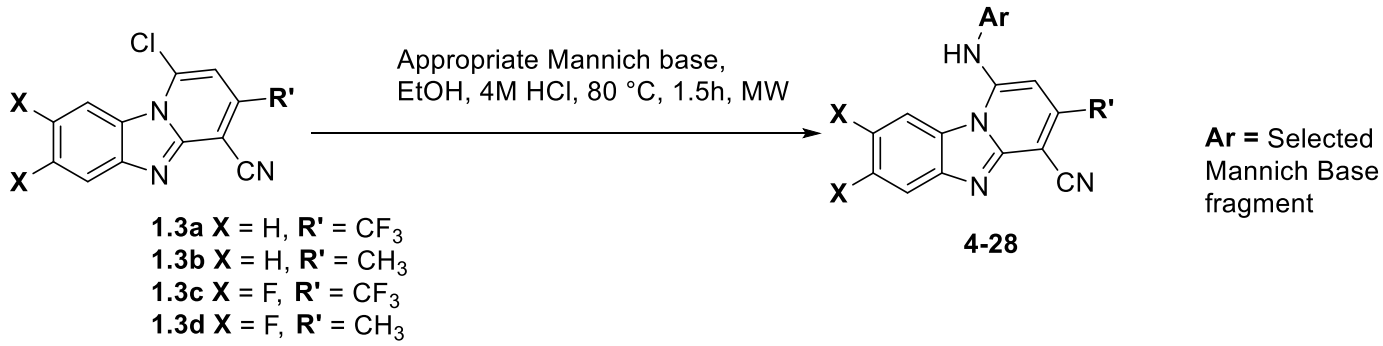

1.3a X = H, **R'** = CF_3
1.3b X = H, **R'** = CH_3
1.3c X = F, **R'** = CF_3
1.3d X = F, **R'** = CH_3

4-28

Scheme 2.17: Reaction and conditions for the final coupling reaction performed to obtain **SAR-1** and **SAR-2** target compounds **4-16**

The same reaction conditions were used for the synthesis of **SAR-1** and **SAR-2** target compounds. However, chlorinated PBI **1.3a** was used for **SAR-1** target compounds with the appropriate Mannich base inputs (**2.2a–2.2b** and **3.3a–3.3j**) to deliver compounds **4-16** (**Table 2.2**) in low to moderate yields. For **SAR-2**, the various PBI modifications required use of different chlorinated PBI intermediates **1.3a–1.3d** to allow synthesis of the desired analogues. The respective yields and associated Mannich base inputs used for each compound are listed in **Table 2.2.**

Table 2.2: Isolated yields of target compounds **4-28** showing Mannich based fragments used in the final coupling reaction to afford desired compounds

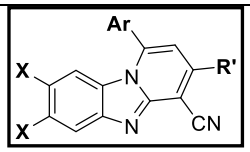

(Ar)

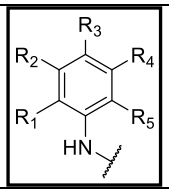

Compound	PBI Core X, R'	R_1, R_2, R_3, R_4, R_5	Mannich Base	Yield (%)
4	X = H, R' = CF_3	**R_1** = H, **R_2** = H, **R_3** = OH, **R_4** = H, **R_5** = H	4-aminophenol	38
5	X = H, R' = CF_3	**R_1** = H, **R_2** = CH_2NHEt, **R_3** = OH, R_4 = H, **R_5** = H **(M1)**	3.3a	37
6	X = H, R' = CF_3	**R_1** = H, **R_2** = $CH_2N(Et)_2$, **R_3** = OH, R_4 = H, **R_5** = H **(P1)**	3.3i	37
7	X = H, R' = CF_3	**R_1** = H, **R_2** = OH, **R_3** = CH_2NHEt, **R_4** = H, **R_5** = H	3.3b	23
8	X = H, R' = CF_3	**R_1** = H, **R_2** = CH_2NHEt, **R_3** = F, R_4 = H, **R_5** = H	2.2a	34
9	X = H, R' = CF_3	**R_1** = H, **R_2** = CH_2NHEt, **R_3** = Cl, R_4 = H, **R_5** = H	2.2b	18
10	X = H, R' = CF_3	**R_1** = OH, **R_2** = CH_2NHEt, **R_3** = H, R_4 = F, **R_5** = H	3.3d	31
11	X = H, R' = CF_3	**R_1** = OH, **R_2** = CH_2NHEt, **R_3** = Cl, R_4 = H, **R_5** = H	3.3e	9
12	X = H, R' = CF_3	**R_1** = OH, **R_2** = CH_2NHEt, **R_3** = H, R_4 = Cl, **R_5** = H	3.3f	18
13	X = H, R' = CF_3	**R_1** = OH, **R_2** = CH_2NHEt, **R_3** = H, R_4 = H, **R_5** = Me	3.3h	13
14	X = H, R' = CF_3	**R_1** = OH, **R_2** = CH_2NHEt, **R_3** = H, R_4 = Me, **R_5** = H **(M2)**	3.3g	32
15	X = H, R' = CF_3	**R_1** = OH, **R_2** = CH_2NHEt, **R_3** = H, R_4 = H, **R_5** = H	3.3c	26
16	X = H, R' = CF_3	**R_1** = OH, **R_2** = $CH_2N(Et)_2$, **R_3** = H, R_4 = Me, **R_5** = H **(P2)**	3.3j	26
17	X = H, R' = CH_3	M1	3.3a	33
18	X = H, R' = CH_3	M2	3.3g	34
19	X = F, R' = CH_3	M1	3.3a	25
20	X = F, R' = CH_3	M2	3.3g	39
21	X = F, R' = CF_3	M1	3.3a	22
22	X = F, R' = CF_3	M2	3.3g	29
23	X = H, R' = CH_3	P1	3.3i	29
24	X = H, R' = CH_3	P2	3.3j	25
25	X = F, R' = CH_3	P1	3.3i	18
26	X = F, R' = CH_3	P2	3.3j	12
27	X = F, R' = CF_3	P1	3.3i	12
28	X = F, R' = CF_3	P2	3.3j	25

The final compounds from **SAR-1** were evaluated for antiplasmodium activity and results obtained used to select Mannich base side chain inputs for the synthesis of **SAR-2** target compounds. Mannich base side chains present in the most active compounds selected from **SAR-1** were used along with other modifications around the PBI core in **SAR-2** as shown in **Figure 2.17.** More specifically**,** compounds **6** and **14** showed promising potency against *P. falciparum,* and the Mannich base side-chains in these compounds were explored further in **SAR-2**.

Compound **5** is the presumed metabolite (**M1**) of the parent compound **6** while compound **16** is the parent of the presumed metabolite **14**.

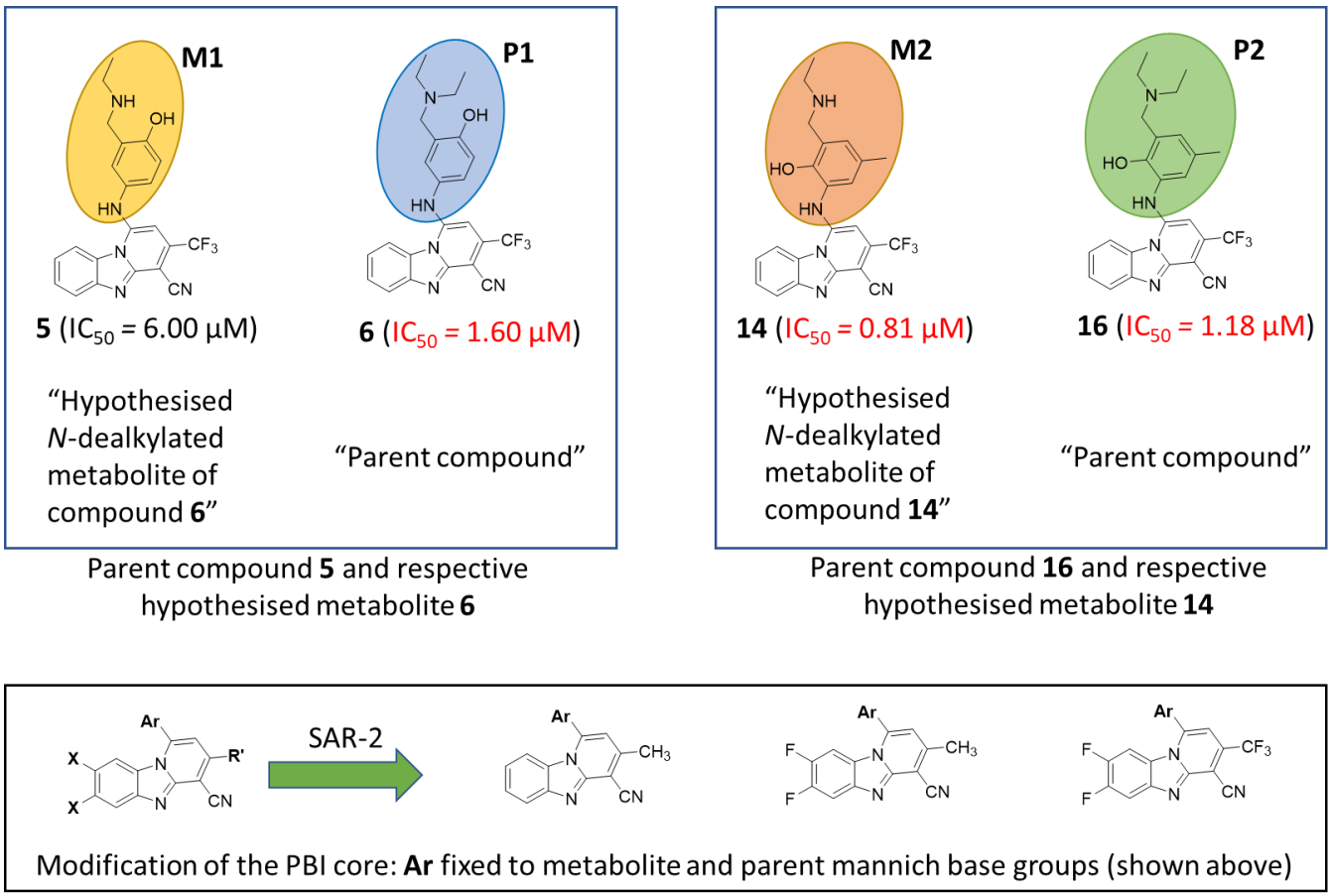

Parent compound **5** and respective hypothesised metabolite **6**

Parent compound **16** and respective hypothesised metabolite **14**

Figure 2.17: Lead compound parent-metabolite pairs **5** and **6** and **14** and **16** selected from SAR-1 and SAR-2.

PBI core modifications in **SAR-2** included modifications at positions **R'** and **X** (**Figure 2.17**). The final compounds were achieved through a coupling reaction with the appropriate Mannich base group and the appropriate chlorinated PBI intermediates

1.3b, **1.3c** and **1.3d** shown in **Figure 2.18**. The Mannich bases are maintained from **SAR-1** and therefore modifications of the PBI core only will be discussed.

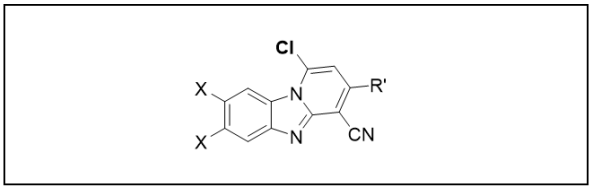

Appropriate chlorinated PBIs necessary for SAR-2 final coupling reaction

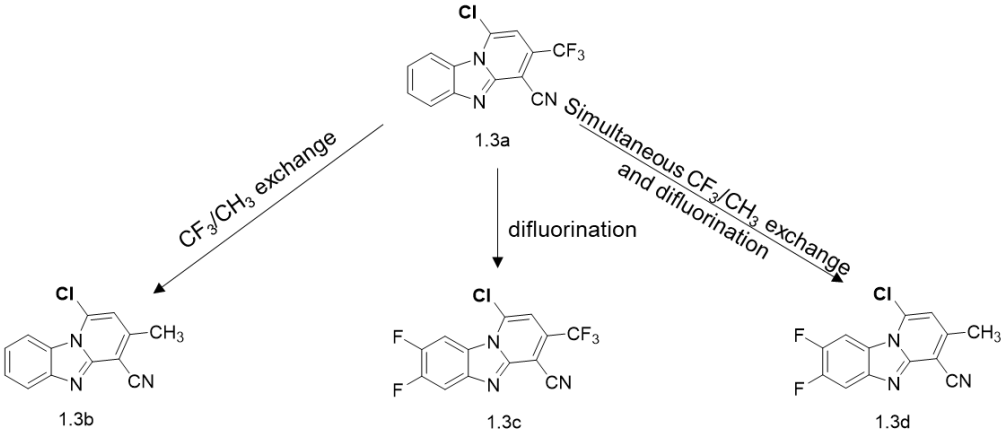

Figure 2.18: Appropriate chlorinated PBI intermediates to diversify **SAR-2** used in the final coupling reaction

Three changes are employed for **SAR-2** namely; (i) CF_3/CH_3 exchange at the **R'** position (**1.3b**), (ii) difluorination at **X** (**1.3c**), and finally (iii) a combination of CF_3/CH_3 exchange at **R'** with fluorination at **X** (**1.3d**). For (i) exchanging CF_3 for CH_3 results in a significant decrease in molecular weight with little implications on electronic potentials of the compounds. The second modification was (ii) difluorination at position **X,** which was shown to improve the pharmacological activity and microsomal metabolic stability of PBIs in previous studies.[92] The third and final modification explored in **SAR-2** was (iii) a combination of CF_3/CH_3 exchange at **R'** with difluorination at the **X-**position, combining the aforementioned modifications to develop a new PBI core scaffold and explore new chemical spaces.

The previously discussed final coupling reaction between the appropriate Mannich base inputs and chlorinated PBI intermediates was utilised as shown in **Scheme 2.17**. The synthetic procedure and characterization of final compounds will be exemplified by compound **28** as an illustrative example for the final N-arylation coupling reaction between chlorinated PBI intermediates and MBFs.

Synthesis and characterization of target compounds from a coupling reaction between a Mannich base salt and PBI intermediate

The synthesis of final compounds **4–28** was outlined in **Scheme 2.17** earlier and the reaction mechanism is shown in **Scheme 2.18.** Synthesis of final compounds began with the appropriately substituted chlorinated PBI intermediates **1.3a–1.3d**, which reacted with (i) free Mannich base inputs (1.2 eq) or (ii) [Mannich base]•2HCl salts dissolved in EtOH (2 mL). It is important to note that the reaction favoured acidic conditions, and that the desired product was not formed unless HCl was present. It is for this reason that free Mannich bases **2.2a** and **2.2b** required the dropwise addition of 4 M HCl for formation of the product. For Mannich base inputs that were isolated as salts, there was dual protonation on the primary and secondary amines respectively and therefore addition of KH_2PO_4 was necessary to facilitate the aromatic nucleophilic substitution reaction.

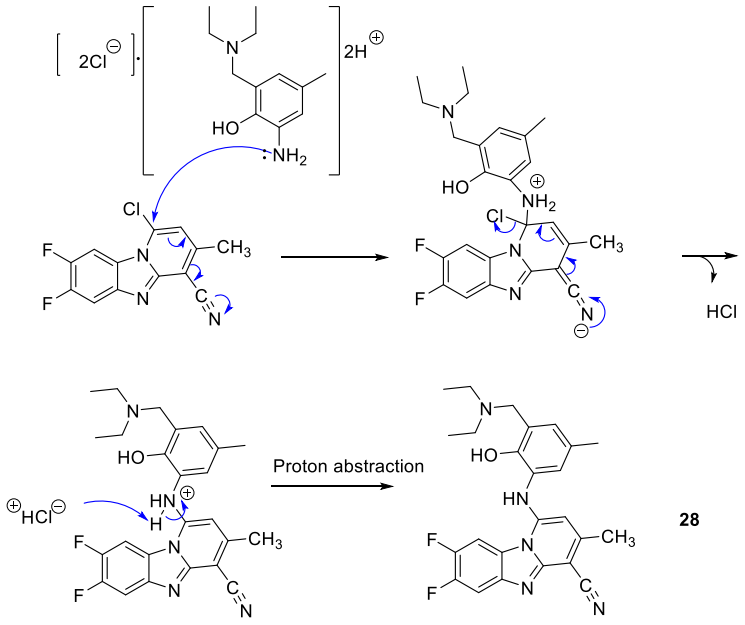

Scheme 2.18: Proposed mechanism for the nucleophilic aromatic substitution reaction performed to afford final compound 28

The formation of target compound **28** via nucleophilic aromatic substitution is shown in **Scheme 2.18**. The reaction proceeds via regioselective nucleophilic attack of the primary amine at the carbon of the chloro-position on the PBI. For Mannich base isolates which had a secondary amine on the Mannich base side chain, a

regioselective nucleophilic addition of the primary amine over the secondary amine occurred, as the less nucleophilic primary amine is sterically unhindered compared to the more nucleophilic secondary amine. The reaction mechanism proposed includes a nucleophilic aromatic substitution reaction, which begins with nucleophilic addition of the primary amine (aniline) at the carbon of the PBI core to which the chloro is attached. The cyano-substituent acts as an electron-sink. To confirm the success of the reaction, ^{1}HNMR spectroscopy analysis of **28** was performed and the spectrum is shown in **Figure 2.19**.

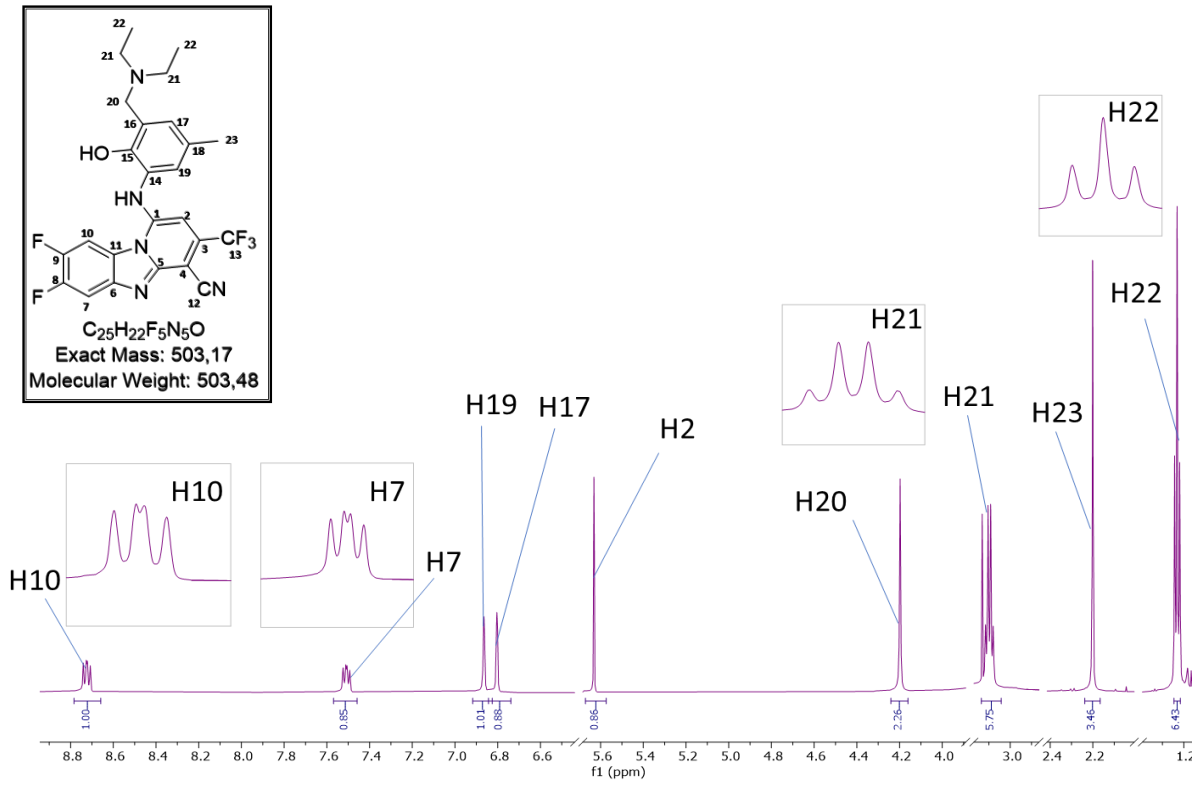

Figure 2.19: ^{1}H-NMR (DMSO-d_6, 600 MHz) spectrum of 28

The diagnostic peaks include key proton signals from the Mannich base (**Ar**) side-chain and PBI core of the molecule. Successful substitution at the **C1**-position was confirmed by an upfield shift of proton **H2** compared to that in **1.3c,** which appeared as a singlet integrating for one proton at δ 5.63 ppm. Furthermore, protons belonging to the PBI core underwent ortho-fluorine coupling (*J* = 11.4 Hz) and meta-coupling (*J* = 8.1 and 7.4 Hz), and are assigned as two doublet of doublets at δ 8.72 ppm and δ 7.51 ppm, each integrating for a single proton, corresponding to **H10** and **H7,** respectively. The aromatic proton signals associated with the Mannich base side-chain (**Ar**) of the compound are two singlets, each integrating for a single proton at δ 6.86 ppm and δ 6.80 ppm, corresponding to **H19** and **H17,** respectively. The methylene linker was assigned to a singlet at δ 4.20 ppm integrating for two protons corresponding to **H20**. The diethylamine protons were assigned to two signals at δ 3.10 ppm and δ 1.23 ppm as a quartet integrating for four protons (*J* = 7.2 Hz) and a triplet integrating for six protons corresponding to **H21** and **H22** respectively. The final peak in the ^{1}H spectrum for **28** is that of **H23** which appears as a singlet, integrating for three protons at δ 2.20 ppm.

To further confirm the success of the reaction, ^{13}C-NMR analysis was also performed (**Figure 2.20**). Characteristic features of the ^{13}C-NMR spectrum include 19 carbon peaks in the aromatic region (89–155 ppm) corresponding to aromatic regions from both the PBI and Mannich base side-chain portions of the final compound and finally the CF_3 carbon signal. The splitting pattern associated with the ^{13}C-NMR spectrum of **28** is attributed to fluorine atoms at **C7, C8**, **C9, C10,** and **C13,** as these have a nuclear spin of ½ and therefore split the carbon signals from singlets into doublets. Meta-coupling to the fluorine atom in the PBI core was observed for C7 and C10. Finally, the success of the reaction was confirmed by the remaining aliphatic ^{13}C-NMR peaks attributed to the diethylamine chain at δ 51.17 ppm corresponding to **C20**, and two peaks remaining, each equivalent to two carbons at δ 47.14 ppm and δ 8.97 ppm corresponding to **C21** and **C22,** respectively. The final remaining peak is that at δ 20.64 ppm corresponding to **C23**.

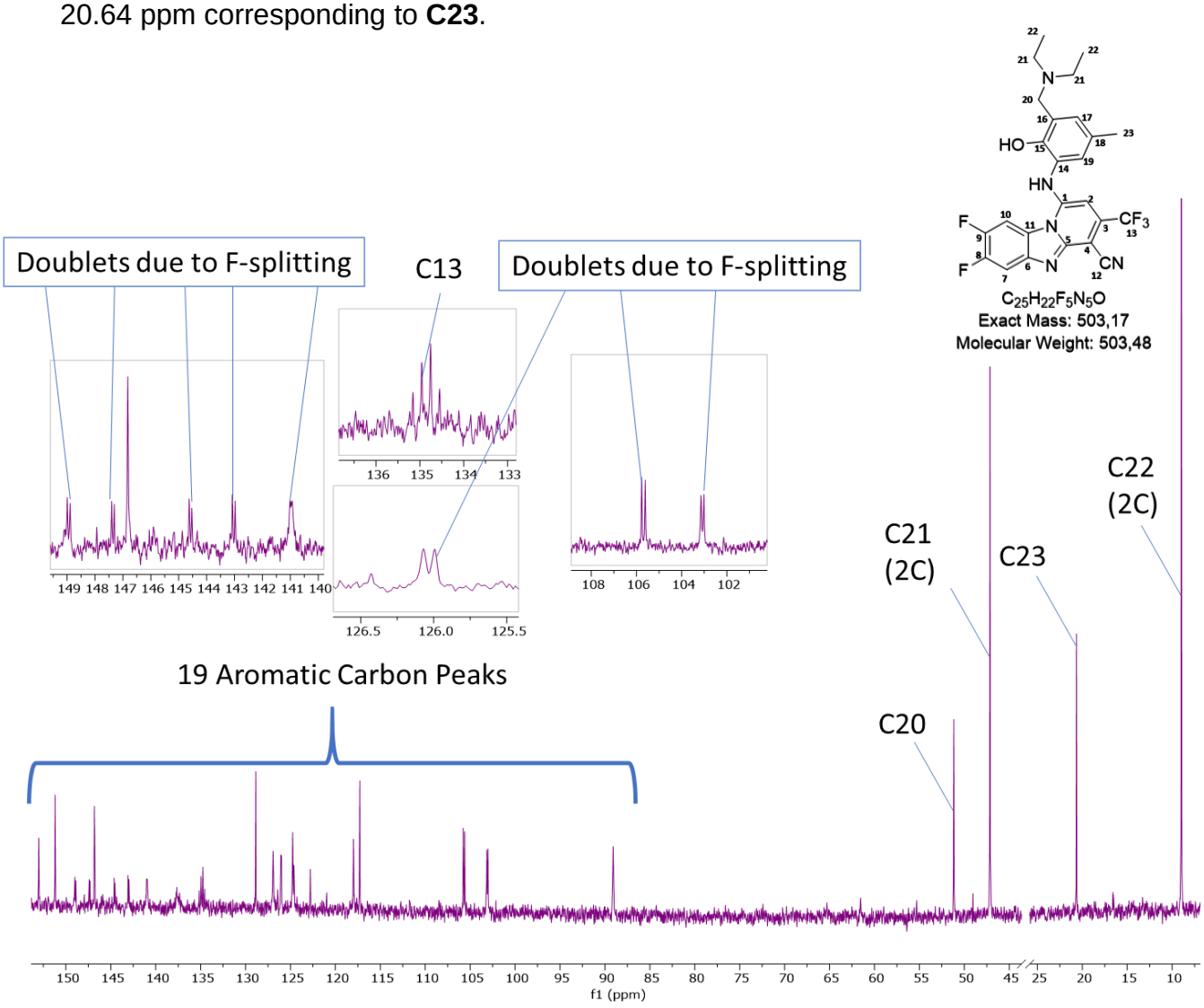

Figure 2.20: ^{13}C-NMR (DMSO-d_6, 151 MHz) spectrum of 28

Mass analysis of compound **28** was performed using ESI^+ and the parent peak indicated an *m*/z of 504.20 $[M+H]^+$, which was obtained to corroborate the calculated mass for $C_{25}H_{22}F_5N_5O$ (503.17)**.**

2.5 Chapter conclusion

This chapter described the synthesis and characterization of target compounds designed for SAR studies. Furthermore, the parent and corresponding presumed N-dealkylated metabolite pairs were selected from **SAR-1** to investigate further in **SAR-2**. The compounds were synthesized using standard protocols adapted from published synthetic methods. All compounds synthesized were fully characterized using NMR, and chromatographic methods including TLC and HPLC-MS, along with measurement of physical attributes such as melting point and appearance. The final target compounds were submitted for biological evaluation and physicochemical profiling as detailed in **Chapter 3**. In addition, data relating to the characterization of each of the compounds synthesized are fully described in **Chapter 4**.

CHAPTER 3: Biological results and discussion

3.1 Chapter overview

This chapter details the studies conducted to assess the antiplasmodium activity, β-hematin inhibition potential, cytotoxicity, metabolic stability, and physicochemical properties of target PBIs. A simplified illustration of the test sequence used for biological and physicochemical profiling is included to highlight the key assays used.

3.2 Screening cascade for target compounds

The studies performed here followed the screening cascade shown in **Figure 3.1**, which lists the various assays and progression criteria (cut-off values) used. First, all compounds were initially screened to determine *in vitro* antiplasmodium activity against the *NF*54 (CQ-sensitive) asexual blood stage (ABS) strain of *P. falciparum* and sexual blood-stage gametocytes. The potential for compounds to inhibit -hemozoin formation was evaluated using an in-house β-hematin inhibition cell-free assay. It is noteworthy that β-hematin is synthetic hemozoin. Emerging front-runner compounds exhibiting IC_{50} < 2 µM against ABS parasites were deemed active and were further tested for cytotoxicity and microsomal metabolic stability. Cytotoxicity was evaluated in both Caucasian hepatocellular carcinoma cells (Hep-G2) and Chinese hamster ovarian (CHO) cells to determine the compounds' selectivity towards the parasite. Compounds displaying IC_{50} > 10 µM against mammalian cells were considered non-cytotoxic.

Furthermore, two synthesized compounds were evaluated for microsomal metabolic stability in mouse liver microsomes (MLMs), towards identifying compounds for proof-of-concept *in vivo* antimalarial efficacy studies in a mouse model. Microsomal stability was determined via incubation with MLMs after which the percentage parent compound remaining after 30 min was determined via LC-MS.

The solubility of all target compounds was determined using the turbidimetric kinetic solubility assay and the melting points determined.

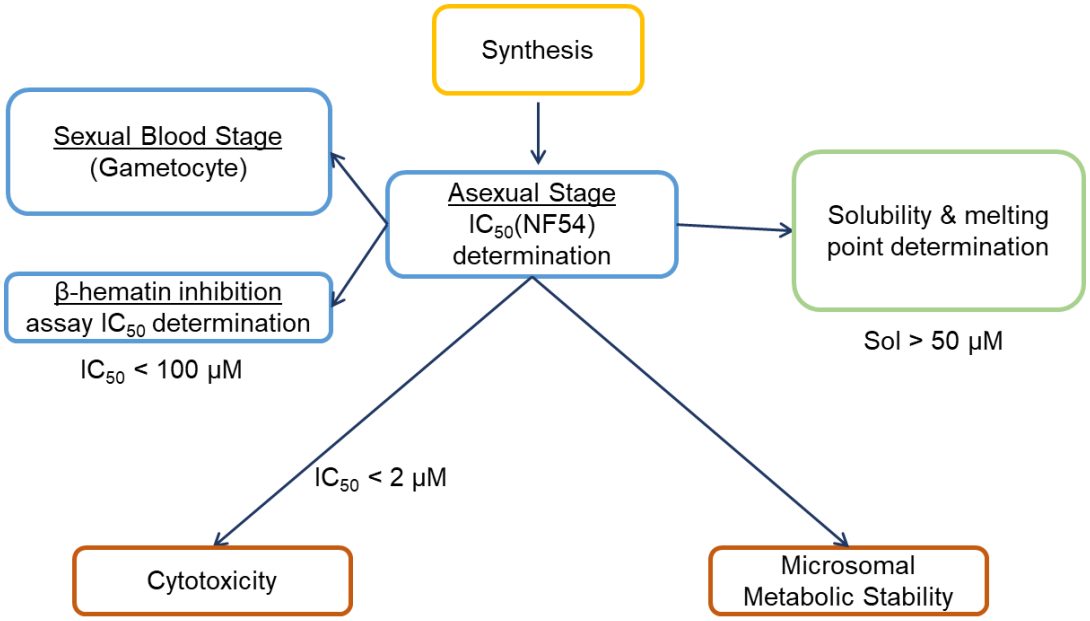

Figure 3.1: Screening cascade for various biological and physicochemical studies depicting cut-offs for the progression of compounds

3.3 *In vitro* antiplasmodium activity

The PBI analogues selected from **SAR-1** and **SAR-2** were evaluated *in vitro* for multi-stage activity against the asexual erythrocytic CQ-sensitive (NF54) strain as well as early- and late-stage sexual stage parasites (gametocytes) using a modified luciferase assay (NF54-PfS16-GFP-Luc) for gametocyte viability determination.[95] A discussion of the *in vitro* antiplasmodium activities of **SAR-1** and **SAR-2** compounds follows below.

3.3.1 SAR-1

The *in vitro* antiplasmodium activities of **SAR-1** compounds were evaluated against asexual and sexual stages of *P. falciparum*. The mean values obtained for **SAR-1** compounds are shown in **Table 3.1**.

Table 3.1**:** *In vitro* activity of **SAR-1** compounds against asexual-stage (NF54) and gametocyte (NF54) *P. falciparum* parasites

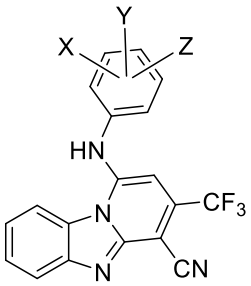

Compound	Phenolic Mannich base side-chain	ABS parasites IC_{50} (µM)[a]	% inhibition in early-stage gametocytes		% inhibition in late-stage gametocytes	
	X, Y, Z	*NF*54	1 µM	5 µM	1 µM	5 µM
4	X =H, Y =4-OH, Z = H	6.00	0	12	25	27
5	X =H, Y =4-OH, Z = 3-CH_2NHEt	6.00	33	14	26	41
6	X =H, Y =4-OH, Z = 3-$CH_2N(Et)_2$	1.60	19	29	60	60
7	X =H, Y =3-OH, Z = 4-CH_2NHEt	6.00	0	0	66	67
8	X =H, Y =4-F, Z = 3-CH_2NHEt	5.82	16	49	77	43
9	X =H, Y =4-Cl, Z = 3-CH_2NHEt	6.00	-	-	-	-
10	X =5-F, Y =2-OH, Z = 3-CH_2NHEt	6.00	-	-	-	-
11	X =4-Cl, Y =2-OH, Z = 3-CH_2NHEt	6.00	-	-	-	-
12	X =5-Cl, Y =2-OH, Z = 3-CH_2NHEt	2.56	-	-	-	-
13	X =6-Me, Y =2-OH, Z = 3-CH_2NHEt	5.78	-	-	-	-
14	X =5-Me, Y =2-OH, Z = 3-CH_2NHEt	0.81	-	-	-	-
15	X =H, Y =2-OH, Z = 3-CH_2NHEt	4.86	2.0	4.5	14.9	0.9
16	X =5-Me, Y =2-OH, Z = 3-$CH_2N(Et)_2$	1.18	6.6	84.6	0	12.5

[a] Mean values were calculated from at least two independent experiments (individual values within ± 2-fold). Artesunate (IC_{50} = 0.007 µM) and chloroquine (IC_{50} = 0.012 µM) were used as reference drugs.

For the purpose of this study, compounds were classified as showing high activity (IC_{50} ≤ 2 µM), moderate activity (2 < IC_{50} < 6 µM), or poor activity (IC_{50} ≥ 6 µM). For **SAR-1,** all compounds synthesized contained the same PBI-core and are therefore discussed in terms of their substituents at the **X, Y,** and **Z** positions of the phenolic Mannich base side-chain (**Table 3.1**). The presence or absence of the monoethylated Mannich side chain was not critical for antiplasmodium activity as highlighted by the 4-hydroxy aromatic (**Ar**) group in **4** (IC_{50} = 6.00 µM), and **5** (IC_{50} = 6.00 µM). The diethylated Mannich side chain was crucial as exemplified by the activity of compound

6. The substituent at the 3rd position (**Z** = 3-$CH_2N(Et)_2$) of the Mannich base side-chain drastically improved activity as exemplified by compound **6** (IC_{50} = 1.60 µM), which showed a 4-fold increase in activity compared to that of desethyl metabolite **5**. One of the structural modifications implemented to overcome the liabilities associated with quinone-imine formation included swapping the position of the substituents at the 3rd and 4th positions of the Mannich base side-chain. Unfortunately, this resulted in loss of activity as shown for compound **7** (IC_{50} = 6.00 µM). Another strategy involving substituting the hydroxyl group at the 4th position of the Mannich base side-chain with a halogen (F or Cl) was detrimental to activity as shown by the poor activities of analogues **8** and **9** (IC_{50} = 5.82 and 6.00 µM, respectively).

Exploitation of the 2nd and 3rd positions of the Mannich base side-chain was investigated for the remaining **SAR-1** compounds. Compounds **10**–**16** all contained a Mannich base side-chain with the 2nd position occupied by a hydroxyl substituent (**Y** = 2-OH). Compounds **10–12** are the halogenated analogues of **SAR-1**. Addition of a fluorine substituent at the 5th position (**X** = 5-F) and a chlorine substituent at the 4th position (**X** = 4-Cl) led to loss of antiplasmodium activity as shown by **10** and **11** ((IC_{50} = 6.00 µM). The presence of a chlorine atom in the 5th position (**X** = 5-Cl) was somewhat tolerated, as represented by the moderate activity of compound **12** (IC_{50} = 2.56 µM).

The position of the methyl substituent influenced antiplasmodium activity, as was shown by both analogues **13** and **14**. Compound **13** containing a methyl substituent at the 6th position (IC_{50} = 5.78 µM), was significantly less active compared to compound **14** (IC_{50} of 0.81 µM)**,** which contains a methyl substituent at the 5th position. When there is no substituent present (i.e., **X** = H, as in **15**), activity decreased 6-fold (IC_{50} = 4.86 µM) compared to that of **14**, thus highlighting the importance of a 5-methyl substituent. High antiplasmodium activity was observed for compound **16** (IC_{50} = 1.18 µM) in which a diethylaminomethylene group is at position 3 (**Z** = 3-$CH_2N(Et)_2$). When compared to the monoethylated analogue **14** (IC_{50} = 0.81 µM), it appears monoethylation has similar activity compared to diethylation.

In summary, eight compounds (**4, 5, 7, 8, 9, 10, 11,** and **13**) from the **SAR-1** series showed poor antiplasmodium activity, IC_{50} = 6.00 µM. In comparison, analogue **6** showed an IC_{50} of 1.60 µM. The most active compounds from **SAR-1** were **6**, **14,** and

16. These active compounds were used as a starting point in the rationalization of compounds selected for **SAR-2**. Of the remaining compounds, **12** (IC_{50} = 2.56 µM) and **15** (IC_{50} = 4.86 µM) showed moderate antiplasmodium activity.

From **SAR-1**, seven compounds were selected for testing against both late- and early-stage gametocytes. For the purpose of discussion, compounds were classified as indicated below:

- High activity: >70% inhibition at 5 µM and >50% inhibition at 1 µM
- Moderate activity: >70% inhibition at 5 µM and <50% inhibition at 1 µM, <70% inhibition at 5 µM and >50% inhibition at 1 µM, or 50–70% inhibition at 5 µM and <50% inhibition at 1 µM
- No/ minimal activity: <50% inhibition at 5 µM and <50% inhibition at 1 µM

Based on these criteria, all compounds selected for gametocyte testing, with the exception of **16**, showed no/minimal activity against early-stage gametocytes. Compound **16** exhibited moderate activity against early-stage gametocytes with 84.6% inhibition at 5 µM. Compounds **6, 7,** and **8** showed moderate activity against late-stage gametocytes while compounds **4**, **5**, **15,** and **16** showed minimal activity against late-stage gametocytes. Compounds **6** and **16** were considered active against both sexual and asexual stage parasites and analogues containing the Mannich base side-chains present in these active compounds were evaluated in **SAR-2**. The relationships between parent and desethyl metabolites were explored in **SAR-2** with respect to antiplasmodium activity and metabolic stability. A brief comparison of the parent compounds and desethyl metabolites is provided using representative compounds from **SAR-1** (compounds **5**, **6, 14,** and **16**).

3.3.2 Selection of parent and desethyl metabolite pairs from SAR-1 for exploration in SAR-2

In **SAR-1,** only compounds **6** and **16** contained a diethylamine group at the 3rd position (**Z** = 3-$CH_2N(Et)_2$). These were classified as parent compounds based on the assumption that they will undergo metabolism to the corresponding desethyl metabolites based on previous metabolite identification studies.[92] Desethyl metabolites of **6** and **16** were synthesized and evaluated in **SAR-1**, and these

contained an ethylamine substituent at the 3rd position (**Z** = 3-CH_2NHEt), as represented by **5** and **14,** respectively. Noticeably, when comparing the activity of parent and desethyl metabolite pairs **6** and **5,** the parent compound **6** (IC_{50} = 1.60 µM) was active against asexual-stage parasites and moderately active against late-stage gametocytes (60% inhibition at 1 µM), although the desethyl metabolite (**5**) showed no activity against sexual or asexual parasites (IC_{50} = 6 µM). In comparison, the desethyl metabolite **14** (IC_{50} = 0.81 µM) showed similar activity against asexual-stage parasites compared to that of the parent **16**. The parent was still considered active against asexual-stage parasites (IC_{50} = 1.18 µM) as well and moderately active against early-stage gametocytes (84.6 % inhibition at 5 µM).

Based on the antiplasmodium activity data described in **SAR-1**, the comparison between the antiplasmodium activities of parent compounds and desethyl metabolites was further investigated in **SAR-2**. The selection criteria used for **SAR-2** analogues is shown in **Figure 3.2**.

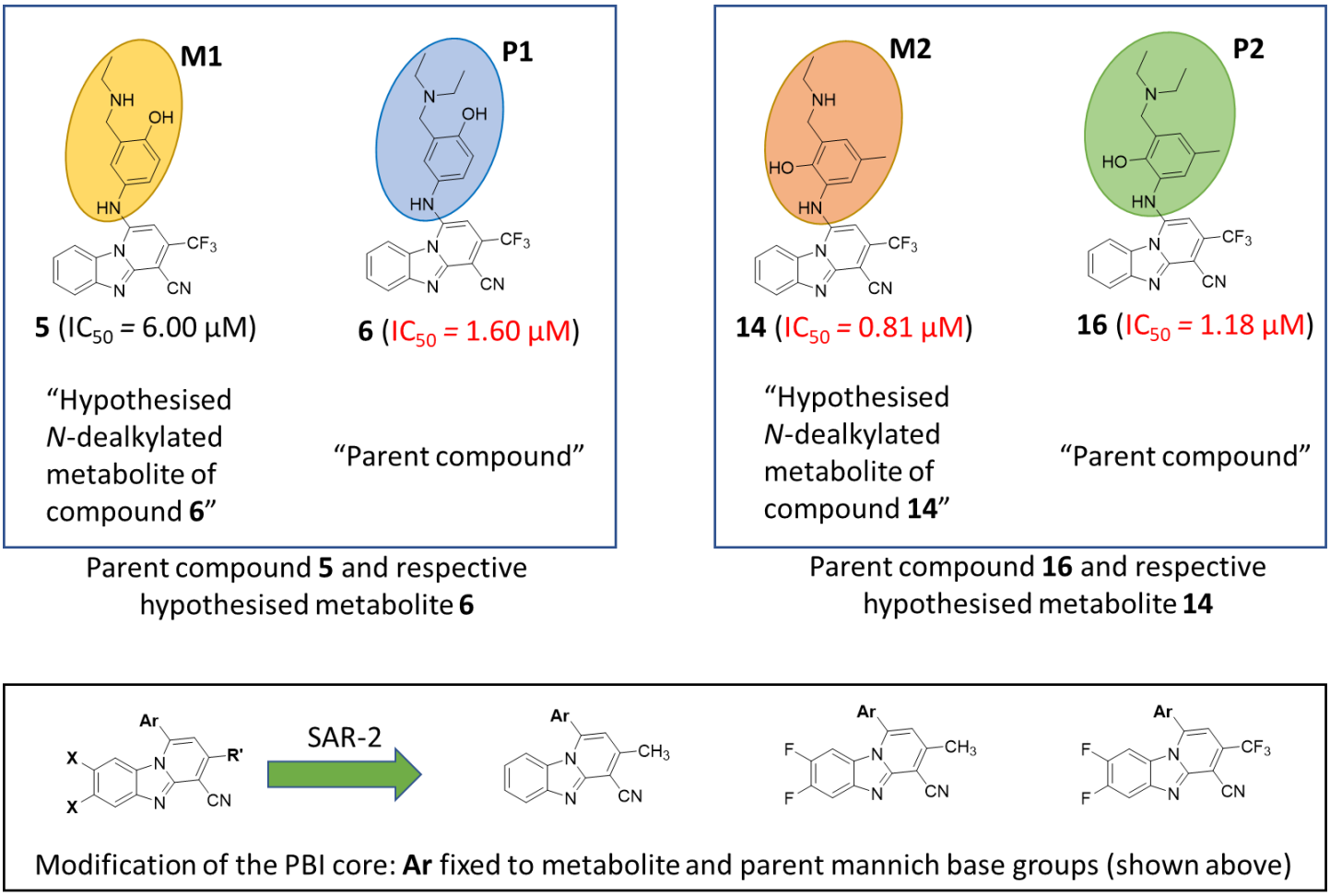

Figure 3.2: Mannich base fragments used for all SAR-2 compounds

The Mannich base side-chains selected for **SAR-2** are highlighted in **Figure 3.2**. Briefly, the first metabolite-parent pair, desethyl metabolite **5** and parent **6**, contain Mannich base side-chains **M1** and **P1,** respectively. The second metabolite-parent pair is desethyl metabolite **14** and parent **16,** which contain Mannich base side-chains **M2** and **P2**, respectively. The two parent-metabolite pairs maintained their respective Mannich base side-chains whilst three changes were made to the PBI core, including a CF_3/CH_3 exchange at the **R′** position, difluorination at the **X**-position, and a combination of CF_3/CH_3 substitutions and difluorination at the **R′-** and **X**-positions respectively. While the CF_3 and CH_3 substitutions were intended to broaden the SAR, introduction of fluorine atoms in the left hand side of the PBI core was designed to improve metabolic stability as fluorination is known to improve metabolic stability in phase I oxidation metabolism.[96] The parent-metabolite pairs synthesized are shown in **Table 3.2** along with their antiplasmodium activities against both sexual- and asexual-stage parasites.

3.3.3 SAR-2 *in vitro* antiplasmodium activity

The *in vitro* antiplasmodium activities of **SAR-2** compounds were evaluated against asexual stages of *P. falciparum* (NF54 strain) and selected compounds evaluated against early- and late-stage gametocytes. The mean values obtained for **SAR-2** compounds are shown in **Table 3.2**.

Table 3.2: *In vitro* activity of SAR-2 compounds against asexual-stage and gametocyte *P. falciparum* parasites (NF54 strain)

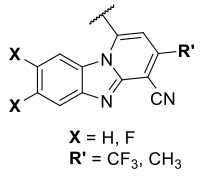

PBI core

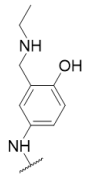

M1

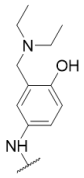

P1

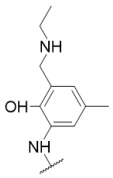

M2

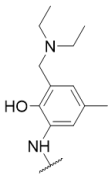

P2

Mannich Base Fragments

Compound	PBI core X, R'	Mannich base side-chain M1, P1, M2, P2	IC_{50} in ABS (μM)[a]	%Gametocyte inhibition[b]			
				Early stage		Late stage	
			*NF*54	1 μM	5 μM	1 μM	5 μM
5	X = H R' = CF_3	M1	6.00	33	14	26	41
6	X = H R' = CF_3	P1	1.60	19	29	60	60
14	X = H R' = CF_3	M2	0.81	-	-	-	-
16	X = H R' = CF_3	P2	1.18	6.6	84.6	0	12.5
17	X = H R' = CH_3	M1	3.70	0	57.5	0	14.8
18	X = H R' = CH_3	M2	1.20	0	90.3	0	9.8
19	X = F R' = CH_3	M1	0.59	0	77.1	0	10.2
20	X = F R' = CH_3	M2	0.63	17.9	92.8	0	3.6
21	X = F R' = CF_3	M1	3.06	0	23.2	0	0
22	X = F R' = CF_3	M2	2.08	0	29.3	0	8.9
23	X = H R' = CH_3	P1	1.50	0	30.9	0	1.7
24	X = H R' = CH_3	P2	0.64	52.8	88.7	0	9.3
25	X = F R' = CH_3	P1	0.47	0	52.6	0	0
26	X = F R' = CH_3	P2	0.54	81.4	84.6	0	7.8
27	X = F R' = CF_3	P1	2.31	0	17.1	0	12.2
28	X = F R' = CF_3	P2	0.35	0	0	0	41.9

[a]Mean values were calculated from at least two independent experiments (individual values within ± 2-fold). Artesunate (IC_{50} = 0.007 μM) and chloroquine (IC_{50} = 0.012 μM) were used as reference drugs. [b]Reference compounds typically produce the following average % inhibition of gametocyte viability at 1 μM: methylene blue, 95% in early gametocytes and 92% in late gametocytes), MMV390048 (UCT MMV internal reference), 56% in early gametocytes and 86% in late gametocytes).

Compounds **5**, **6**, **14,** and **16** have already been discussed in **SAR-1** but are included in **Table 3.2** for comparison purposes. Overall, **SAR-2** compounds showed higher antiplasmodium activity than **SAR-1** compounds**.** Six compounds from **SAR-2** showed sub-micromolar antiplasmodium activity, including both parent compounds and desethyl metabolites. The desethyl metabolites showing sub-micromolar activity contain Mannich base side-chains **M1** and **M2, 19** (IC_{50} = 0.59 µM) and **20** (IC_{50} = 0.63 µM), respectively. The four parent compounds with sub-micromolar activity are: **24** (IC_{50} = 0.64 µM), **25** (IC_{50} = 0.47 µM), **26** (IC_{50} = 0.54 µM), and **28** (IC_{50} = 0.35 µM) containing Mannich base side-chains **P2**, **P1, P2,** and **P2,** respectively.

The SAR for modifications made to the PBI-core will be highlighted using selected representative compounds based on CF_3/CH_3 substitutions and other modifications of the PBI-core. These modifications will be compared to **SAR-1** compounds with an unmodified PBI core, as represented by compounds **5** (IC_{50} = 6.00 µM)**, 6** (IC_{50} = 1.60 µM)**, 14** (IC_{50} = 0.81 µM), and **16** (IC_{50} = 1.18 µM)**.**

Overall, replacement of the CF_3 substituent with a CH_3 group either resulted in an increase in activity for the desethyl metabolites **17** (IC_{50} = 3.70 µM,) or in comparable activity as in **18** (IC_{50} = 1.20 µM,). In case of the parent compounds, there was comparable activity in case of **23** (IC_{50} = 1.50 µM) and an increase in activity in case of **24** (IC_{50} = 0.64 µM). In general, difluorination at the **X**-position resulted in an increase in activity as shown by desethyl metabolites **21** (IC_{50} = 3.06 µM,) and **22** (IC_{50} = 2.08 µM) and parent compound **28** (IC_{50} = 0.35 µM) but a slight decrease in activity for parent compounds **27** (IC_{50} = 2.31 µM). Simultaneous replacement of the CF_3 substituent with a CH_3 group with difluorination at the **X**-position resulted in an increase in activity for both parents and desethyl metabolites, as exemplified by desethyl metabolites **19** (IC_{50} = 0.59 µM) and **20** (IC_{50} = 0.63 µM,) and parent compounds **25** (IC_{50} = 0.47 µM), and **26** (IC_{50} = 0.54 µM).

In summary, all structural modifications to the PBI core at positions **X** and **R′** with respect to replacement of the CF_3 substituent with a CH_3 group and difluorination improved antiplasmodium activity across all Mannich base side-chains (**M1, M2, P1,** and **P2**), with the exception of difluorination at the **X**-position for Mannich base side-chains **M2** and **P1**, as exemplified by **22** and **27,** respectively, which was detrimental to antiplasmodium activity.

All 12 compounds from **SAR-2** were selected for testing against both late- and early-stage gametocytes. Two compounds showed high activity against early stage gametocytes: these were parent compounds **24** and **26,** which showed 52.8% and 81.4%, inhibition, respectively, at 1 µM. Three desethyl metabolites showed moderate activity against early-stage gametocytes: **18** (90.3% inhibition at 5 µM), **19** (77.1% inhibition at 5 µM), and **20** (92.8% inhibition at 5 µM). The remaining seven compounds from **SAR-2** (**17, 21, 22, 23, 25, 27,** and **28**) showed minimal inhibition of early-stage gametocytes. No clear trend towards early-stage gametocyte activity was observed across transformations made around the PBI-core. All compounds from **SAR-2** showed minimal inhibition of late-stage gametocytes. Overall, compounds showed a preference for early-stage gametocytes, which suggests stage-specificity.

3.4 β-hematin inhibition studies and turbidimetric solubility studies for final compounds

The mechanistic potential of analogues synthesized in **SAR-1** and **SAR-2** to inhibit hemozoin formation was evaluated *in vitro* by investigating their ability to inhibit β-hematin formation. A Nonidet-P-40 (NP-40) detergent-mediated assay was performed in acetate buffer (pH 4.8) at 37 °C, with the activity cut-off set at $IC_{50} < 100$ µM. The approximate aqueous solubility of the compounds synthesized was measured using turbidimetric kinetic solubility assay. The turbidimetric solubility assay relies on the appearance of turbidity in solution once a compound exceeds its solubility limit in the assay and generally results in an over-estimated solubility compared to HPLC-based methods. Compound solubility was determined as the concentration value (IC_{50}) above which the compounds precipitated out of an aqueous buffer (phosphate-buffered saline, pH 7.4). Results of the β-hematin inhibition and turbidimetric solubility assays are shown in **Table 3.3**.

Table 3.3: Results of the β-hematin inhibition assay and turbidimetric solubility studies of all compounds

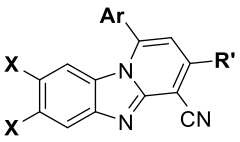

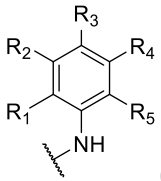

(Ar)

Compound	PBI core **X**, **R'**	Mannich base fragment (**Ar**)	β-hematin inhibition IC_{50} (μM)	Solubility (μM)
4	X = H R' = CF_3	**R_1** = H, **R_2** = H, **R_3** = OH, **R_4** = H, **R_5** = H	241	200
5	X = H R' = CF_3	**R_1** = H, **R_2** = CH_2NHEt, **R_3** = OH, R_4 = H, **R_5** = H **(M1)**	14.68	160
6	X = H R' = CF_3	**R_1** = H, **R_2** = $CH_2N(Et)_2$, **R_3** = OH, R_4 = H, **R_5** = H **(P1)**	6.502	5
7	X = H R' = CF_3	**R_1** = H, **R_2** = OH, **R_3** = CH_2NHEt, **R_4** = H, **R_5** = H	43.86	10
8	X = H R' = CF_3	**R_1** = H, **R_2** = CH_2NHEt, **R_3** = F, R_4 = H, **R_5** = H	22.43	5
9	X = H R' = CF_3	**R_1** = H, **R_2** = CH_2NHEt, **R_3** = Cl, R_4 = H, **R_5** = H	111.4	5
10	X = H R' = CF_3	**R_1** = OH, **R_2** = CH_2NHEt, **R_3** = H, R_4 = F, **R_5** = H	8.341	10
11	X = H R' = CF_3	**R_1** = OH, **R_2** = CH_2NHEt, **R_3** = Cl, R_4 = H, **R_5** = H	10.75	20
12	X = H R' = CF_3	**R_1** = OH, **R_2** = CH_2NHEt, **R_3** = H, R_4 = Cl, **R_5** = H	7.77	40
13	X = H R' = CF_3	**R_1** = OH, **R_2** = CH_2NHEt, **R_3** = H, R_4 = H, **R_5** = Me	10.39	40
14	X = H R' = CF_3	**R_1** = OH, **R_2** = CH_2NHEt, **R_3** = H, R_4 = Me, **R_5** = H **(M2)**	13.44	40
15	X = H R' = CF_3	**R_1** = OH, **R_2** = CH_2NHEt, **R_3** = H, R_4 = H, **R_5** = H	14.17	20
16	X = H R' = CF_3	**R_1** = OH, **R_2** = $CH_2N(Et)_2$, **R_3** = H, R_4 = Me, **R_5** = H **(P2)**	182.4	20
17	X = H R' = CH_3	**M1**	59.58	80
18	X = H R' = CH_3	**M2**	33.56	80
19	X = F R' = CH_3	**M1**	27.86	40

20	X = F R' = CH_3	**M2**	16.41	40
21	X = F R' = CF_3	**M1**	7.84	20
22	X = F R' = CF_3	**M2**	8.21	10
23	X = H R' = CH_3	**P1**	71.08	200
24	X = H R' = CH_3	**P2**	56.66	<5
25	X = F R' = CH_3	**P1**	>200	<5
26	X = F R' = CH_3	**P2**	5.86	20
27	X = F R' = CF_3	**P1**	>200	10
28	X = F R' = CF_3	**P2**	>200	<5

For the purpose of discussion, Mannich base side-chains (**Ar**) maintained from **SAR-1** and carried through to **SAR-2** are highlighted in **Table 3.3**. Compounds **5**, **6**, **14,** and **16** contain Mannich base side-chains **M1**, **P1**, **M2,** and **P2,** respectively. These abbreviated Mannich base side-chains are used to describe the **Ar** groups for compounds **17**–**28** from **SAR-2**. Most compounds were shown to be active inhibitors of β-hematin formation (**Table 3.3**). To illustrate how PBI core modifications influenced both β-hematin inhibition and solubility, a bar graph was constructed (**Figure 3.3**)**.**

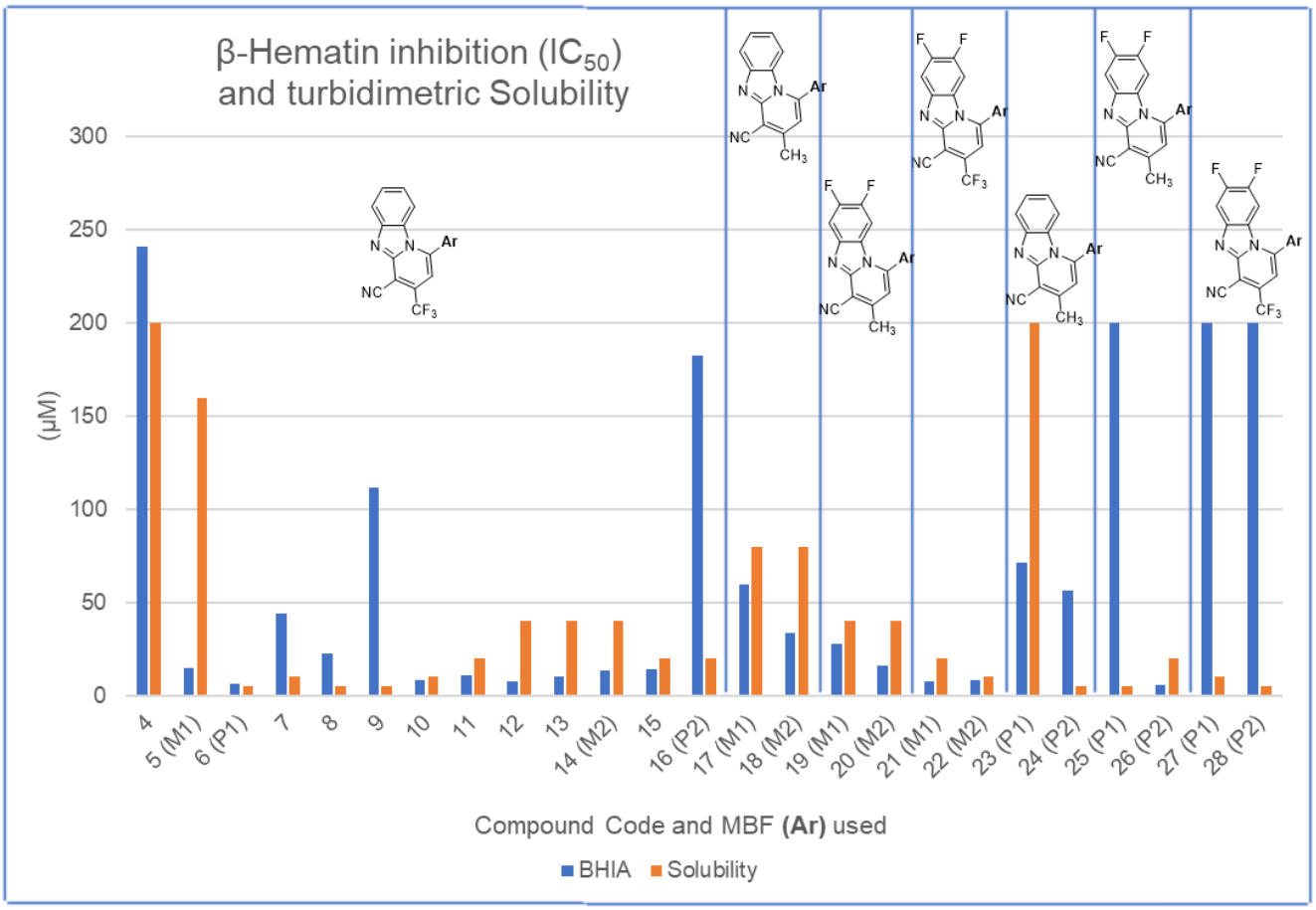

Figure 3.3: Graphical representation of β-hematin inhibition (IC_{50}) and turbidimetric solubility (µM) for all compounds

The most potent inhibitor of synthetic hemozoin formation was **26** (IC_{50} = 5.86 µM). However, there were 16 compounds that inhibited hemozoin formation with an IC_{50} < 50 µM. Of these 16 compounds, 10 were from **SAR-1** (**5–8** and **10–15**), and six were from **SAR-2** (**18–22** and **26)**. Interestingly, although compound **26** was the most potent inhibitor of the β-hematin pathway, parent MBFs (**6**, **16**, and **23–28**) overall exhibited low β-hematin inhibition when compared to desethyl analogues, with the exception of **6** and **26**. Although substitutions made around the PBI core were envisaged to potentially have an influence on β-hematin activity, there was no obvious correlation. Rather, the potential to inhibit the β-hematin pathway seems to correlate more closely with the Mannich base side-chains selected. Compounds **4**, **9**, **16**, **25**, **27**, and **28** showed minimal inhibition of β-hematin with IC_{50} values > 100 µM. In summary, of the 25 PBI analogues, 16 displayed strong potential (IC_{50} < 50), three displayed moderate potential (50 < IC_{50} < 100), and six compounds showed minimal potential to inhibit the

β-hematin formation pathway. There was a correlation between the inhibition of the β-hematin inhibition and the antiplasmodium activity of compounds. Compounds with potent antiplasmodium activity (IC_{50} < 2 µM) showed the highest inhibition of the β-hematin formation. Exceptions of this trend are compounds **16**, **25**, and **28**, which have good antiplasmodium activity with poor inhibition of the β-hematin formation, which may indicate an alternative mechanism of action for these compounds.

As mentioned, the solubility of compounds was tested via a turbidimetric solubility assay. The solubility concentration values obtained are shown in **Table 3.3** and are graphically presented in **Figure 3.4.** Turbidity was detected by measuring the ultraviolet-visible (UV-VIS) absorbance of the suspension at 620 nm as most compounds, including those synthesized, do not absorb light in this region. The positive control used was a solution of the compound in dimethyl sulfoxide (DMSO). The aqueous solubility of compounds was defined as a point of inflection from the baseline of a graph (DMSO plot) showing corrected absorbance at 620 nm and compound concentration, as shown for compounds **17** and **21** in **Figure 3.4**.

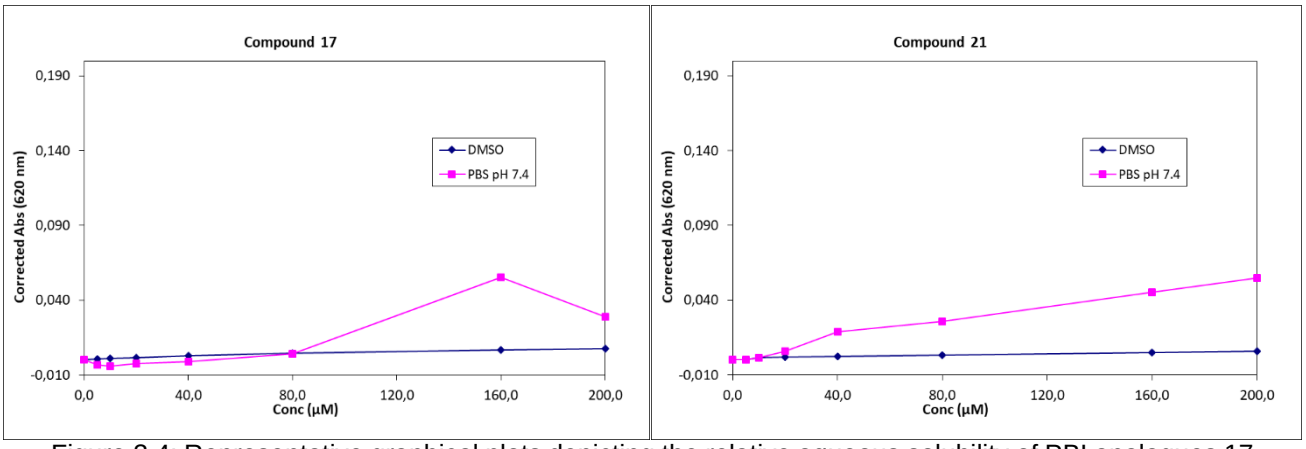

Figure 3.4: Representative graphical plots depicting the relative aqueous solubility of PBI analogues 17 and 21

The majority of the compounds showed low (<20 µM) or moderate solubility (20–100 µM; **Table 3.3**). Three compounds (**4**, **5,** and **23**) did, however, display high solubility. Compound **4** (200 µM) is used as a reference compound as it is the only analogue that does not contain a Mannich base side-chain.

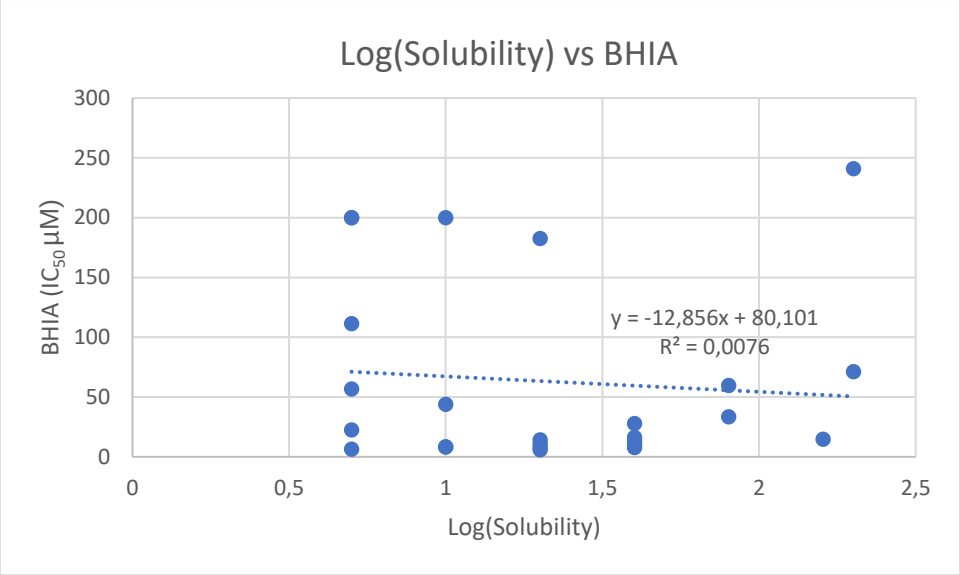

Figure 3.5: Plot of Log[Solubility] vs β-Hematin inhibition assay IC_{50}.

In an attempt to correlate the potential for a compound to inhibit synthetic hemozoin formation with solubility, a graph of the β-hematin inhibition assay (BHIA) vs Log(Solubility) was plotted (**Figure 3.5**). It is expected that increased solubility correlates with a decrease in the IC_{50} value determined for the BHIA, relating to more soluble compound's ability to inhibit the beta-hematin formation pathway than insoluble ones which are likely to aggregate in solution. From the figure above, there is evidently no correlation between the BHIA and solubility for this series of compounds with an R^2 value of <0.01. This could be due to the similarity of all the compounds across the series, since modest modifications are introduced focusing on microsomal metabolic liabilities, rather than an exploration of various solubilizing groups as in a structure-property relationship (SPR) guided project. This results in a flat series of compounds with little chemical diversity which could be addressed by introducing substituents from various regions of a Craig-plot to gauge the correlation between inhibition of β-hematin formation and solubility.

3.5 Cytotoxicity evaluation

Table 3.4: Cytotoxicity of target compounds

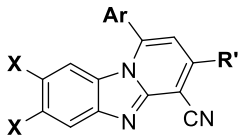

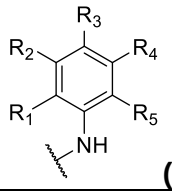

(Ar)

Compound	PBI Core **X**, **R'**	Mannich base fragment (**Ar**)	Cytotoxicity	
			HepG2 (% toxicity)	CHO IC_{50} (µM)
4	X = H, R' = CF_3	**R_1** = H, **R_2** = H, **R_3** = OH, **R_4** = H, **R_5** = H	-156.3	
5	X = H, R' = CF_3	**R_1** = H, **R_2** = CH_2NHEt, **R_3** = OH, R_4 = H, **R_5** = H **(M1)**	-97.3	41.71
6	X = H, R' = CF_3	**R_1** = H, **R_2** = $CH_2N(Et)_2$, **R_3** = OH, R_4 = H, **R_5** = H **(P1)**	-148.7	
7	X = H, R' = CF_3	**R_1** = H, **R_2** = OH, **R_3** = CH_2NHEt, **R_4** = H, **R_5** = H	-13.9	
8	X = H, R' = CF_3	**R_1** = H, **R_2** = CH_2NHEt, **R_3** = F, R_4 = H, **R_5** = H	- 55.9	
9	X = H, R' = CF_3	**R_1** = H, **R_2** = CH_2NHEt, **R_3** = Cl, R_4 = H, **R_5** = H	-	
10	X = H, R' = CF_3	**R_1** = OH, **R_2** = CH_2NHEt, **R_3** = H, R_4 = F, **R_5** = H	-	
11	X = H, R' = CF_3	**R_1** = OH, **R_2** = CH_2NHEt, **R_3** = Cl, R_4 = H, **R_5** = H	-	
12	X = H, R' = CF_3	**R_1** = OH, **R_2** = CH_2NHEt, **R_3** = H, R_4 = Cl, **R_5** = H	-	
13	X = H, R' = CF_3	**R_1** = OH, **R_2** = CH_2NHEt, **R_3** = H, R_4 = H, **R_5** = Me	-	
14	X = H, R' = CF_3	**R_1** = OH, **R_2** = CH_2NHEt, **R_3** = H, R_4 = Me, **R_5** = H **(M2)**	17.3	
15	X = H, R' = CF_3	**R_1** = OH, **R_2** = CH_2NHEt, **R_3** = H, R_4 = H, **R_5** = H	-	
16	X = H, R' = CF_3	**R_1** = OH, **R_2** = $CH_2N(Et)_2$, **R_3** = H, R_4 = Me, **R_5** = H **(P2)**	49.7	29.84
17	X = H, R' = CH_3	**R_1** = H, **R_2** = CH_2NHEt, **R_3** = OH, R_4 = H, **R_5** = H **(M1)**	0	-
18	X = H, R' = CH_3	**R_1** = OH, **R_2** = CH_2NHEt, **R_3** = H, R_4 = Me, **R_5** = H **(M2)**	24.2	29.07
19	X = F, R' = CH_3	**R_1** = H, **R_2** = CH_2NHEt, **R_3** = OH, R_4 = H, **R_5** = H **(M1)**	0	46.54

20	X = F, R' = CH_3	**R_1** = OH, **R_2** = CH_2NHEt, **R_3** = H, R_4 = Me, **R_5** = H **(M2)**	22.3	30.67
21	X = F, R' = CF_3	**R_1** = H, **R_2** = CH_2NHEt, **R_3** = OH, R_4 = H, **R_5** = H **(M1)**	37.8	-
22	X = F, R' = CF_3	**R_1** = OH, **R_2** = CH_2NHEt, **R_3** = H, R_4 = Me, **R_5** = H **(M2)**	26.5	-
23	X = H, R' = CH_3	**R_1** = H, **R_2** = $CH_2N(Et)_2$, **R_3** = OH, R_4 = H, **R_5** = H **(P1)**	100	> 50
24	X = H, R' = CH_3	**R_1** = OH, **R_2** = $CH_2N(Et)_2$, **R_3** = H, R_4 = Me, **R_5** = H **(P2)**	100	> 50
25	X = F, R' = CH_3	**R_1** = H, **R_2** = $CH_2N(Et)_2$, **R_3** = OH, R_4 = H, **R_5** = H **(P1)**	56.1	> 50
26	X = F, R' = CH_3	**R_1** = OH, **R_2** = $CH_2N(Et)_2$, **R_3** = H, R_4 = Me, **R_5** = H **(P2)**	83.1	28.06
27	X = F, R' = CF_3	**R_1** = H, **R_2** = $CH_2N(Et)_2$, **R_3** = OH, R_4 = H, **R_5** = H **(P1)**	37.8	-
28	X = F, R**'** = CF_3	**R_1** = OH, **R_2** = $CH_2N(Et)_2$, **R_3** = H, R_4 = Me, **R_5** = H **(P2)**	3.7	> 50

Synthesized analogues from **SAR-1** and **SAR-2** were evaluated for *in vitro* cytotoxicity against HepG2 cells as a single-point concentration assay at 2 µM, and selected compounds were evaluated against CHO cells to determine the compound concentration value detrimental to cell survival. For HepG2 cytotoxicity studies, a compound leading to >50% cell death was regarded as cytotoxic and in CHO studies compounds which had an IC_{50} < 20 µM were regarded as cytotoxic (**Table 3.4**). All **SAR-1** compounds evaluated against HepG2 cells were non-cytotoxic at 2 µM. The negative cytotoxicity values (**Table 3.4**) indicate treated cells that proliferated, in comparison to the control cell line (untreated), thus confirming the compounds are non-cytotoxic. Furthermore, compounds **5** and **16** showed no cytotoxicity against CHO cells.

SAR-2 compounds were generally non-cytotoxic in both HepG2 and non-cytotoxic in all CHO cells. Cytotoxicity was observed for compounds **23** (100% HepG2 toxicity), **24** (100% HepG2 toxicity), **25** (56.1% HepG2 toxicity) and **26** (83.1% HepG2 toxicity). in HepG2 cells. Compounds **23 – 26** showed cytotoxicity against HepG2 but not CHO cells. These observations highlight the importance of testing across multiple cell lines, as susceptibility across various cell lines may vary.

3.6 Microsomal stability studies on SAR-2 compounds

The most potent (IC_{50} < 2 µM) PBIs were selected for *in vitro* microsomal metabolic stability. This assay was conducted by Dr Mathew Njoroge at the UCT Drug Discovery and Development Centre, H3D. The protocol used for the microsomal stability assay is described in detail in Chapter 5. The LC-MS/MS mass peak readout was used to determine the percentage remaining compound after 30 min incubation with MLMs (**Table 3.5**). For illustrative purposes, microsomal stability is also graphically presented in **Figure 3.6**.

Table 3.5**:** *In vitro* metabolic stability in mouse liver microsomes

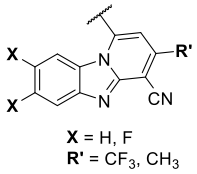

PBI core

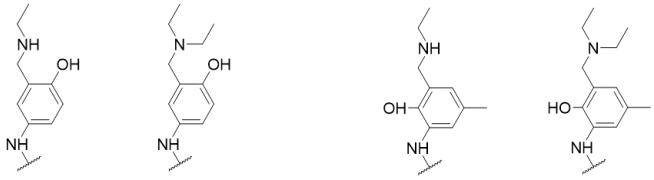

Mannich base fragments (MBFs)

Compound	PBI core **X**, **R'**	MBF **M1, P1, M2, P2**	Microsomal stability in **MLMs** **% remaining after 30 min**
5	X = H R' = CF_3	M1	-
6	X = H R' = CF_3	P1	12.05
14	X = H R' = CF_3	M2	>99
16	X = H R' = CF_3	P2	28.91
17	X = H R' = CH_3	M1	-
18	X = H R' = CH_3	M2	34.96
19	X = F R' = CH_3	M1	>99
20	X = F R' = CH_3	M2	63.19
21	X = F R' = CF_3	M1	-
22	X = F R' = CF_3	M2	-
23	X = H R' = CH_3	P1	60.35
24	X = H R' = CH_3	P2	7.58
25	X = F R' = CH_3	P1	51.18
26	X = F R' = CH_3	P2	17.48
27	X = F R' = CF_3	P1	-
28	X = F R' = CF_3	P2	5.20

.

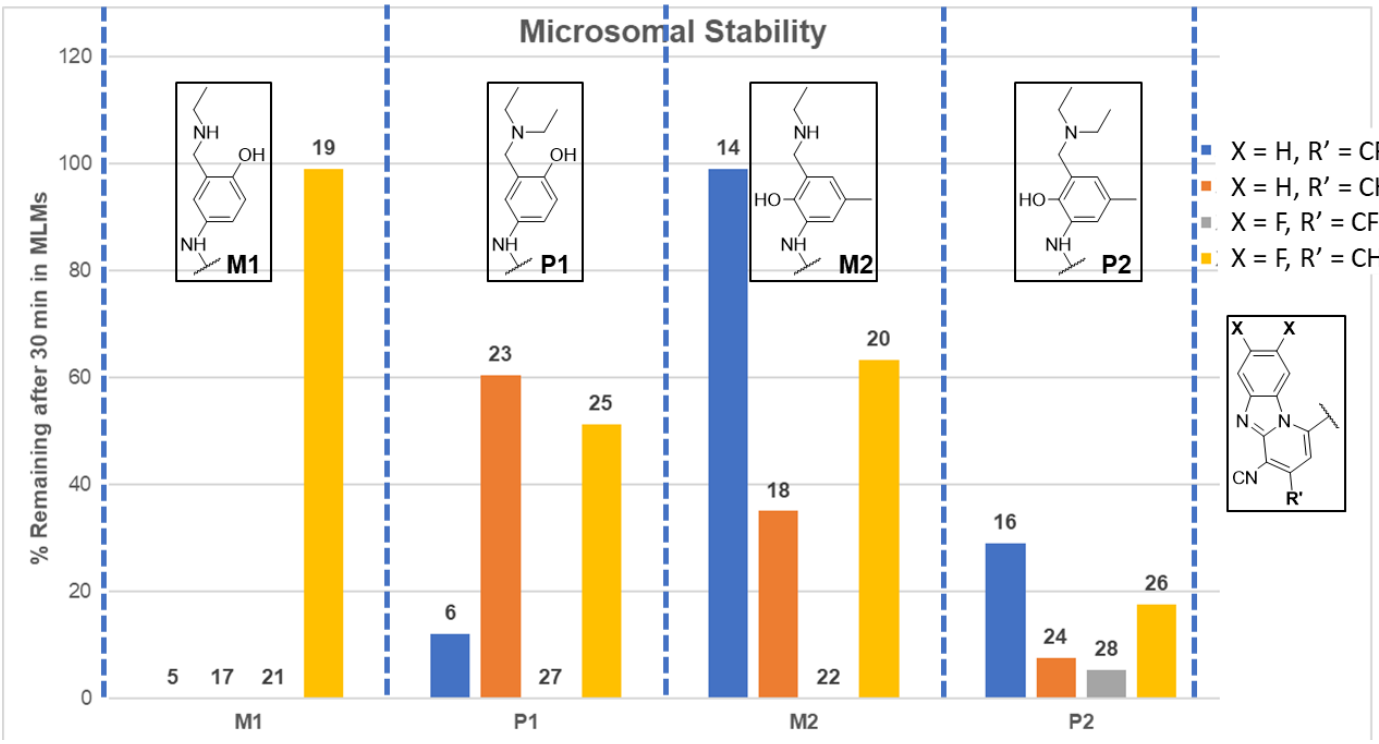

Figure 3.6: SAR-2 selected compounds evaluated for microsomal stability in mouse liver microsomes (MLMs)

Two PBI analogues from **SAR-2** displayed high stability in MLMs, showing >99% remaining after 30 min incubation. The poor microsomal stability shown by compound **16** is likely a result of the metabolically labile *N,N*-diethyl moiety, which undergoes rapid mono-desethylation. Similarly, compound **25** showed moderate microsomal stability (51.18% remaining), which is likely also due to mono-desethylation.

When comparing the parent and desethyl metabolite of compounds containing the same PBI core, the most metabolically stable compounds contained the monoethylated desethyl metabolite Mannich base side-chain as opposed to the diethylated parent Mannich base side chain. Exemplified by monoethylated compound **14**, the most stable compound (**X** = H, **R'** = CF_3, blue bar, notably from **SAR-1**) with >99% parent compound remaining after 30 min. Conversely, diethylated compound **18** (**X** = H, **R'** = CH_3; orange bar) exhibited overall reduced metabolic stability through with approximately 35% remaining. Difluorination (where **X** = F and **R'** = CH_3, yellow bar;) improved metabolic stability with compound **20** showing approximately 60% parent compound remaining after 30 min, an improvement from **18**. A similar trend was observed for analogues **16**, **24**, **26** and **28,** with the most stable PBI core containing **X** = H and **R'** = CF_3 observed for **16** (28.91% remaining), followed by a drop

in microsomal stability for compound **24** (7.58% remaining) and a slight increase through difluorination as in compound **26** (17.48% remaining) and low microsomal stability for **28** (5.20% remaining).

In contrast to these trends observed for **14** and **16**, the most stable compound of the P1 analogues was compound **23** (60.35% remaining), where **X** = H and **R'** = CH_3. Furthermore, the effect of simultaneous difluorination and methyl substitution resulted in a decrease in metabolic stability as seen in compound **25** (51% remaining). Although compound **19** (**X** = F and **R'** = CH_3) showed very high microsomal stability, with >99% parent compound remaining after 30 min, there were no analogues containing the **M1** Mannich base side-chain showing potent antiplasmodium activity to prioritize microsomal stability testing.

In summary, the nature of the Mannich base side chain, when comparing the same PBI-core, influenced the *in vitro* microsomal stability of compounds with desethyl metabolites showing greater stability than their corresponding parent compounds. The effects of PBI core modification on microsomal metabolic stability were not obvious and would need to be investigated further as part of future work.

Compounds **14** and **19** exhibited high microsomal metabolic stability and are potential candidates for *in vivo* antimalarial efficacy studies. It is important to note that compounds **14** and **19** are hypothesized desethyl metabolites of parent compounds **16** and **25** respectively (**Figure 3.7**). The rapid metabolism of both these parent compounds is likely due to the metabolically labile *N,N*-diethyl moiety, which undergoes rapid mono-desethylation. This hypothesis would need to be investigated through metabolite identification studies of parent compounds to confirm the presence of desethyl metabolites.

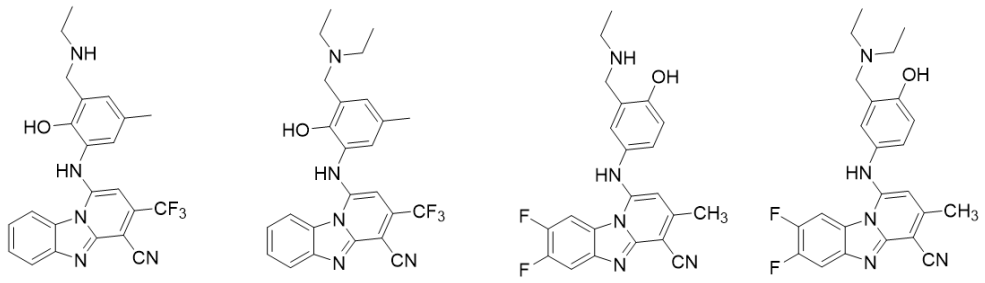

Figure 3.7: Compounds **14** and **19** exhibiting high microsomal metabolic stability and their respective parent compounds **16** and **25.**

CHAPTER 4: Summary, conclusions, and recommendations for future work

4.1 General summary and conclusions

Two series of PBI compounds containing various Mannich base side-chains were successfully synthesized for antiplasmodium structure-activity relationship studies. They were characterized using spectroscopic (^{1}H-NMR, ^{13}C-NMR, and LC-MS), and melting point determination.

SAR-1 specifically investigated the activity of hypothesized *N*-dealkylated metabolites, which were further investigated in **SAR-2** alongside their corresponding parent compounds, whilst simultaneously investigating the effect of modifications around the PBI core. **SAR-2** modifications included systematic changes at the **R'-** and **X**-positions (**Figure 4.1**) via difluorination (**X** = F) to improve microsomal metabolic stability and antiplasmodium potency, and replacement of the CF_3 substituent with a CH_3 group, along with a combination of both difluorination and replacement of the CF_3 substituent with a CH_3 group. The antiplasmodium activities of all synthesized compounds were evaluated against the NF54 strain of *P. falciparum*, as was their ability to inhibit the formation of β-hematin. Solubility was also determined using the turbidimetric kinetic solubility assay. Finally, the cytotoxicity of compounds showing high antiplasmodium activity (IC_{50} < 2 µM) was evaluated in HepG2 and CHO cell lines and their microsomal stability determined in MLMs.

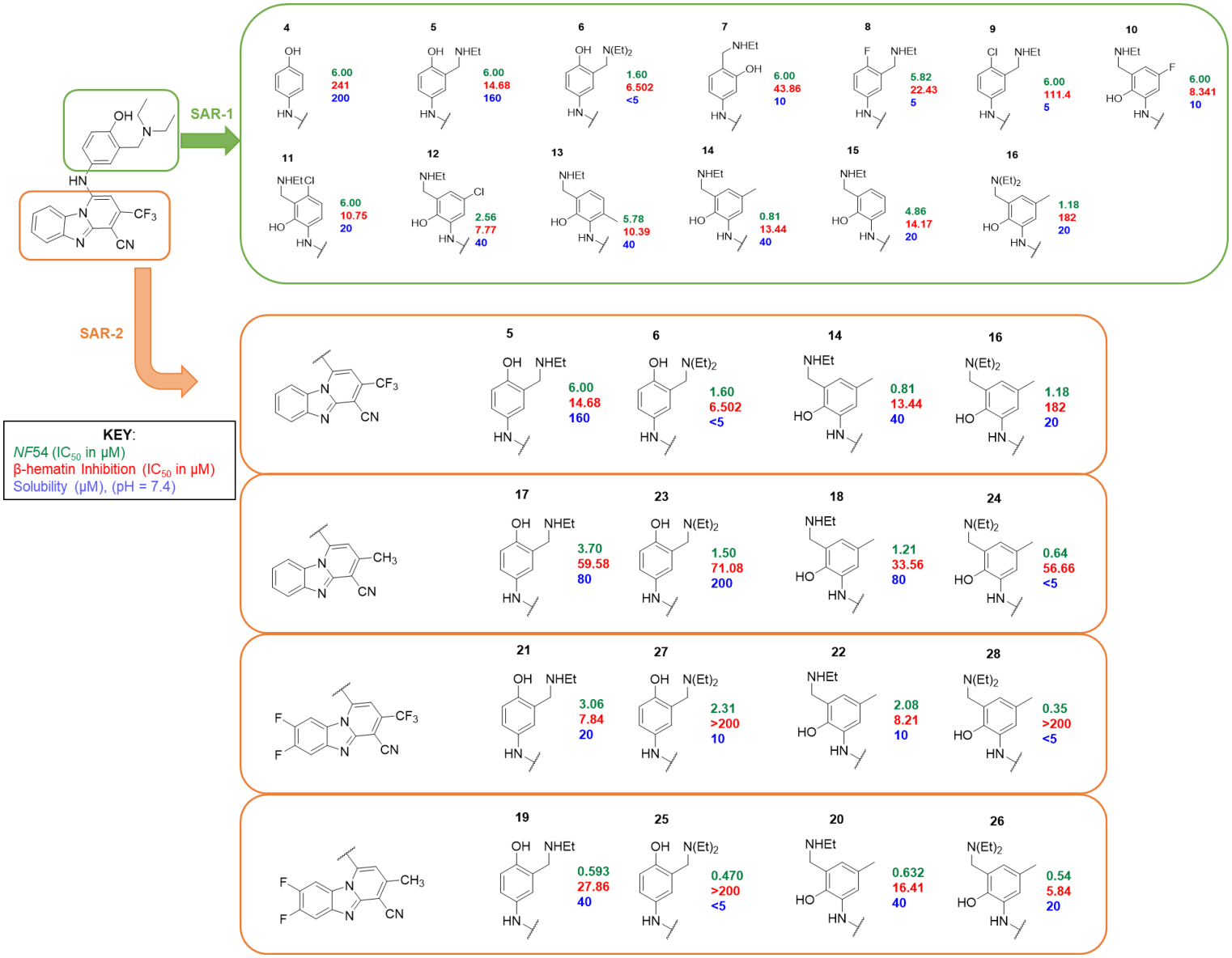

Figure 4.1: Summary of antiplasmodium activity, β-hematin inhibition, and turbidimetric solubility for final compounds from SAR-1 and SAR-2

In summary, the following observations were made with regard to **SAR-1** compounds:

- Three compounds showed high antiplasmodium activity (IC_{50} < 2 µM).
- The hydroxyl group on the Mannich base side-chain appears to be crucial for antiplasmodium activity since its replacement with a halogenation was detrimental to activity.
- Analogues containing 1,4-aminophenol and 1,2-aminophenol moieties both showed high antiplasmodium activity, as exemplified by **6**, **14**, and **16**.

- Most compounds potently inhibited the formation of synthetic hemozoin (β-hematin) and are therefore likely inhibitors of the hemoglobin degradation pathway.
- Only two compounds showed high solubility, whereas poor and moderate solubility was observed for the remaining 11 analogues.
- This series of compounds showed no cytotoxicity against HepG2 cells.

The MBFs of compounds that showed high antiplasmodium activities (**4, 6,** and **16**) were investigated further in parent-desethyl metabolite pairs in **SAR-2,** with simultaneous modifications around the PBI core.

In summary, the following observations were made with regard to **SAR-2** compounds:

- Eight compounds showed high antiplasmodium activity (IC_{50} < 2 µM).
- High antiplasmodium activity was observed in both parent and hypothesized metabolite regardless of modifications made around the PBI core.
- A combination of difluorination and substitution of the CF_3 with a methyl group resulted in the most potent compounds.
- Most compounds potently inhibited the formation of synthetic hemozoin and are likely inhibitors of the hemoglobin degradation pathway.
- In general, synthesized desethyl metabolites were more soluble than their corresponding parent compounds.
- All compounds showed poor or moderate solubility, with the exception of one compound that was highly soluble.
- Four compounds showed cytotoxicity against HepG2 and CHO cells.
- Three compounds showed moderate microsomal stability while two compounds showed high stability (> 99% remaining after 30 min) when incubated in MLMs
- In general, synthesized desethyl metabolites showed greater stability in MLMs than their corresponding parent analogues, presumably due to rapid *N*-dealkylation of the parent analogues.

4.2 Future outlook and recommendations

- Metabolite identification should be performed on potent parent analogues to confirm the hypothesis that rapid *N*-dealkylation is responsible for the poor microsomal stability observed in parent analogues and also identify other metabolic soft spots.
- Strategies aiming to improve the solubility of compounds should be employed to enhance the physicochemical profiles of compounds in this series for progression to *in vivo* animal model studies. The recommended changes to improve the aqueous solubility of future compounds are shown in **Figure 4.2**.

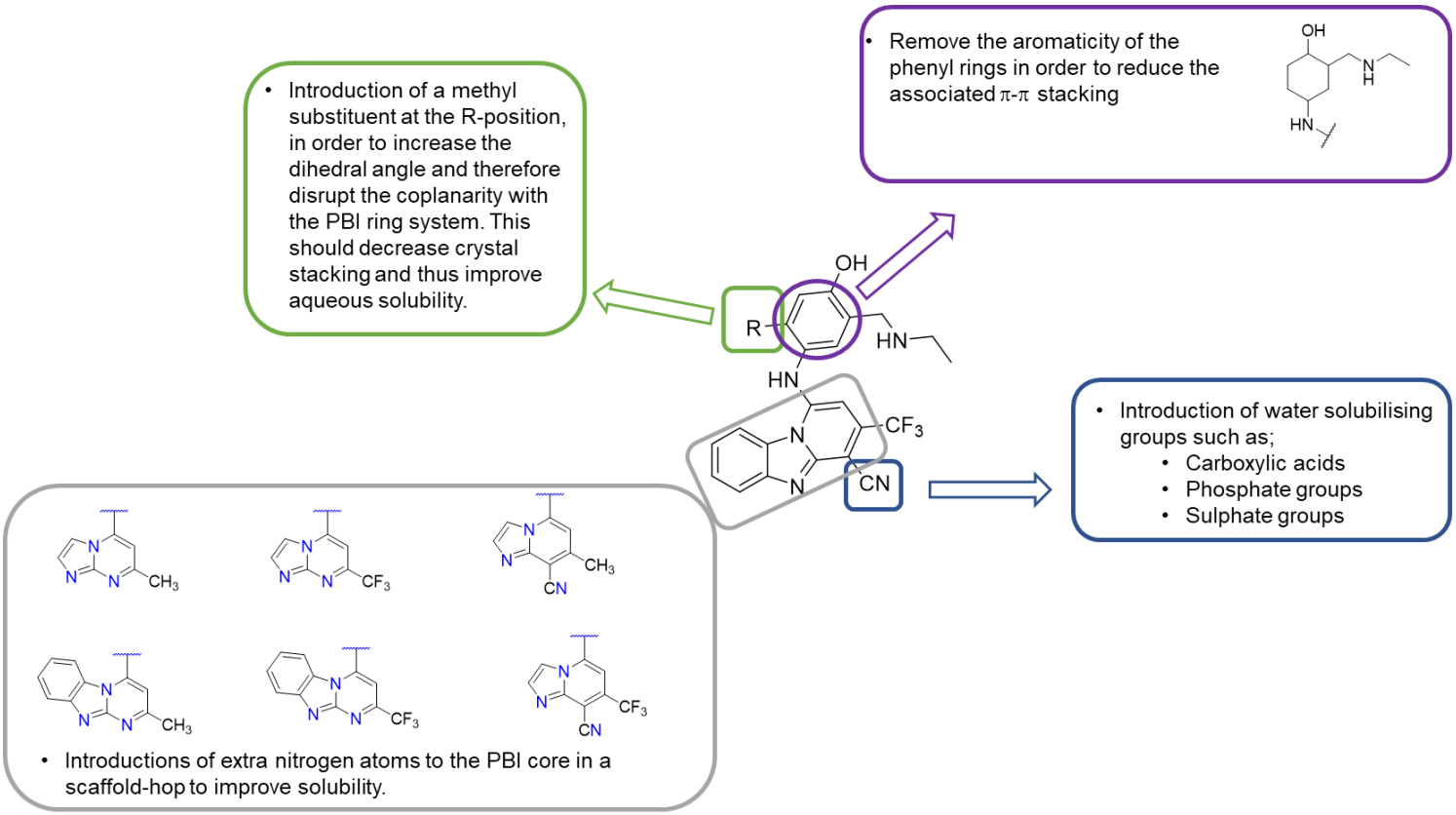

Figure 4.2: Recommended future work to improve aqueous solubility of compounds.

CHAPTER 5: Experimental

5.1 Chapter overview

This chapter supplements the results from chapters 2 and 3 by describing the detailed experimental protocols involved, particularly those that have not been outlined in the main text. In addition, this chapter provides characterization data for all compounds synthesized.

5.2. Biology

5.2.1. *In vitro* antiplasmodium evaluation protocols

Lactate dehydrogenase assay for asexual blood-stage parasites

Samples were tested in triplicate on one occasion against the CQ-sensitive NF54 strain of *P. falciparum*. Continuous *in vitro* cultures of asexual erythrocyte-stage *P. falciparum* were maintained using a modified version of the method described by Trager and Jensen.[97] *In vitro* antiplasmodial activity was quantitatively determined via a parasite lactate dehydrogenase assay. Test samples were prepared as 20-mg/mL stock solution in 100% DMSO or were tested as suspensions if not completely dissolved. Stock solutions were stored at low temperatures of -20 °C. Further dilutions were prepared on the day of the experiment. CQ and artesunate served as reference drugs in all experiments. A full dose-response analysis was performed on all test compounds to determine the concentration inhibiting 50% parasite growth (IC_{50}). Compounds were initially tested at a concentration of 100 µg/mL, which was then serially diluted 2-fold to produce 10 solutions (0.2 µg/mL being the lowest concentration). The same dilution technique was used for all samples. Reference drugs were tested at a starting concentration of 1000 ng/mL. The highest concentration of solvent to which the parasites were exposed had no measurable effect on parasite viability. IC_{50} values were obtained using a non-linear dose-response curve fitting analysis using GraphPad Prism v.4.0 software.

Luciferase reporter assay for early and late gametocyte parasites

A luciferase reporter assay[95] was established to enable accurate, reliable, and quantifiable investigations of the stage-specific action of gametocytocidal compounds in the early- and late-stage gametocyte marker cell line NF54-PfS16-GFP-Luc. Drug assays were set up on days 5 and 10 (representing >90% of early stage II/III or mature stage IV/V gametocytes, respectively). In each instance, assays were set up using parasite culture containing 2–3% gametocytemia and 1.5% hematocrit, which were incubated for 48 h under drug pressure in a gas chamber (90% N_2, 5% O_2, and 5% CO_2) at 37 °C. Luciferase activity was determined in 30 µL parasite lysates by adding 30 µL luciferin substrate (Promega Luciferase Assay System) at room temperature and the resultant bioluminescence was detected at an integration constant of 10 s using the GloMax® Explorer Detection System and Instinct® Software. Methylene blue (5 µM) and internal project specific controls (MMV390048, 5 µM) are routinely included as controls. Dual point screens are routinely performed as technical triplicates for a single biological assay.

β-hematin inhibition assay

This assay quantifies the inhibition of β-hematin formation at a particular drug concentration. It involves the addition of pyridine solution, which complexes with free heme (absorbance at 405 nm) but not β-hematin, thus allowing for quantification of hemozoin formation. The controls used were CQ and AQ, both known β-hematin-inhibiting antimalarials, and the non-inhibitor pyrimethamine. Stock solutions of controls and test compounds (20 mM) were prepared in DMSO. A solution containing water/305.5 µM NP40/DMSO at a v/v ratio of 70%/20%/10% respectively, was added to every well in columns 1-11 while 140 µL water and 40 µL 305.5 µM NP40 were added to column 12 to mediate the formation of β-hematin. Drug (20 µL, 20 mM) was added to column 12 and 100 µL of this solution was serially diluted to column 2, with column 1 left as the blank (no compound). In case the compound was colored, the absorbance was pre-measured at 405 nm on a SpectraMax plate-reader. A 178.8-µL aliquot of hematin stock was suspended in 20 mL 1 M acetate buffer (pH 4.9) and 100 µL of this hematin suspension was added to each well. Plates were then incubated for

5 h at 37 °C after which 32 µL pyridine solution (20% water, 20% acetone, 10% 2 M HEPES buffer (pH 7.4), 50% pyridine) was added. This was followed by addition of 60 µL acetone to all wells. Plate absorbance was measured again at 405 nm and IC_{50} values were plotted using GraphPad 6 software.

3.6.2 Cytotoxicity evaluation protocols

Cytotoxicity evaluation in CHO cells

The *in vitro* cytotoxicity of the compounds synthesized was evaluated in CHO cancer cells using 3-(4,5-dimethylthiazolyl-2)-2,5-diphenyltetrazolium bromide (MTT), a colorimetric assay based on assessing cellular metabolic activity.[98] The compounds synthesized were assayed in triplicate. Stock solutions of test samples (2 mg/mL) were prepared in DMSO and poorly soluble samples were tested as suspensions. The compounds were stored at -20 °C until use. In all experiments, emetine was used as a reference drug. Starting with an initial concentration of 100 µg/mL, 10-fold serial dilutions were made in complete medium to obtain six solutions (lowest concentration = 0.001 µg/mL). Cell viability was not affected by the highest concentration of solvent used. Full dose-response curves were plotted using a non-linear dose-response curve fitting analysis in GraphPad Prism v.4 software and the minimum concentration required for 50% inhibition (IC_{50}) was determined for each compound.

Cytotoxicity evaluation in HepG2 cells

The compounds' cytotoxicity was determined in HepG2 cells using a CytoSelect™ LDH Cytotoxicity Assay Kit (Cell Biolabs Inc., CBA-241) at 2 µM for 48 h. Screens were performed as technical duplicates for three biological assays. HepG2 cells were maintained as previously described[99] in Dulbecco's modified Eagle's medium (DMEM, HyClone) supplemented with 5% heat-inactivated fetal bovine serum (FBS) and 1% penicillin/streptomycin (Sigma-Aldrich) at 37 °C in 5% CO_2. Cell viability was monitored microscopically using 0.2% Trypan blue. Cells were treated with trypsin (1× Trypsin-EDTA, Sigma) and approximately 1×10^5 cells were plated in 96-well plates

and incubated for 24 h. The cells were treated with 2 μM compound and incubated for a further 48 h at 37 °C in 5% CO_2. Cytotoxicity was determined using a CytoSelect™ LDH Cytotoxicity Assay Kit and the reagent was added to the supernatant before measuring absorbance at 450 nm. Data obtained were analyzed in Excel and experiments were performed in technical duplicates for one biological repeats (n = 1).

3.7 Metabolic stability

This assay was conducted by Dr Mathew Njoroge at the Division of Clinical Pharmacology, UCT. In this study, MLMs were selected as it was anticipated that *in vivo* PK and efficacy studies would be conducted in mouse models, if compounds were to be progressed to *in vivo* studies. Briefly, a single time-point (30-min) assay protocol was used. Test compounds were appropriately diluted to 0.1 μM using phosphate buffer at pH 7.4 in a 96-well microtiter plate. MLMs (0.4 mg/mL) were then added into the wells along with NADPH, which served as an enzyme cofactor for initiation of the enzymatic reactions involved. This mixture was then incubated at 37 ºC for 30 min, with shaking, and the reaction was stopped by the addition of ice-cold acetonitrile. The mixture was then centrifuged to remove proteins as sediments, while the supernatant was analyzed via LC-MS/MS. This readout was used to determine the percentage intact compound remaining after 30 min of incubation with MLMs.

5.3 Chemistry

5.3.1 Reagents and solvents

All commercially available chemicals and reagents were purchased from either Sigma-Aldrich or Combi-Blocks Limited (USA), and were used without prior purification. Anhydrous solvents such as 1,4-dioxane, acetonitrile, and DMF were purchased as such from Sigma-Aldrich. In addition, column chromatography solvents such as ethyl acetate, DCM, hexane (Hex), and methanol were purchased as analytical reagent (AR)-grade solvents from Kimix Chemicals, South Africa, and used directly. HPLC-grade acetonitrile and methanol for LC-MS (ESI^+) mobile phase preparation were purchased from Romil Ltd (Cambridge, UK).

5.3.2 Physical and spectroscopic characterization

Reported compounds were characterized via ^{1}H-NMR, ^{13}C-NMR, HPLC-MS (ESI^{+}), and melting point determination. Melting points were determined using a Lasec Stuart SMP40 hot-stage microscope and are reported as uncorrected values. NMR spectra were recorded on a Varian Mercury spectrometer (^{1}H, 300 MHz; ^{13}C, 75 MHz), Bruker Ultrashield-Plus Spectrometer (^{1}H, 400 MHz; ^{13}C, 101 MHz), or Bruker Ascend™-600 spectrometer (^{1}H, 600 MHz; ^{13}C, 150 MHz). Samples for NMR spectroscopy were prepared by dissolving in deuterated DMSO (DMSO-d_6), or methanol (methanol-d_4). Chemical shifts (δ) are reported in parts per million (ppm) and are rounded to two decimal places, while coupling constants (J) are reported in Hz and are rounded to one decimal place. Abbreviations used to describe ^{1}H-NMR signal multiplicities include: d (doublet), dd (doublet of doublets), ddd (doublet of doublet of doublets), dt (doublet of triplets), dtd (doublet of triplet of doublets), hept (heptet), m (multiplet), q (quartet), s (singlet), t (triplet), td (triplet of doublets), tdd (triplet of doublet of doublets), and tt (triplet of triplets). ^{13}C-NMR spectra were recorded in complete proton-decoupled mode and chemical shifts are listed without assigning to the corresponding carbon atoms, a format accepted by most international journals. The splitting patterns observed in the ^{13}C-NMR spectra as a result of fluorine splitting were reported as either a doublet (d) or quartet (q) and *J* values were not recorded but were reported in the form d or q, *CJF*.

5.3.3 Chromatography

Target compound peak purity, retention time, and molecular ions were determined using an Agilent HPLC system equipped with Agilent 1260® Infinity Binary Pump, Agilent 1260® Infinity Diode Array Detector (DAD), Agilent 1290® Infinity Column Compartment, Agilent 1260® Infinity Autosampler, Agilent 6120® Quadrupole LC/MS, and Peak Scientific® Genius 1050 Nitrogen Generator. The column used was an X-bridge® C18, 2.5 µm, 3.0 mm (ID) × 50 mm (length) maintained at 35 °C. The composition and gradient conditions of the mobile phase used at a flow rate of 0.9 mL/min are listed in **Table 5.1**. The injection volume was 2 µL and mass spectra were obtained both via ESI^{+} and atmospheric pressure chemical ionization (APCI). All

reported LC-MS (ESI^+) purity values were based on maximum chromatograms resulting from DAD (210–640 nm) scans.

Table 5.1: HPLC gradient conditions

Time (min)	%A	%B
0.00-1.00	90	10
1.00-3.00	5	95
3.00-5.00	5	95
5.00-6.50	90	10
6.50-7.00	90	10

A, 10 mM NH_4OAc in buffer (0.4% acetic acid); B, 10 mM NH_4OAc (0.4% acetic acid) in 90% HPLC grade CH_3OH in H_2O

Reactions were monitored via analytical TLC using Fluka or Merck F254 aluminium-backed pre-coated silica gel plates, which were visualized under UV light at a wavelength of 254 or 366 nm. Staining was performed in some instances to facilitate direct visualization. Gravity column chromatography was performed using Merck Kieselgel® 60 (70–230 mesh) silica gel, while Biotage SNAP® cartridges were packed with 40–65 µm diameter KP-Sil silica gel for flash column chromatography on a Biotage Isolera One® system (Biotage AB, Uppsala, Sweden).

5.4 Synthesis and characterization

5.4.1 Synthesis and characterization of PBI intermediates

2-(5,6-difluoro-1H-benzo[d]imidazol-2-yl)acetonitrile **(1.1a)**

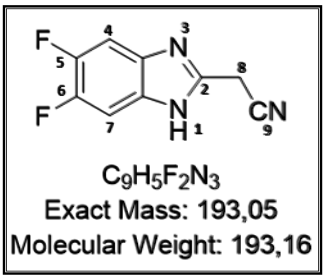

A mixture of commercially available 4,5-difluorobenzene-1,2-diamine (0.500 g, 1.0 eq) and ethyl carbonocyanidate (1.11 mL, 3.0 eq) was dissolved in anhydrous DMF (5 mL). The mixture was irradiated in a microwave reactor at 100 °C for 7 h. The reaction mixture was left to cool to 23 °C. Cold ethyl acetate (20 mL) was added to the reaction mixture and transferred to a separating funnel. The organic layer was washed with water (4 × 30 mL) to remove residual DMF. The organic layer was dried using magnesium sulphate, filtered and reduced *in vacuo* to isolate **1.1a** as a brown solid (0.605 g, 90%), R_f = 0.61 (5% MeOH/DCM); **^{1}H-NMR (400 MHz, DMSO-*d*$_6$)** δ 7.59 (m, 2H, H7/ H4), 4.38 (s, 2H, H8); **^{13}C-NMR (101 MHz, DMSO-*d*$_6$)** δ 157.88, 149.58, 139.15, 123.69, 121.19, 114.58, 105.57 (d, *CJF*), 102.47, 101.56 (d, *CJF*); **LC-MS (ESI$^+$):** Purity 82% (t_R 1.18 min), m/z 194.1 $[M + H]^+$.

General procedure for cyclocondensation to afford intermediate compounds 1.2a-1.2d

The appropriately substituted or unsubstituted 2-benzimidazole acetonitrile (1.0 eq), appropriate diketo-ester (1.2 eq), and NH_4OAc (2.0 eq) were stirred at 150 °C under pressure for 12 h. The reaction mixture was left to cool to 23 °C. Cold MeCN (20 mL) was added to the mixture and left to cool to 0 °C on ice. The cold mixture was then filtered, the residue washed with cold acetonitrile (4 × 10 mL), and dried *in vacuo* to isolate intermediates **1.2a–1.2d.**

1-oxo-3-(trifluoromethyl)-1,5-dihydrobenzo[4,5]imidazo[1,2-a]pyridine-4-carbonitrile **(1.2a)**

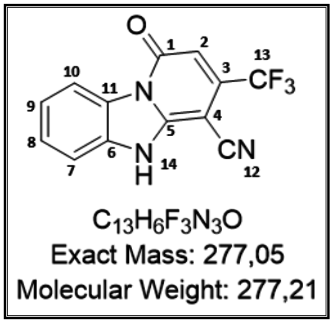

Obtained from commercially available 2-benzimidazole acetonitrile (0.800 g, 1.0 eq), ethyl 4,4,4-trifluoro-3-oxobutanoate (0.89 mL, 1.2 eq), and NH_4OAc (0.785 g, 2.0 eq) to isolate intermediate **1.2a** as a brown powder (1.20 g, 86%), R_f = 0.70 (50% EtOAC/Hex); **^{1}H-NMR (400 MHz, DMSO-*d*$_6$)** δ 8.61 (dd, *J* = 8.2, 1.9 Hz, 1H, H10), 7.65 (dd, *J* = 8.1, 1.8 Hz, 1H, H7), 7.45 (td, *J* = 8.3, 1.2 Hz, 1H, H9), 7.25 (td, *J* = 8.3, 1.1 Hz, 1H, H8), 6.03 (s, 1H, H2); **^{13}C-NMR (101 MHz, DMSO-*d*$_6$)** δ 158.35, 148.52, 138.70, 133.89, 128.18, 127.43, 124.07, 123.01, 121.34, 116.64, 115.02, 112.83, 102.10; **LC-MS (ESI$^+$):** Purity 95%, (t_R 2.97 min), m/z 278.2 $[M + H]^+$.

3-methyl-1-oxo-1,5-dihydrobenzo[4,5]imidazo[1,2-a]pyridine-4-carbonitrile **(1.2b)**

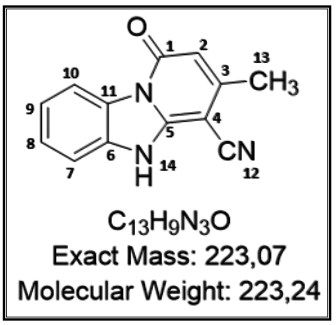

Obtained from commercially available 2-benzimidazole acetonitrile (500 mg, 1.0 eq), ethyl 3-oxobutanoate (0.48 mL, 1.2 eq) and NH_4OAc (491 mg, 2.0 eq) to isolate intermediate **1.2a** as a brown powder (0.650 g, 92%), R_f = 0.39 (50% EtOAC/Hex); **^{1}H-NMR (400 MHz, DMSO-*d*$_6$)** δ 8.49 (d, *J* = 8.0 Hz, 1H, H10), 7.48 (d, *J* = 8.0 Hz, 1H, H7), 7.33 (t, *J* = 7.6 Hz, 1H, H9), 7.12 (t, *J* = 7.6 Hz, 1H, H8), 5.55 (s, 1H, H2), 2.31 (s, 3H, H13); **^{13}C-NMR (101 MHz, DMSO-*d*$_6$)** δ 172.41, 160.28, 151.37, 150.48, 141.10, 130.05, 124.81, 119.54, 115.82, 114.76, 100.03, 71.52, 20.90; **LC-MS (ESI$^+$):** Purity 90%, (t_R 2.36 min), m/z 224.1 $[M + H]^+$.

7,8-difluoro-1-oxo-3-(trifluoromethyl)-1,5-dihydrobenzo[4,5]imidazo[1,2-a]pyridine-4-carbonitrile **(1.2c)**

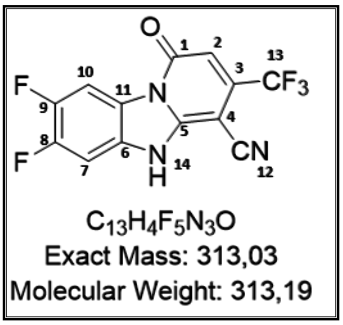

Obtained from **1.1a** (1.2 g, 1.0 eq), ethyl 4,4,4-trifluoro-3-oxobutanoate (1.82 mL, 2.0 eq), and NH_4OAc (0.959 g, 2.0 eq) to isolate intermediate **1.2c** as a brown powder (0.831 g, 43%), R_f = 0.86 (10% MeOH/DCM); **^{1}H-NMR (400 MHz, DMSO-*d*$_6$)** δ 8.48 (dd, *J* = 10.3, 7.4 Hz, 1H, H10), 7.66 (dd, *J* = 10.1, 7.0 Hz, 1H, H7), 6.37 (s, 1H, H2); **^{13}C-NMR (101 MHz, DMSO-*d*$_6$)** δ 157.88, 149.58, 147.28, 139.15, 138.84, 129.92, 123.69, 121.19, 114.58, 105.57 (d, *CJF*), 102.47, 101.56 (d, *CJF*), 65.45; **^{19}F NMR (377 MHz, DMSO-*d*$_6$)** δ -62.98, -136.59 (d, *J* = 21.8 Hz), -142.25 (d, *J* = 21.5 Hz). **LC-MS (ESI$^+$):** Purity 94%, (t_R 2.47 min), m/z 314.1 $[M + H]^+$.

7,8-difluoro-3-methyl-1-oxo-1,5-dihydrobenzo[4,5]imidazo[1,2-a]pyridine-4-carbonitrile **(1.2d)**

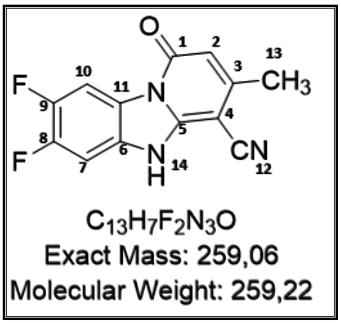

Obtained from **1.1a** (0.600 g, 1.0 eq), ethyl 3-oxobutanoate (0.79 mL, 2.0 eq) and NH_4OAc (0.479 g, 2.0 eq) to isolate intermediate **1.2d** as a brown powder (0.742 g, 86%), R_f = 0.63 (10% MeOH/DCM); **^{1}H-NMR (400 MHz, DMSO-*d*$_6$)** δ 8.35 (dd, *J* = 11.1, 8.1 Hz, 1H, H10), 7.95 (s, 1H, H2), 7.43 (dd, *J* = 11.8, 7.5 Hz, 1H, H7), 2.29 (s, 3H, H13); **^{13}C-NMR (101 MHz, DMSO-d$_6$)** δ 157.04, 142.27, 135.84, 128.16, 125.61, 118.91, 115.54, 112.16, 109.54, 105.97, 102.47, 101.56, 20.68; **LC-MS (ESI$^+$):** Purity 85% (t_R 2.82 min), m/z 260.1 $[M + H]^+$.

General procedure for chlorination to afford intermediate compounds 1.3a–1.3d

The appropriate intermediates **1.2a-1.2d** (1.0 eq) were mixed with excess phosphorous oxychloride ($POCl_3$, 20 eq) and heated to 130 °C under reflux for 12 h. Excess $POCl_3$ was removed under reduced pressure and the solution was neutralized with $NaHCO_3$ in cold water (50 mL) to a pH of 7-8. The cold mixture was then filtered, and the residue washed with cold water (4 × 10mL). The residue was dried of residual

water by using anhydrous magnesium sulphate in 10% methanol/DCM, then filtered and reduced *in vacuo* to isolate intermediates **1.3a–1.3d.**

1-chloro-3-(trifluoromethyl)benzo[4,5]imidazo[1,2-a]pyridine-4-carbonitrile **(1.3a)**

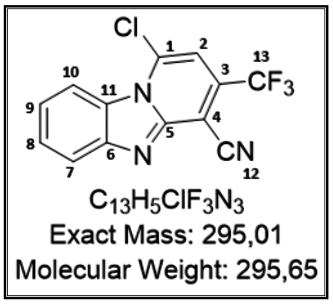

Obtained from **1.2a** (1.0 g, 1 eq) and $POCl_3$ (6.75 mL, 20 eq) to isolate **1.3a** as a yellow powder (956 mg, 90%), R_f = 0.65 (50% EtOAC/Hex); **^{1}H-NMR (400 MHz, DMSO-*d*$_6$)** δ 8.76 (dd, *J* = 8.7, 0.9 Hz, 1H, H10), 8.10 (dd, *J* = 8.3, 1.3 Hz, 1H, H7), 7.81 – 7.74 (m, 2H, H2 & H9), 7.62 (td, *J* = 8.4, 1.2 Hz, 1H, H8); **^{13}C-NMR (101 MHz, DMSO-d$_6$) δ** 158.37, 146.65, 145.30, 137.25, 129.79, 128.31, 127.42, 123.99, 122.99, 120.66, 116.68, 112.90, 107.76; **LC-MS (ESI$^+$):** Purity 94%, (t_R 2.42 min), m/z 296.0 $[M + H]^+$.

1-chloro-3-methylbenzo[4,5]imidazo[1,2-a]pyridine-4-carbonitrile **(1.3b)**

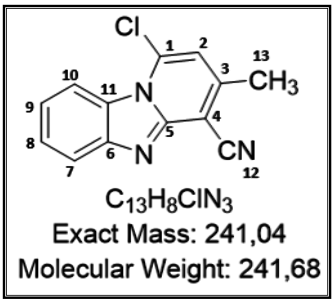

Obtained from **1.2b** (0.650 g, 1.0 eq) and $POCl_3$ (5.45 mL, 20 eq) to isolate **1.3b** as a brown powder (652 mg, 93%), R_f = 0.74 (5% MeOH/DCM); **^{1}H-NMR (400 MHz, DMSO-*d*$_6$)** δ 8.58 (d, *J* = 8.6 Hz, 1H, H10), 7.93 (d, *J* = 8.3 Hz, 1H, H7), 7.63 (t, *J* = 8.2 Hz, 1H, H9), 7.45 (t, *J* = 8.7, Hz, 1H, H8), 7.31 (s, 1H, H2), 2.62 (s, 3H, H13); **^{13}C-NMR (101 MHz, DMSO-d$_6$)** δ 150.29, 147.62, 144.65, 134.22, 129.89, 127.08, 122.47, 120.01, 116.03, 115.03, 114.10, 98.35, 20.68; **LC-MS (ESI$^+$):** Purity 95%, (t_R 2.45min), m/z 242.5 $[M + H]^+$.

1-chloro-7,8-difluoro-3-(trifluoromethyl)benzo[4,5]imidazo[1,2-a]pyridine-4-carbonitrile **(1.3c)**

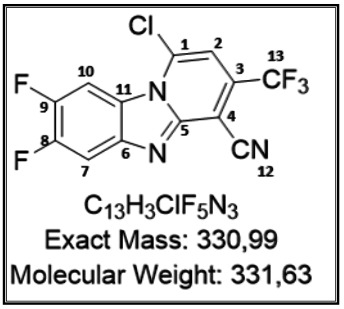

Obtained from **1.2c** (0.890 g, 1.0 eq) and $POCl_3$ (5.16 mL, 20 eq) to isolate **1.3c** as a brown powder (0.784 g, 83%), R_f = 0.81 (10% MeOH/DCM); **^{1}H-NMR (400 MHz, DMSO-*d*$_6$)** δ 8.79 (dd, *J* = 11.1, 7.4 Hz, 1H, H10), 8.19 (dd, *J* = 10.8, 7.6 Hz, 1H, H7), 7.82 (s, 1H, H2); **^{13}C-NMR (101 MHz, DMSO-*d*$_6$)** δ 157.67, 149.10, 147.97, 136.83, 114.23, 112.38, 108.29 (d, *CJF*), 107.71 (d, *CJF*), 105.69 (d, *CJF*), 105.22 (d, *CJF*), 103.26 (d, *CJF*), 101.33 (d, *CJF*), 97.74; **LC-MS (ESI$^+$):** Purity 95%, (t_R 2.81 min), m/z 332.7 $[M + H]^+$.

1-chloro-7,8-difluoro-3-methylbenzo[4,5]imidazo[1,2-a]pyridine-4-carbonitrile **(1.3d)**

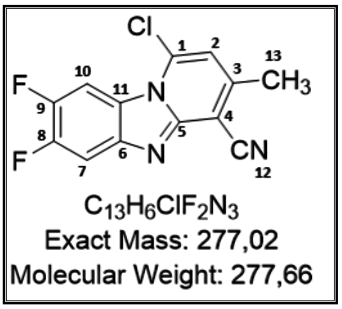

Obtained from **1.2d** (0.600 g, 1.0 eq) and $POCl_3$ (4.23 mL, 20 eq) to isolate **1.3d** as a brown powder (0.544 g, 85%), R_f = 0.72 (5% MeOH/DCM). **^{1}H-NMR (400 MHz, DMSO-*d*$_6$)** δ 8.59 (dd, *J* = 11.2, 7.5 Hz, 1H, H10), 7.98 (dd, *J* = 11.0, 7.7 Hz, 1H, H7), 7.35 (s, 1H, H2), 2.62 (s, 3H, H13); **^{13}C-NMR (101 MHz, DMSO-*d*$_6$)** δ 150.64, 140.77, 133.73, 125.03, 124.91, 114.68, 114.55, 107.10, 106.90, 104.69, 104.44, 98.41, 20.69; **LC-MS (ESI$^+$):** Purity 98%, (t_R 2.45 min), m/z 278.1 $[M + H]^+$.

5.4.2 Synthesis and characterization of Mannich base intermediates

Reductive amination reaction to form intermediates 2.1a and 2.1b

N-(2-fluoro-5-nitrobenzyl)ethanamine **(2.1a)**

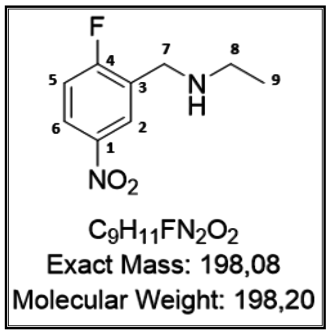

2-Fluoro-5-nitrobenzaldehyde (500 mg, 1.0 eq) and ethylamine (0.25 mL, 1.5 eq) in methanol (10 mL) were stirred at 23 °C for 3 h (monitored via TLC). The reaction mixture was cooled to 0 °C and $NaBH_4$ (559 mg, 5 eq) was added. The reaction mixture was stirred at 23 °C for 3 h. The reaction mixture was neutralized using 1 M hydrogen chloride solution to pH 7 and reduced *in vacuo*. The residue was recrystallized using DCM to isolate compound **2.1a** (545 mg, 95%) as a black oil, R_f = 0.16 (1% Hex/ EtOAc); **^{1}H-NMR (400 MHz, DMSO-*d*$_6$)** δ 8.41 (dd, *J* = 6.3, 2.9 Hz, 1H, H2), 8.23 (ddd, *J* = 9.1, 4.4, 2.9 Hz, 1H, H6), 7.35 (dd, *J* = 10, 8.6 Hz, 1H, H5), 4.82 (s, 2H, H7), 2.72 (q, *J* = 7.2 Hz, 2H, H8), 1.19 (t, *J* = 7.2 Hz, 3H, H9); **^{13}C-NMR (101 MHz, DMSO-*d*$_6$)** δ 204.96, 144.51, 126.37 (d, *CJF*), 125.24 (d, *CJF*), 117.03 (d, *CJF*), 94.68, 45.11, 43.29, 14.87; **^{19}F-NMR (377 MHz, DMSO-*d*$_6$) δ** -107.97; **LC-MS (ESI$^+$):** Purity 84%, (t_R 0.137 min), m/z 199.1 $[M + H]^+$.

N-(2-chloro-5-nitrobenzyl)ethanamine **(2.1b)**

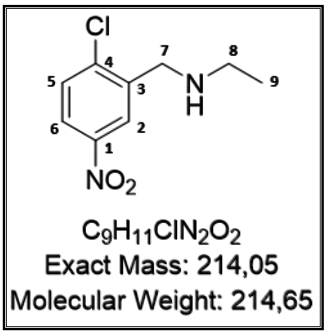

2-Chloro-5-nitrobenzaldehyde (500 mg, 1.0 eq) and ethylamine (0.183 mL, 1.2 eq) in methanol (10 mL) were stirred at 23 °C for 3 h (monitored using TLC). The reaction mixture was cooled to 0 °C and $NaBH_4$ (559 mg, 5 eq) was added. The reaction mixture was stirred at 23 °C for 1 h. The reaction mixture was neutralized using 1 M hydrogen chloride solution to pH 7-8 and reduced *in vacuo*. The residue was recrystallized using DCM to isolate compound **2.1b** (547 mg, 95%) as a yellow oil, R_f = 0.73 (1% MeOH/ DCM); **^{1}H-NMR (400 MHz, DMSO-*d*$_6$)** δ 8.40 (d, *J* = 2.8 Hz, 1H, H2), 8.10 (dd, *J* = 8.7, 2.8 Hz, 1H, H6), 7.71 (d, *J* = 8.8 Hz, 1H, H5), 3.84 (s, 2H, H7), 2.72 (q, *J* = 7.2 Hz, 2H, H8), 1.19 (t, *J* = 7.2 Hz, 3H, H9); **^{13}C-NMR (101 MHz, DMSO-*d*$_6$)** δ 146.96, 141.31, 139.68, 130.76, 124.27, 123.29, 49.88, 43.58, 15.58; **LC-MS (ESI$^+$):** Purity 81%, (t_R 0.167 min), m/z 215.1 $[M + H]^+$.

Reduction of nitro group using stannous chloride to form intermediates 2.2a and 2.2b

3-((ethylamino)methyl)-4-fluoroaniline **(2.2a)**

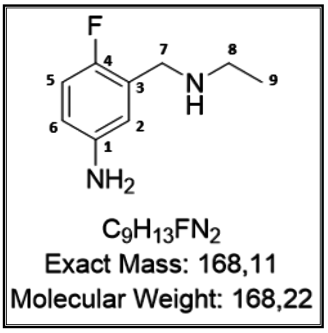

$SnCl_2$ (1.91 g, 4 eq) in THF (5 mL) was added to compound **2.1a** (500 mg, 1.0 eq) and stirred at room temperature while adding 1 M aqueous hydrogen chloride solution (7.8 mL, 3.1 eq). The solution was refluxed at 70 °C for 12 h. The reaction mixture was allowed to cool and reduced *in vacuo*. The reaction mixture was neutralized using saturated sodium bicarbonate to pH 9. The compound was extracted using 10% MeOH:EtOAc and the organic layer dried using $MgSO_4$, filtered, and concentrated to isolate compound **2.2a** (547 mg, 95%) as a black oil, R_f = 0.15 (10% MeOH/DCM); **^{1}H-NMR (400 MHz, DMSO-*d*$_6$)** δ 6.77 (dd, *J* = 10, 8.6 Hz, 1H, H5), 6.62 (dd, *J* = 6.5, 2.9 Hz, 1H, H2), 6.41 (ddd, *J* = 8.6, 4.3, 2.9 Hz, 1H, H6), 3.59 (s, 2H, H7), 2.65 (q, *J* = 7.2 Hz, 2H, H8), 1.03 (t, *J* = 7.1 Hz, 3H, H9); **^{13}C-NMR (101 MHz, DMSO-*d*$_6$)** δ 153.05 (d, *CJF*), 145.25, 127.87 (d, *CJF*), 115.34 (d, *CJF*), 115.08, 113.31 (d, *CJF*), 46.57, 43.38, 15.48; **^{19}F-NMR (377**

MHz, DMSO-d_6) δ -136.16; **LC-MS (ESI$^+$):** Purity 70%, (t_R 0.137min), m/z 169.1 [M + H]$^+$.

4-chloro-3-((ethylamino)methyl)aniline **(2.2b)**

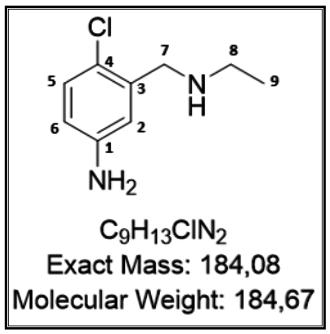

$SnCl_2$ (1.77 g, 4 eq) in THF (5 mL) was added to compound **2.1b** (500 mg, 1.0 eq) and stirred at room temperature while adding 1 M hydrogen chloride solution (7.2 mL, 3.1 eq). The solution was stirred at 70 °C for 12 h. The reaction mixture was allowed to cool and reduced *in vacuo*. The reaction mixture was neutralized using saturated sodium bicarbonate to pH 9. The compound was extracted using 10% EtOAc:MeOH and the organic layer dried using $MgSO_4$, filtered, and concentrated to isolate compound **2.2b** (390.8 mg, 91%) as a yellow oil, R_f = 0.16 (10% MeOH/DCM); **^{1}H-NMR (400 MHz, DMSO-d_6)** δ 6.98 (d, *J* = 8.4 Hz, 1H, H5), 6.72 (d, *J* = 2.8 Hz, 1H, H2), 6.43 (dd, *J* = 8.5, 2.8 Hz, 1H, H6), 3.61 (s, 2H, H7), 2.55 (q, *J* = 7.0 Hz, 2H, H8), 1.04 (t, *J* = 7.1 Hz, 3H, H9); **^{13}C-NMR (101 MHz, DMSO-d_6)** δ 148.13, 138.55, 129.45, 118.87, 115.45, 113.89, 50.76, 43.50, 15.60; **LC-MS (ESI$^+$):** Purity 75%, (t_R 0.157 min), m/z 185.1 [M + H]$^+$.

General procedure for the acetylation reaction to form intermediate compounds 3.1c–3.1g

The appropriate aminophenol (1.0 eq) was dissolved in THF and acetic anhydride (1.2 eq) added. The reaction mixture was stirred at 60 °C under pressure for 1 h, using TLC to monitor the progress of the reaction. The reaction mixture was allowed to cool and reduced *in vacuo* and triturated with diethyl ether, without any further purification.

N-(2-hydroxyphenyl)acetamide **(3.1c)**

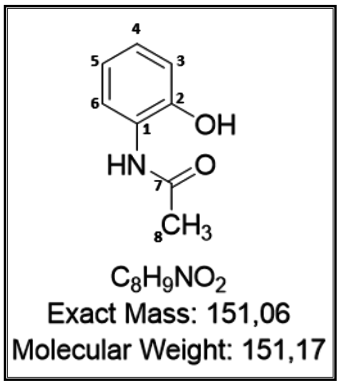

Obtained from commercially available 2-aminophenol (1.00 g, 1.0 eq) and acetic anhydride (1.04 mL, 1.2 eq) in THF (5 mL) to isolate **3.1** as a white powder (1.325 g, 96%), R_f = 0.41 (20% MeOH/DCM); **^{1}H-NMR (400 MHz, MeOH-*d*$_4$)** δ 7.56 (dd, *J* = 7.9, 1.6 Hz, 1H, H6), 6.98 (td, *J* = 7.5, 1.6 Hz, 1H, H4), 6.85 (dd, *J* = 8.0 Hz, 1.4, 1H, H3), 6.79 (td, *J* = 7.6, 1.4 Hz, 1H, H5), 2.16 (s, 3H, H8); **^{13}C-NMR (101 MHz, MeOH-*d*$_4$)** δ 172.2, 149.7, 127.1, 126.8, 124.0, 120.6, 117.3, 23.4; **LC-MS (ESI$^+$):** Purity 95%, (t_R 0.23 min), m/z 152.2 $[M + H]^+$.

N-(5-fluoro-2-hydroxyphenyl)acetamide **(3.1d)**

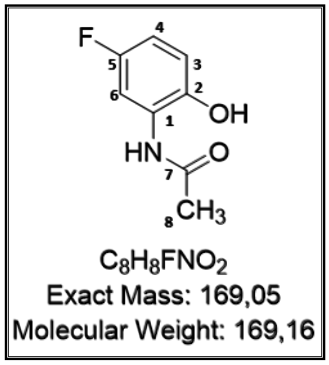

Obtained from commercially available 2-amino-4-fluorophenol (320 mg, 1.0 eq) and acetic anhydride (0.30 mL, 1.2 eq) in THF (2 mL) to isolate **3.1d** as an off-white powder (374 mg, 88%), R_f = 0.4 (8% MeOH/DCM); **^{1}H-NMR (400 MHz, DMSO-*d*$_6$)** δ 7.75 (dd, *J* = 11.0, 3.1 Hz, 1H, H6), 6.83 (dd, *J* = 8.9, 5.5 Hz, 1H, H3), 6.73 (td, *J* = 8.5, 3.2 Hz, 1H, H4), 2.12 (s, 3H, H8); **^{13}C-NMR (101 MHz, DMSO-*d*$_6$)** δ 169.52, 155.35 (d, *CJF*), 143.84, 127.85 (d, *CJF*), 115.93 (d, *CJF*), 110.04 (d, *CJF*), 108.55 (d, *CJF*), 24.27; **LC-MS (ESI$^+$):** Purity 77%, (t_R 0.335 min), m/z 170.1 $[M + H]^+$.

N-(4-chloro-2-hydroxyphenyl)acetamide **(3.1e)**

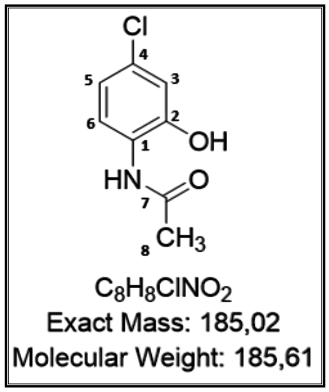

Obtained from commercially available 2-amino-5-chlorophenol (1.0 g, 1.0 eq) and acetic anhydride (0.84 mL, 1.2 eq) in THF (2 mL) to isolate **3.1e** as a brown powder (1.254 g, 97%), R_f = 0.85 (5% MeOH/DCM); **^{1}H-NMR (400 MHz, DMSO-*d*$_6$)** δ 7.78 (d, *J* = 8.6 Hz, 1H, H6), 6.90 (d, *J* = 2.4 Hz, 1H, H3), 6.80 (dd, *J* = 8.6, 2.4 Hz, 1H, H5), 2.10 (s, 3H, H8); **^{13}C-NMR (101 MHz, DMSO-*d*$_6$)** δ 169.41, 149.30, 128.11, 126.15, 123.69, 119.07, 115.83, 24.09; **LC-MS (ESI$^+$):** Purity 87%, (t_R 0.873 min), m/z 186.5 $[M + H]^+$.

N-(5-chloro-2-hydroxyphenyl)acetamide **(3.1f)**

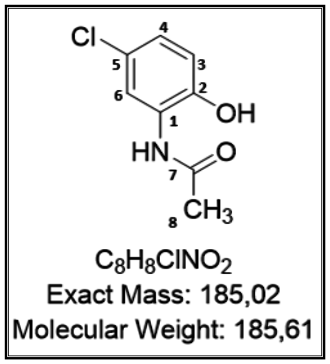

Obtained from commercially available 2-amino-4-chlorophenol (500 mg, 1.0 eq) and acetic anhydride (0.42 mL, 1.2 eq) in THF (3 mL) to isolate **3.1f** as a light brown powder (639 mg, 99%), R_f = 0.23 (5% MeOH/DCM); **^{1}H-NMR (400 MHz, DMSO-*d*$_6$)** δ 7.94 (d, *J* = 2.6 Hz, 1H, H6), 6.95 (dd, *J* = 8.6, 2.6 Hz, 1H, H4), 6.86 (d, *J* = 8.6 Hz, 1H, H3), 2.11 (s, 3H, H8); **^{13}C-NMR (101 MHz, DMSO-*d*$_6$)** δ 169.51, 146.72, 128.28, 123.92, 122.61, 121.49, 116.89, 24.24; **LC-MS (ESI$^+$):** Purity 90%, (t_R 0.841 min), m/z 186.1 $[M + H]^+$.

N-(2-hydroxy-5-methylphenyl)acetamide **(3.1g)**

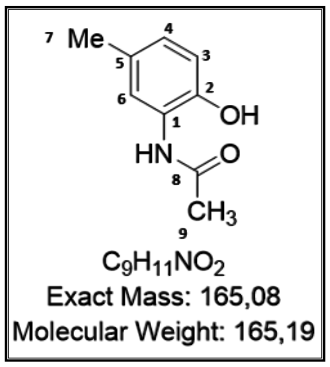

Obtained from commercially available 2-amino-4-methylphenol (1.0 g, 1.0 eq) and acetic anhydride (0.92 mL, 1.2 eq) in THF (3 mL) to isolate **3.1g** as a light brown powder (1.29 mg, 96%), R_f = 0.87 (8% MeOH/DCM); **^{1}H-NMR (600 MHz, MeOH-*d*$_4$)** δ 7.35 (d, *J* = 2.0 Hz, 1H, H6), 6.80 (dd, *J* = 2.2, 8.1 Hz, 1H, H4), 6.73 (d, *J* = 8.1 Hz, 1H, H3), 2.22 (s, 3H, H7), 2.15 (s, 3H, H9); **^{13}C-NMR (151 MHz, MeOH-*d*$_4$)** δ 172.2, 147.4, 130.1, 127.3, 126.8, 124.3, 117.3, 23.4, 20.7; **LC-MS (ESI$^+$):** Purity 90%, (t_R 0.64 min), m/z 166.0 $[M + H]^+$.

N-(2-hydroxy-6-methylphenyl)acetamide **(3.1h)**

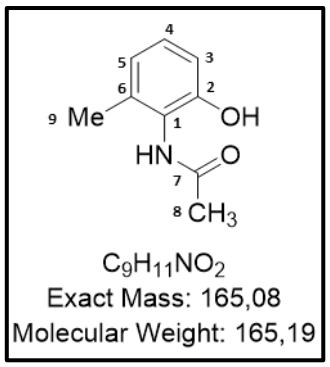

Obtained from commercially available 2-amino-3-methylphenol (1 g, 1.0 eq) and acetic anhydride (0.92 mL, 1.2 eq) in THF (4 mL) to isolate **3.1h** as orange needle-like crystals (1.29 g, 96%), R_f = 0.20 (5% MeOH/DCM); **^{1}H-NMR (400 MHz, DMSO-*d*$_6$)** δ 6.96 (t, *J* = 7.8 Hz, 1H, H4), 6.69 (dd, 1H, *J* = 8.2, 1.4 Hz H3), 6.66 (dd, *J* = 8.2, 1.4 Hz, 1H, H5), 2.10 (s, 3H, H9), 2.04 (s, 3H, H8); **^{13}C-NMR (101 MHz, DMSO-*d*$_6$)** δ 169.10, 153.10, 136.54, 127.14, 124.60, 120.97, 114.20, 23.25, 18.51; **LC-MS (ESI$^+$):** Purity 90%, (t_R 0.26 min) m/z 166.2 $[M + H]^+$.

General procedure for the Mannich reaction used to afford compounds 3.2a–3.2j

The appropriate acetanilide (1.0 eq) was dissolved in ethanol and a mixture of formaldehyde (1.5 eq) and ethylamine (1.5 eq) were added. The reaction mixture was stirred at 85 °C while monitoring with TLC for formation of product for approximately 3 h. The reaction mixture was cooled to 23 °C and reduced *in vacuo*. The compound was dissolved in DCM (15 mL) and acidified using 1 M aqueous hydrogen chloride solution (15 mL), causing the compound to be extracted from DCM into the aqueous layer as a salt. The solution was then neutralized using 1 M aqueous NaOH solution to pH 8-10 and partitioned using DCM (3 × 15 mL). The organic layer was dried using $MgSO_4$ and reduced *in vacuo* to isolate intermediates **3.2a–3.2j.**

N-(3-((ethylamino)methyl)-4-hydroxyphenyl)acetamide **(3.2a)**

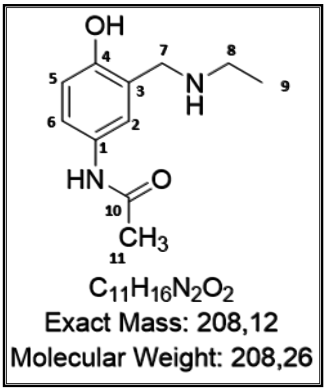

Obtained from commercially available (4-hydroxyphenyl)acetamide (300 mg, 1.0 eq), formaldehyde (0.09 mL, 1.5 eq), and ethylamine (0.17 mL, 1.5 eq) as a brown oil (0.242 g, 59%), R_f = 0.17 (EtOAc); **^{1}H-NMR (400 MHz, DMSO-d$_6$)** δ 7.28 (d, *J* = 2.6 Hz, 1H, H2), 7.23 (dd, *J* = 8.6, 2.6 Hz, 1H, H6), 6.61 (d, *J* = 8.5 Hz, 1H, H5), 3.78 (s, 2H, H7), 2.56 (q, *J* = 7.3 Hz, 2H, H8), 1.98 (s, 3H, H11), 1.05 (t, *J* = 7.2 Hz, 3H, H9); **^{13}C-NMR (101 MHz, DMSO-d$_6$) δ** 169.34, 158.54, 130.23, 126.42, 122.51, 119.56, 117.04, 106.41, 51.85, 45.67, 13.99; **LC-MS (ESI$^+$):** Purity 81%, (t_R 0.217 min), m/z 209.0 $[M + H]^+$.

N-(4-((ethylamino)methyl)-3-hydroxyphenyl)acetamide **(3.2b)**

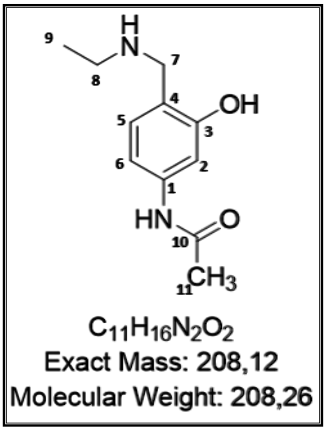

Obtained from commercially available (3-hydroxyphenyl) acetamide (1.4 g, 1.0 eq), formaldehyde (0.39 mL, 1.5 eq), and ethylamine (0.787 mL, 1.5 eq) to isolate **3.2b** as a brown oil (911 mg, 47%), R_f = 0.17 (20% MeOH/DCM); **^{1}H-NMR (400 MHz, DMSO-d$_6$)** δ 7.56 (d, *J* = 8.1 Hz, 1H, H5), 7.07 (d, *J* = 2.2 Hz, 1H, H2), 6.98 (dd, *J* = 8.1, 2.2 Hz, 1H, H6), 4.24 (s, 2H, H7), 3.14 (q, *J* = 7.4 Hz, 2H, H8), 2.00 (s, 3H, H11), 1.37 (t, *J* = 7.3 Hz, 3H, H9); **^{13}C-NMR (101 MHz, DMSO-d$_6$)**

δ 168.46, 158.09, 139.54, 128.82, 119.16, 109.74, 106.91, 49.06, 42.75, 24.44, 14.91; **LC-MS (ESI+):** Purity 80%, (t_R 0.237 min), m/z 209.1 $[M + H]^+$.

N-(3-((ethylamino)methyl)-2-hydroxyphenyl)acetamide **(3.2c)**

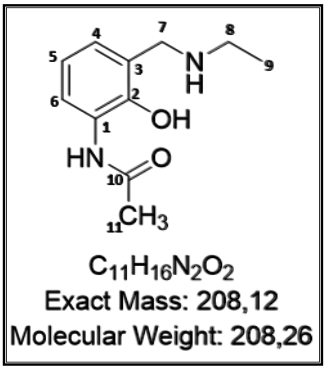

Obtained from **3.1c** (1.0 g, 1.0 eq), formaldehyde (0.27 mL, 1.5 eq), and ethylamine (0.560 mL, 1.5 eq) to isolate **3.2c** as a purple solid (106 mg, 8%), R_f = 0.14 (20% MeOH/DCM); **^{1}H-NMR (400 MHz, DMSO-*d*$_6$)** δ 7.61 (dd, *J* = 8.0, 1.6 Hz, 1H, H6), 6.94 (dd, *J* = 7.6, 1.6 Hz, 1H, H4), 6.61 (t, *J* = 7.8 Hz, 1H, H5), 3.89 (s, 2H, H7), 2.59 (q, *J* = 7.3 Hz, 2H, H8), 2.08 (s, 3H, H11), 1.06 (t, *J* = 7.2 Hz, 3H, H9); **^{13}C-NMR (101 MHz, DMSO-*d*$_6$)** δ 196.40, 177.67, 156.46, 148.41, 126.39, 125.35, 119.51, 52.28, 42.40, 24.18, 14.36; **LC-MS (ESI$^+$):** Purity 65%, (t_R 0.179 min), m/z 209.1 $[M + H]^+$.

N-(3-((ethylamino)methyl)-5-fluoro-2-hydroxyphenyl)acetamide **(3.2d)**

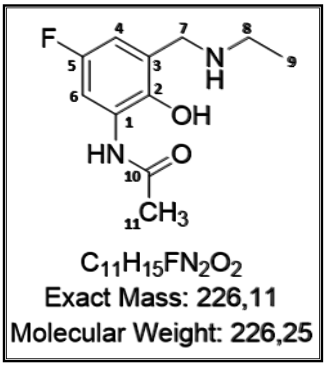

Obtained from **3.1d** (350 mg, 1.0 eq), formaldehyde (0.09 mL, 1.5 eq), and ethylamine (0.176 mL, 1.5 eq) to isolate **3.2d** as a white powder (381 mg, 81%), R_f = 0.14 (5% MeOH/DCM); **^{1}H-NMR (400 MHz, DMSO-d$_6$)** δ 7.76 (dd, *J* = 11.1, 3.2 Hz, 1H, H6), 6.63 (dd, *J* = 8.8, 3.1 Hz, 1H, H4), 3.89 (s, 2H, H7), 2.58 (q, *J* = 7.2 Hz, 2H, H8), 2.12 (s, 3H, H11) 1.08 (t, *J* = 7.0 Hz, 3H, H9); **^{13}C-NMR (101 MHz, DMSO-*d*$_6$)** δ 169.27, 154.44 (d, *CJF*), 145.01, 127.59 (d, *CJF*), 123.49 (d, *CJF*), 109.06 (d, *CJF*), 106.43 (d, *CJF*), 51.10, 42.55, 24.34, 14.57; **LC-MS (ESI$^+$):** Purity 80%, (t_R 0.137 min), m/z 227.1 $[M + H]^+$.

N-(4-chloro-3-((ethylamino)methyl)-2-hydroxyphenyl)acetamide **(3.2e)**

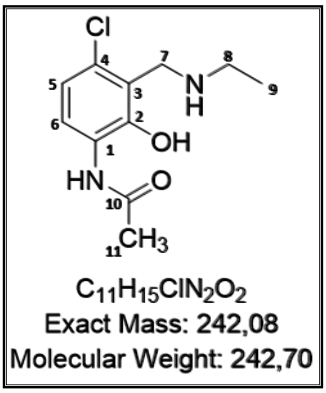

Obtained from **3.1e** (1 g, 1.0 eq), formaldehyde (0.23 mL, 1.5 eq) and ethylamine (0.459 mL, 1.5 eq) to isolate **3.2e** as a brown oil (541.3 mg, 41%), R_f = 0.13 (20% MeOH/DCM); **^{1}H-NMR (400 MHz, MeOH-*d*$_4$)** δ 7.83 (d, *J* = 8.7 Hz, 1H, H5), 6.57 (d, *J* = 8.6 Hz, 1H, H6), 4.28 (s, 2H, H7), 2.93 (q, *J* = 7.3 Hz, 2H, H8), 2.18 (s, 3H, H11), 1.27 (t, *J* = 7.2 Hz, 3H, H9); **^{13}C-NMR (101 MHz, MeOH-*d*$_4$)** δ 169.91, 156.05, 128.35, 126.92, 120.58, 116.86, 114.45, 46.60, 41.65, 22.51, 11.27; **LC-MS (ESI$^+$):** Purity 98%, (t_R 1.765 min), m/z 243.1 $[M + H]^+$.

N-(5-chloro-3-((ethylamino)methyl)-2-hydroxyphenyl)acetamide **(3.2f)**

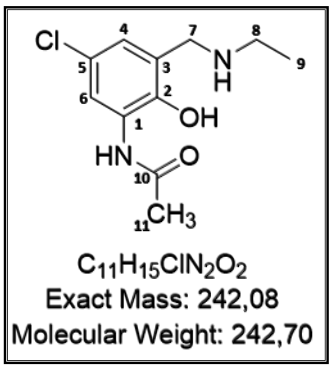

Obtained from **3.1f** (500 mg, 1.0 eq), formaldehyde (0.11 mL, 1.5 eq) and ethylamine (0.22 mL, 1.5 eq) to isolate **3.2f** as a yellow solid (343 mg, 52%), R_f = 0.11 (20% MeOH/DCM); **^{1}H-NMR (400 MHz, DMSO-*d*$_6$)** δ 7.94 (d, *J* = 2.7 Hz, 1H, H6), 6.81 (d, *J* = 2.7 Hz, 1H, H4), 3.91 (s, 2H, H7), 2.60 (q, *J* = 7.2 Hz, 2H, H8), 2.10 (s, 3H, H11), 1.08 (t, *J* = 7.2 Hz, 3H, H9); **^{13}C-NMR (101 MHz, DMSO-*d*$_6$)** δ 169.13, 149.03, 128.31, 123.60, 122.57, 120.29, 119.05, 50.88, 42.32, 24.37, 14.35; **LC-MS (ESI$^+$):** Purity 79%, (t_R 0.195 min), m/z 243.1 $[M + H]^+$.

N-(3-((ethylamino)methyl)-2-hydroxy-5-methylphenyl)acetamide **(3.2g)**

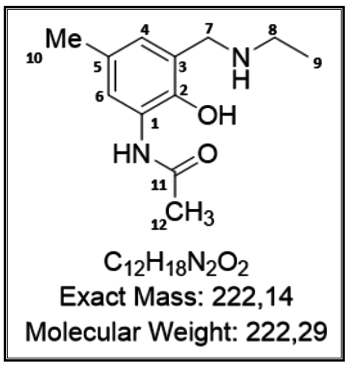

Obtained from previously synthesised *N*-(2-hydroxy-5-methylphenyl)acetamide (500 mg, 1.0 eq), formaldehyde (0.13 mL, 1.5 eq) and ethylamine (0.26 mL, 1.5 eq) to isolate **3.2g** as an orange oil (560.7 mg, 83%), R_f = 0.1 (5% MeOH/DCM); **^{1}H-NMR (400 MHz, DMSO-*d*$_6$)** δ 7.59 (d, *J* = 2.2 Hz, 1H, H6), 6.61 (d, *J* = 2.2 Hz, 1H, H4), 3.84 (s, 2H, H7), 2.56 (q, *J* = 7.2 Hz, 2H, H8), 2.19 (s, 3H, H10), 2.08 (s, 3H, H12), 1.07 (t, *J* = 7.2 Hz, 3H, H9); **^{13}C-NMR (101 MHz, DMSO-*d*$_6$)** δ 168.84, 146.59, 126.56, 126.44, 124.17, 123.10, 121.03, 51.36, 42.62, 24.27, 20.97, 14.77; **LC-MS (ESI$^+$):** Purity 65%, (t_R 0.156 min), m/z 223.2 $[M + H]^+$.

N-(3-((ethylamino)methyl)-2-hydroxy-6-methylphenyl)acetamide **(3.2h)**

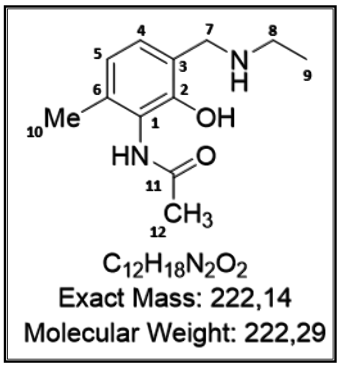

Obtained from **3.1h** (1.20 g, 1.0 eq), formaldehyde (0.27 mL, 1.5 eq) and ethylamine (0.55 mL, 1.5 eq) to isolate **3.2h** as an off-white solid (788 mg, 49%), R_f = 0.17 (20% MeOH/DCM); **^{1}H-NMR (400 MHz, MeOH-*d*$_4$)** δ 7.11 (d, *J* = 7.7 Hz, 1H, H4), 6.78 (d, *J* = 7.7 Hz, 1H, H5), 4.11 (s, 2H, H7), 2.99 (q, *J* = 7.3 Hz, 2H, H8), 2.23 (s, 3H, H10), 1.91 (s, 3H, H12), 1.29 (t, *J* = 7.2 Hz, 3H, H9); **^{13}C-NMR (101 MHz, MeOH-*d*$_4$)** δ 172.10, 152.39, 137.01, 128.68, 123.76, 120.64, 118.44, 42.05, 22.71, 21.35, 16.88, 10.79; **LC-MS (ESI$^+$):** Purity 65%, (t_R 0.140 min), m/z 223.1 $[M + H]^+$.

N-(3-((diethylamino)methyl)-4-hydroxyphenyl)acetamide **(3.2i)**

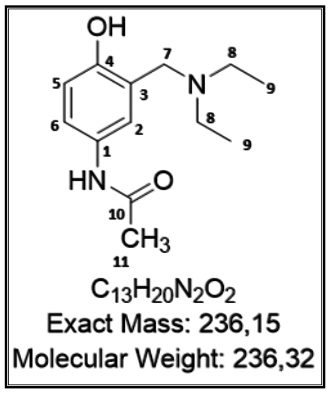

Obtained from **3.1i** (1.00 g, 1.0 eq), formaldehyde (0.27 mL, 1.5 eq) and diethylamine (1.03 mL, 1.5 eq) to isolate **3.2i** as a white solid (0.560 g, 36%), R_f = 0.18 (5% MeOH/DCM); **^{1}H-NMR (400 MHz, MeOH-*d*$_4$)** δ 7.23 (d, *J* = 2.6 Hz, 1H, H2), 7.18 (dd, *J* = 8.6, 2.6 Hz, 1H, H6), 6.66 (d, *J* = 8.6 Hz, 1H, H5), 3.75 (s, 2H, H7), 2.63 (q, *J* = 7.2 Hz, 4H, H8), 2.07 (s, 3H, H11), 1.10 (t, *J* = 7.2 Hz, 6H, H9); **^{13}C-NMR (101 MHz, MeOH-*d*$_4$)** δ 169.91, 154.69, 129.95, 122.31, 121.30, 120.91, 115.30, 56.14, 46.16 (2C), 22.10, 10.20 (2C); **LC-MS (ESI$^+$):** Purity 84%, (t_R 0.136 min), m/z 237.3 $[M + H]^+$.

N-(3-((diethylamino)methyl)-2-hydroxy-5-methylphenyl)acetamide **(3.2j)**

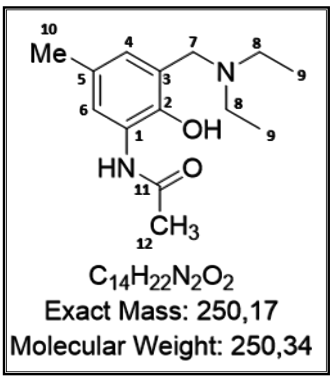

Obtained from **3.1j** (0.700 g, 1.0 eq), formaldehyde (0.18 mL, 1.5 eq) and diethylamine (0.66 mL, 1.5 eq) to isolate **3.2j** as a white solid (0.521 g, 49%), R_f = 0.18 (5% MeOH/DCM); **^{1}H-NMR (600 MHz, MeOH-*d*$_4$)** δ 7.61 (d, *J* = 2.0 Hz, 1H, H6), 6.61 (d, *J* = 2.0 Hz, 1H, H4), 3.76 (s, 2H, H7), 2.64 (q, *J* = 7.2 Hz, 4H, H8), 2.20 (s, 3H, H10), 2.14 (s, 3H, H12), 1.11 (t, *J* = 7.2 Hz, 6H, H9); **^{13}C-NMR (151 MHz, MeOH-*d*$_4$)** δ 171.6,

148.0, 128.5, 126.7, 125.9, 122.9, 122.8, 57.6, 47.4 (2C), 23.8, 20.9 and 11.5 (2C); **LC-MS (ESI$^+$):** Purity 98%, (t_R 0.151 min), m/z 251.2 $[M + H]^+$.

General procedure for the deacetylation reaction used to form intermediates 3.3a–3.3j

The appropriate protected Mannich base/-protected amine (1.0 eq) was stirred in 6 M hydrogen chloride solution (4 eq) at 100 °C for 2 h. The reaction mixtures were allowed to cool, triturated with diethyl ether or DCM and reduced *in vacuo* to isolate [Mannich base]•[2HCl] salts of intermediate compounds **3.3a–3.3j**.

4-amino-2-((ethylamino)methyl)phenol **(3.3a)**

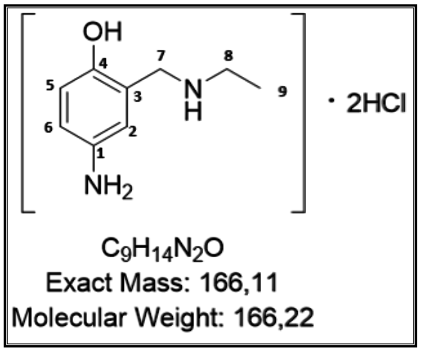

Obtained from compound **3.2a** (0.360 g, 1.0 eq) and 6M hydrogen chloride solution as a brown oil (0.241 g, 84%), R_f = 0.1 (15% MeOH/DCM); **^{1}H-NMR (400 MHz, DMSO-*d*$_6$)** δ 7.44 (s, 1H, H2), 7.29 (d, *J* = 8.7 Hz, 1H, H5), 7.09 (d, *J* = 8.6 Hz, 1H, H6), 4.05 (s, 2H, H7), 2.95 (q, *J* = 6.6 Hz, 2H, H8), 1.24 (t, *J* = 7.2 Hz, 3H, H9); **^{13}C-NMR (101 MHz, DMSO-*d*$_6$)** δ 158.42, 132.64, 130.48, 124.20, 119.71, 115.42, 44.35, 42.16, 11.22; **LC-MS (ESI$^+$):** Purity 99%, (t_R 0.142 min), m/z 167.1 $[M + H]^+$.

5-amino-2-((ethylamino)methyl)phenol **(3.3b)**

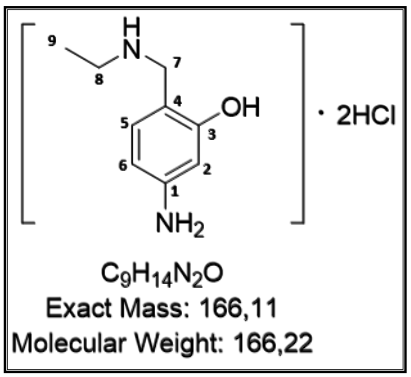

Obtained from compound **3.2b** (200 mg, 1.0 eq) and 6 M hydrogen chloride solution as a brown oil (120.4 mg, 75%), R_f = 0.13 (20% MeOH/DCM); **^{1}H-NMR (400 MHz, DMSO-*d*$_6$)** δ 7.50 (d, *J* = 8.1 Hz, 1H, H5), 7.08 (d, *J* = 2.0 Hz, 1H, H2), 6.84 (dd, *J* = 8.1, 2.1 Hz, 1H, H6), 3.85 (s, 2H, H7), 2.93 (q, *J* = 6.5 Hz, 2H, H8), 1.23 (t, *J* = 7.3 Hz, 3H, H9); **^{13}C-NMR (101 MHz, DMSO-*d*$_6$)** δ 157.32, 134.60, 132.98, 118.20, 113.71, 110.40, 44.35, 42.16, 11.22; **LC-MS (ESI$^+$):** Purity 99%, (t_R 0.122 min), m/z 167.1 $[M + H]^+$.

2-amino-6-((ethylamino)methyl)phenol **(3.3c)**

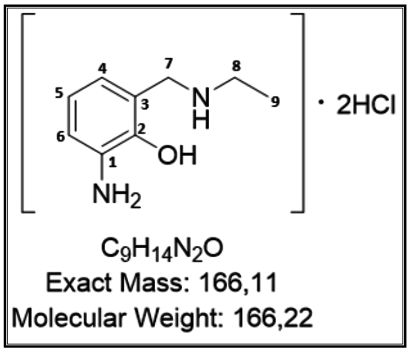

Obtained from compound **3.2c** (100 mg, 1.0 eq) and 6 M hydrogen chloride solution (4 eq) as a brown oil (65.1 mg, 81%), R_f = 0.10 (20% MeOH/DCM); **^{1}H-NMR (400 MHz, MeOH-*d*$_4$) δ** 7.86 (dd, *J* = 7.9, 1.8 Hz, 1H, H6), 6.77 (dd, *J* = 7.5, 1.8 Hz, 1H, H4), 6.32 (t, *J* = 7.7 Hz, 1H, H5), 3.71 (s, 2H, H7), 2.62 (q, *J* = 7.2 Hz, 2H, H8), 1.12 (t, *J* = 7.2 Hz, 3H, H9); **^{13}C-NMR (101 MHz, MeOH-*d*$_4$)** δ 174.11, 149.44, 127.07, 123.70, 120.64, 117.49, 51.13, 42.59, 14.79; **LC-MS (ESI$^+$):** Purity 94%, (t_R 0.126 min), m/z 167.1 $[M + H]^+$.

2-amino-6-((ethylamino)methyl)-4-fluorophenol **(3.3d)**

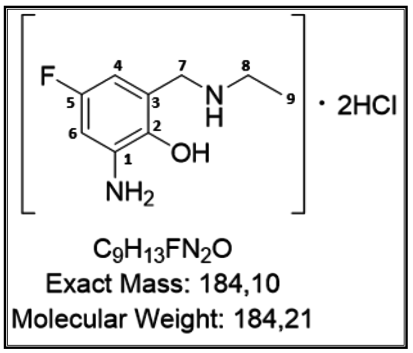

Obtained from compound **3.2d** (100 mg, 1.0 eq) and 6M hydrogen chloride solution (4 eq) as a brown oil (65 mg, 80%), R_f = 0.08 (10% MeOH/DCM); **^{1}H-NMR (400 MHz, MeOH-*d*$_4$)** δ 7.72 (dd, *J* = 10.7, 3.2 Hz, 1H, H6), 6.58 (dd, *J* = 9.1, 3.2 Hz, 1H, H4), 3.88 (s, 2H, H7), 2.73 (q, *J* = 7.2 Hz, 2H, H8), 1.20 (t, *J* = 7.6 Hz, 3H, H9); **^{13}C-NMR (101 MHz, MeOH-*d*$_4$)** δ 156.09 (d, *CJF*), 145.20, 123.09 (d, *CJF*), 117.58–116.85 (m) (2C), 111.99 (d, *CJF*), 44.96, 42.89, 10.09; **LC-MS (ESI$^+$):** Purity 83%, (t_R 0.149 min), m/z 185.1 $[M + H]^+$.

2-amino-4-chloro-6-((ethylamino)methyl)phenol **(3.3e)**

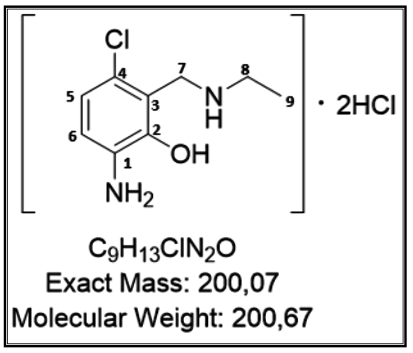

Obtained from compound **3.2e** (100 mg, 1.0 eq) and 6M hydrogen chloride solution (4 eq) as a brown oil (75.6 mg, 91%). R_f = 0.06 (8% MeOH/DCM); **^{1}H-NMR (400 MHz, MeOH-*d*$_4$)** δ 7.51 (d, *J* = 8.5 Hz, 1H, H5), 7.30 (d, *J* = 8.6 Hz, 1H, H6), 4.51 (s, 2H, H7), 3.25 (q, *J* = 7.3 Hz, 2H, H8), 1.42 (t, *J* = 7.2 Hz, 3H, H9); **^{13}C-NMR (101 MHz, MeOH-*d*$_4$)** δ 150.90, 136.27, 126.15, 122.43, 120.52, 120.41, 43.31, 42.68, 9.99; **LC-MS (ESI$^+$):** Purity 72%, (t_R 0.180 min), m/z 201.0 $[M + H]^+$.

2-amino-4-chloro-6-((ethylamino)methyl)phenol **(3.3f)**

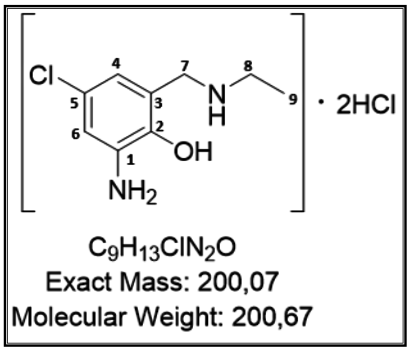

Obtained from compound **3.2f** (150 mg, 1.0 eq) and 6M hydrogen chloride solution (4 eq) as a brown oil (92.1 mg, 74%). R_f = 0.44 (20% MeOH/DCM); **^{1}H-NMR (400 MHz, DMSO-*d*$_6$)** δ 7.27 (d, *J* = 2.5 Hz, 1H, H6), 7.20 (d, *J* = 2.5 Hz, 1H, H4), 4.13(s, 2H, H7), 2.98 (q, *J* = 6.5 Hz, 2H, H8), 1.24 (t, *J* = 7.2 Hz, 3H, H9); **^{13}C-NMR (101 MHz, DMSO-*d*$_6$)** δ 145.86, 125.74, 125.65, 123.96, 123.11, 120.76, 44.77, 42.46, 11.32; **LC-MS (ESI$^+$):** Purity 87%, (t_R 0.180 min), m/z 201.1 $[M + H]^+$.

2-amino-6-((ethylamino)methyl)-4-methylphenol **(3.3g)**

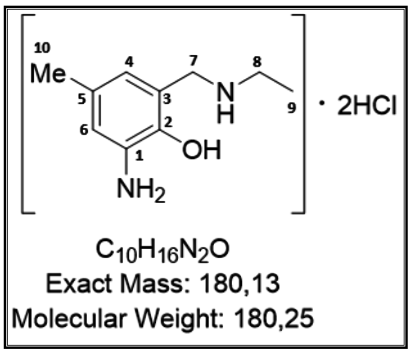

Obtained from compound **3.2g** (100 mg, 1.0 eq) and 6M hydrogen chloride solution (4 eq) as a red oil (65.1 mg, 81%). R_f = 0.12 (15% MeOH/DCM); **^{1}H-NMR (400 MHz, MeOH-*d*$_4$)** δ 7.95 (d, *J* = 2.8 Hz, 1H, H6), 6.75 (d, *J* = 2.8 Hz, 1H, H4), 4.91 (s, 2H, H7), 2.61 (q, *J* = 7.1 Hz, 2H, H8), 2.18 (s, 3H, H10), 1.13 (t, *J* = 7.2 Hz, 3H, H9); **^{13}C-NMR (101 MHz, MeOH-*d*$_4$)** δ 146.59, 126.56, 126.44, 124.17, 123.10, 121.03, 51.36, 42.62, 20.97, 14.77; **LC-MS (ESI$^+$):** Purity 82%, (t_R 0.124 min), m/z 181.2 $[M + H]^+$.

2-amino-6-((ethylamino)methyl)-3-methylphenol **(3.3h)**

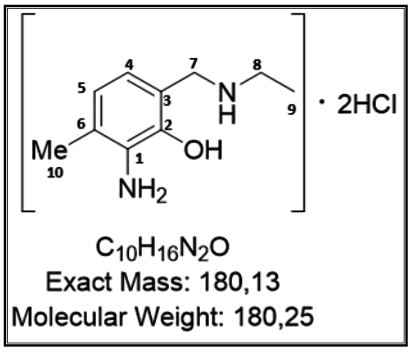

Obtained from compound **3.2h** (100 mg, 1.0 eq) and 6M hydrogen chloride solution (4 eq) as a brown oil (76.2 mg, 92%). R_f = 0.44 (27% MeOH/DCM); **^{1}H-NMR (400 MHz, MeOH-*d*$_4$)** δ 7.21 (d, *J* = 7.8 Hz, 1H, H4), 6.84 (d, *J* = 7.7 Hz, 1H, H5), 4.19 (s, 2H, H7), 3.10 (q, *J* = 7.0 Hz, 2H, H8), 2.26 (s, 3H, H10), 1.35 (t, *J* = 7.3 Hz, 3H, H9); **^{13}C-NMR (101 MHz, MeOH-*d*$_4$)** δ 172.39, 151.52, 137.53, 129.35, 121.32, 117.41, 46.32, 42.20, 16.94, 10.10; **LC-MS (ESI$^+$):** Purity 85%, (t_R 0.126 min), m/z 181 $[M + H]^+$.

4-amino-2-((diethylamino)methyl)phenol **(3.3i)**

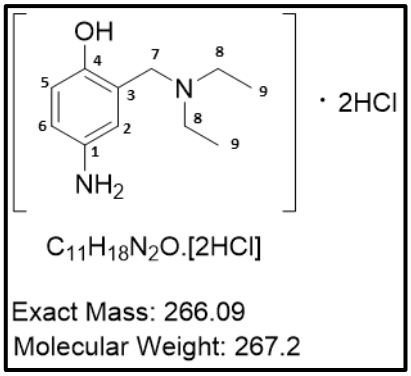

Obtained from compound **3.2i** (100 mg, 1.0 eq) and 6M hydrogen chloride solution (4 eq) as a brown oil (79.0 mg, 96%). R_f = 0.15 (15% MeOH/DCM); **^{1}H-NMR (400 MHz, DMSO)** δ 7.56 (d, *J* = 2.6 Hz, 1H, H2), 7.34 (dd, *J* = 8.7, 2.6 Hz, 1H, H6), 7.16 (d, *J* = 8.7 Hz, 1H, H5), 4.22 (d, *J* = 4.6 Hz, 2H, H7), 3.07 (dq, *J* = 13.9, 7.0 Hz, 4H, H8), 1.27 (t, *J* = 7.2 Hz, 6H, H9); **^{13}C-NMR (101 MHz, DMSO)** δ 158.75, 131.29, 128.04, 126.79, 123.84, 118.22, 115.90, 49.64, 45.67 (2C), 7.11(2C); **LC-MS (ESI$^+$):** Purity 99%, (t_R 0.116 min), m/z 209.2 $[M + H]^+$.

2-amino-6-((diethylamino)methyl)-4-methylphenol **(3.3j)**

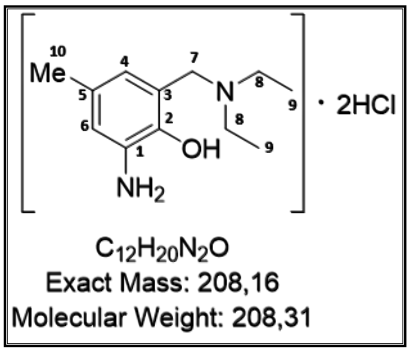

Obtained from compound **3.2j** (100 mg, 1.0 eq) and 6M hydrogen chloride solution (4 eq) as a brown oil (71.0 mg, 85%). R_f = 0.14 (15% MeOH/DCM); **^{1}H-NMR (400 MHz, MeOH-*d*$_4$)** δ 7.44 (d, *J* = 1.9 Hz, 1H, H6), 7.33 (d, *J* = 1.8 Hz, 1H, H4), 4.43 (s, 2H, H7), 3.24 (m, 4H, H8), 2.35 (s, 3H, H10), 1.37 (t, *J* = 7.2 Hz, 6H, H9); **^{13}C-NMR (101 MHz, MeOH-*d*$_4$)** δ 148.6, 134.9, 133.6, 127.6, 122.7, 122.1, 52.1, 48.5 (2C), 20.4, 9.2 (2C); **LC-MS (ESI$^+$):** Purity 95%, (t_R 0.14 min), m/z 209.2 $[M + H]^+$.

5.4.3 Synthesis and characterization of final compounds

General procedures and characterization of final compounds 4, 5, 8, and 9

The appropriate amine/Mannich base (1.2 eq) was dissolved in EtOH (2 mL) and added to compound **1.3a** (1.0 eq), followed by the dropwise addition of 4 M hydrogen chloride solution (1 eq) and allowed to stir at 23 °C for 10 min. The mixture was irradiated in a microwave reactor at 80 °C for 1.5 h. Once cooled to 23 °C, the mixture was dissolved in EtOH (5 mL) and reduced *in vacuo*. The resulting residue was purified using column chromatography (DCM/MeOH) and reduced *in vacuo*. The residue was then triturated using pentane or diethyl ether to isolate final compounds **4, 5, 8,** and **9.**

1-((4-hydroxyphenyl)amino)-3-(trifluoromethyl)benzo[4,5]imidazo[1,2-a]pyridine-4-carbonitrile **(4)**

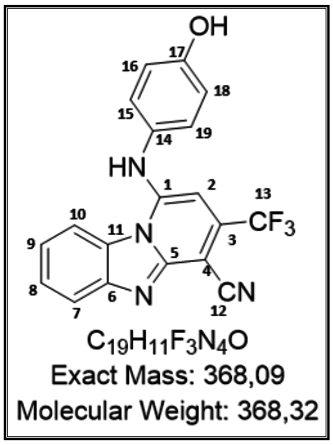

Obtained from commercially available 4-aminophenol (34 mg, 1.2 eq) and intermediate **1.3a** (75 mg, 1 eq) as a yellow solid (35 mg, 38%), M.P. > 350 °C, R_f = 0.83 (20% MeOH/DCM); **^{1}H-NMR (600 MHz, DMSO-*d*$_6$)** δ 9.35 (s, 1H, NH), 8.75 (d, *J* = 8.4 Hz, 1H, H10), 7.86 – 7.77 (m, 2H, H16/H18), 7.62 (t, *J* = 7.7 Hz, 1H, H9), 7.43 (t, *J* = 7.9 Hz, 1H, H8), 7.16 – 7.08 (m, 2H, H15/H19), 6.89 (d, *J* = 8.5 Hz, 1H, H7), 6.15 (s, 1H, H2); **^{13}C-NMR (151 MHz, DMSO-*d*$_6$)** δ 156.02, 149.65, 148.66 (2C), 143.96, 142.31, 135.79, 128.68 (2C), 128.21, 125.47, 123.65, 122.21, 121.83, 120.01, 116.91, 116.84, 114.91, 70.34; **LC-MS (ESI$^+$):** Purity 98%, (t_R 2.734 min), m/z 369.0 $[M + H]^+$.

1-((3-((ethylamino)methyl)-4-hydroxyphenyl)amino)-3-(trifluoromethyl)benzo[4,5]imidazo[1,2-a]pyridine-4-carbonitrile **(5)**

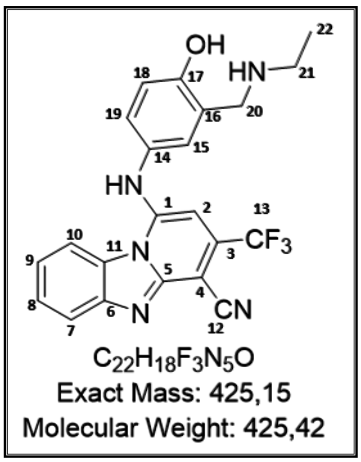

Obtained from **3.3a** (42 mg, 1.5 eq) and **1.3a** (50 mg, 1 eq) as a brown solid (26 mg, 37%), M.P. 380–382 °C, R_f = 0.48 (20% MeOH/DCM); **^{1}H-NMR (400 MHz, DMSO-*d*$_6$)** δ 10.15 (s, 1H, NH), 8.79 (d, *J* = 8.8 Hz, 1H, H10), 8.79 – 8.77 (m, 1H, H18), 7.69 (d, *J* = 7.2 Hz, 1H, H7), 7.55 (t, *J* = 7.9 Hz, 1H, H9), 7.36 (t, *J* = 7.9 Hz, 1H, H8), 7.25 – 7.07 (m, 1H, H15), 7.07 – 6.93 (m, 1H, H19), 6.11 (s, 1H, H2), 4.09 (s, 2H, H20), 2.97 (q, *J* = 7.7 Hz, 2H, H21), 1.23 (t, *J* = 7.2 Hz, 3H, H22); **^{13}C-NMR (101 MHz, DMSO-*d*$_6$) δ** 187.19, 162.35, 153.49, 149.06, 142.37, 134.84, 128.87, 126.86, 126.21, 124.22, 123.29, 122.15, 121.49, 119.74, 117.17 115.57, 115.38, 92.77, 70.27, 44.77, 42.03, 11.20; **LC-MS (ESI$^+$):** Purity 96%, (t_R 3.502 min), m/z 426.2 $[M + H]^+$.

1-((3-((ethylamino)methyl)-4-fluorophenyl)amino)-3-(trifluoromethyl)benzo[4,5]imidazo[1,2-a]pyridine-4-carbonitrile **(8)**

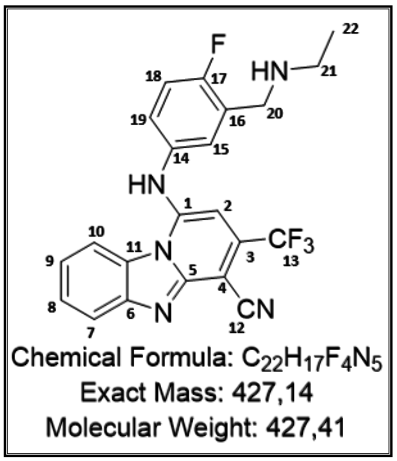

Obtained from **2.2a** (60 mg, 1.5 eq) and **1.3a** (70 mg, 1 eq) as an orange-brown solid (34 mg, 34%), M.P. 235–237 °C, R_f = 0.63 (20% MeOH/DCM); **^{1}H-NMR (400 MHz, DMSO-*d*$_6$)** δ 8.80 (dd, *J* = 8.1, 1.1 Hz, 1H, H10), 7.57 (dd, *J* = 7.9, 1.8 Hz, 1H, H7), 7.34 (td, *J* = 7.2, 1.2 Hz, 1H, H9), 7.30 – 7.24 (m, 1H, H18), 7.17 (dd, *J* = 6.8, 2.7 Hz, 1H, H15), 7.11 (td, *J* = 7.4, 1.2 Hz, 1H, H8), 7.05 (ddd, *J* = 8.7, 4.7, 2.6 Hz, 1H, H19), 5.72 (s, 1H, H2), 4.20 (s, 2H, H20), 3.05 (q, *J* = 7.3 Hz, 2H, H21), 1.23 (t, *J* = 7.3 Hz, 3H, H22); **^{13}C-NMR (101 MHz, DMSO-*d*$_6$) δ** 157.45, 155.06, 151.81, 151.02, 148.01, 145.42, 134.98 (q, *CJF*), 130.98, 125.39 (d, *CJF*), 125.31, 124.68 (d, *CJF*), 124.51, 120.23 (d, *CJF*), 119.03, 118.61, 117.00, 116.78 (d, *CJF*), 116.36, 87.87, 43.68, 42.72, 11.38; **LC-MS (ESI$^+$):** Purity 97%, (t_R 2.382 min), m/z 428.1 [M + H]$^+$.

1-((4-chloro-3-((ethylamino)methyl)phenyl)amino)-3-(trifluoromethyl)benzo[4,5]imidazo[1,2-a]pyridine-4-carbonitrile **(9)**

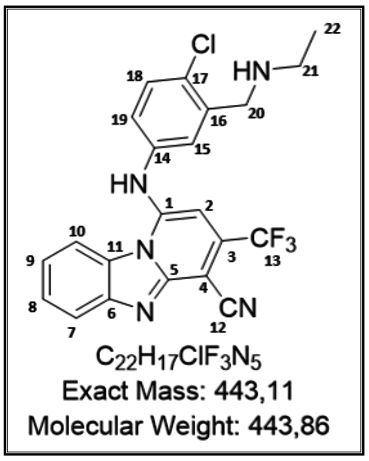

Obtained from **2.2b** (66 mg, 1.5 eq) and **1.3a** (77 mg, 1 eq) as a yellow solid (19.3 mg, 18%), M.P. 273–275 °C, R_f = 0.22 (10% MeOH/DCM); **^{1}H-NMR (400 MHz, DMSO-*d*$_6$)** δ 8.83 (dd, *J* = 8.0, 1.6 Hz, 1H, H10), 7.58 (dd, *J* = 8.1, 1.7 Hz, 1H, H7), 7.49 (d, *J* = 8.5 Hz, 1H, H18), 7.35 (td, *J* = 8.2, 1.3 Hz, 1H, H9), 7.26 (d, *J* = 2.5 Hz, 1H, H15), 7.11 (td, *J* = 8.3, 1.2 Hz, 1H, H8), 7.07 (dd, *J* = 8.5, 2.5 Hz, 1H, H19), 5.74 (s, 1H, H2), 4.14 (s, 2H, H20), 3.03 (q, *J* = 7.2 Hz, 2H, H21), 1.24 (t, *J* = 7.2 Hz, 3H, H22); **^{13}C-NMR (101 MHz, DMSO-*d*$_6$)** δ 151.74, 150.97, 150.84, 145.56, 135.25, 134.96, 131.27, 130.95, 130.81, 125.74, 125.57, 125.28, 124.62, 119.07, 118.51, 117.01, 116.50, 87.63, 64.91, 47.54, 43.00, 11.46; **LC-MS (ESI$^+$):** Purity 99%, (t_R 2.635 min), m/z 444.1 [M + H]$^+$.

General synthetic procedures and characterization for final compounds 6, 7, and 10-16

The appropriate [Mannich base]•2HCl salt (1.2 eq) was dissolved in EtOH (2 mL) and added to a mixture of compound **1.3a** (1.0 eq),and KH_2PO_4 (10 eq) and allowed to stir at 23 °C for 10 min. The mixture was irradiated in a microwave reactor at 80 °C for 1.5 h. Once cooled to 23 °C, the mixture was dissolved in EtOH (5 mL) and reduced *in vacuo*. The resulting residue was purified using column chromatography (DCM/MeOH) and reduced *in vacuo*. The residue was then triturated using pentane or diethyl ether to isolate final compounds.

1-((3-((diethylamino)methyl)-4-hydroxyphenyl)amino)-3-(trifluoromethyl)benzo[4,5]imidazo[1,2-a]pyridine-4-carbonitrile **(6)**

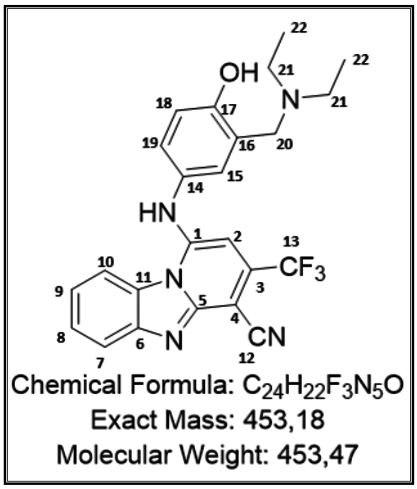

Obtained from **3.3i** (136 mg, 3 eq) and **1.3a** (50 mg, 1 eq) as a brown solid (26 mg, 37%), M.P. 244 – 245 °C, R_f = 0.838 (20% MeOH/DCM); **^{1}H-NMR (600 MHz, DMSO-*d*$_6$)** δ 8.81 (dd, *J* = 8.1, 0.9 Hz, 1H, H10), 7.58 (dd, *J* = 8.1, 1.0 Hz, 1H, H7), 7.36 (td, *J* = 8.2, 1.3 Hz, 1H, H9), 7.14 (td, *J* = 8.3, 1.2 Hz, 1H, H8), 7.02 – 7.01 (m, 1H, H18), 6.94 – 6.93 (m, 2H, H19/H15), 5.84 (s, 1H, H2), 4.16 (s, 2H, H20), 3.07 (q, *J* = 7.2 Hz, 4H, H21), 1.28 – 1.19 (m, 6H, H22); **^{13}C-NMR (151 MHz, DMSO-*d*$_6$)** δ 152.33, 151.57, 150.77, 144.52, 142.10, 134.81, 133.07, 130.77, 126.61, 125.60, 124.73, 122.97, 121.15, 119.39, 118.97, 118.12, 117.04, 116.06, 89.24, 52.14, 47.37 (2C), 9.53 (2C); **LC-MS (ESI$^+$):** Purity 97%, (t_R 2.366 min), m/z 454.2 $[M + H]^+$.

1-((4-((ethylamino)methyl)-3-hydroxyphenyl)amino)-3-(trifluoromethyl)benzo[4,5]imidazo[1,2-a]pyridine-4-carbonitrile **(7)**

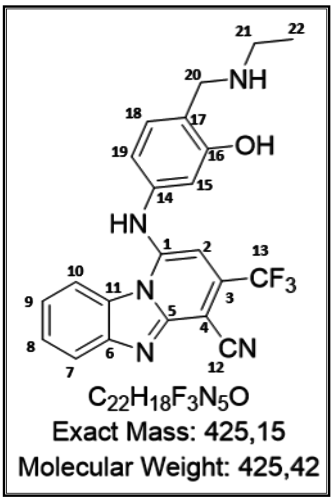

Obtained from **3.3b** (42 mg, 1.5 eq), compound **1.3a** (50 mg, 1.5 eq) and 4M Hydrogen chloride solution (0.1 mL, 1 eq) to isolate **7** as a brown solid (16.9 mg, 23%), M.P. 274 – 276 °C, R_f = 0.15 (10% MeOH/DCM); **^{1}H-NMR (400 MHz, DMSO-*d*$_6$)** δ 8.81 (d, *J* = 8.2 Hz, 1H, H10), 7.62 (d, *J* = 8.2 Hz, 1H, H7), 7.42 (t, *J* = 7.8 Hz, 1H, H9), 7.30 (d, *J* = 7.8 Hz, 1H, H18), 7.21 (t, *J* = 7.9 Hz, 1H, H8), 6.60-6.63 (m, 2H, H15 & H19), 6.00 (s, 1H, H2), 4.20 (s, 2H, H20), 3.15 (q, *J* = 7.2 Hz, 2H, H21), 1.38 (t, *J* = 7.3 Hz, 3H, H22); **^{13}C-NMR (101 MHz, DMSO-*d*$_6$)** δ 202.61, 177.70, 164.23, 153.77, 149.97, 134.09, 132.80, 130.73, 124.75, 121.81, 119.46, 117.06, 113.61, 112.14, 109.00, 106.07, 101.19, 100.02, 85.65, 45.32, 42.25, 11.31; **LC-MS (ESI$^+$):** Purity 96%, (t_R 2.384 min), m/z 426.2 $[M + H]^+$.

1-((3-((ethylamino)methyl)-5-fluoro-2-hydroxyphenyl)amino)-3-(trifluoromethyl)benzo[4,5]imidazo[1,2-a]pyridine-4-carbonitrile **(10)**

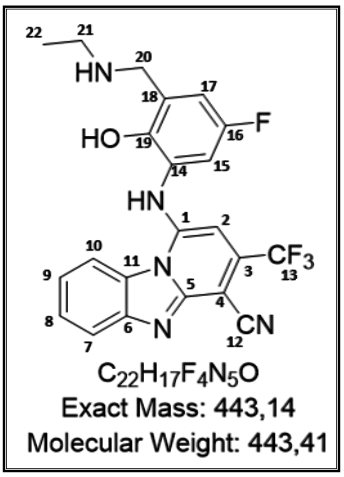

Obtained from **3.3d** (60 mg, 1.2 eq), compound **1.3a** (80 mg, 1.0 eq) and KH_2PO_4 (73 mg, 2 eq) to isolate **10** as a brown powder (31 mg, 31%), M.P. 273 – 275 °C, R_f = 0.21 (10% MeOH/DCM); **^{1}H-NMR (600 MHz, DMSO-*d*$_6$)** δ 8.83 (dd, *J* = 8.0, 1.6 Hz, 1H, H10), 7.58 (dd, *J* = 8.1, 1.7 Hz, 1H, H7), 7.35 (td, *J* = 8.2, 1.3 Hz, 1H, H9), 7.11 (td, *J* = 8.3, 1.2 Hz, 1H, H8), 6.87 (dd, *J* = 9.2, 3.14 Hz, 1H, H17), 6.84 (dd, *J* = 10.3, 3.11 Hz, 1H, H15), 5.74 (s, 1H, H2), 4.14 (s, 2H, H20), 3.03 (q, *J* = 7.2 Hz, 2H, H21), 1.24 (t, *J* = 7.2 Hz, 3H, H22); **^{13}C-NMR (151 MHz, DMSO-*d*$_6$)** δ 156.47, 154.91, 152.17, 151.66, 145.58, 145.09, 140.15 (d, C*J*F), 134.95 (q, C*J*F), 131.21, 124.85, 124.51, 119.20 (d, C*J*F), 118.91, 118.54, 117.77, 116.38, 109.96 (d, C*J*F), 109.50 (d, *CJF*), 87.90, 45.43, 42.61, 11.39; **LC-MS (ESI$^+$):** Purity 98%, (t_R 2.408 min), m/z 444.3 $[M + H]^+$.

1-((4-chloro-3-((ethylamino)methyl)-2-hydroxyphenyl)amino)-3-(trifluoromethyl)benzo[4,5]imidazo[1,2-a]pyridine-4-carbonitrile **(11)**

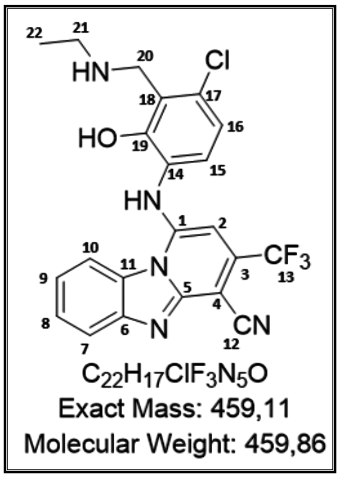

Obtained from **3.3e** (57 mg, 1.2 eq), compound **1.3a** (70 mg, 1.0 eq) and KH_2PO_4 (65 mg, 2 eq) to isolate **11** as a yellow powder (9.8 mg, 9%), M.P. 274 – 275 °C R_f = 0.14 (8% MeOH/DCM); **^{1}H-NMR (600 MHz, DMSO-*d*$_6$)** δ 8.84 (dd, *J* = 8.1, 2.0 Hz, 1H, H10), 7.58 (dd, *J* = 8.0, 1.7 Hz, 1H, H7), 7.35 (td, *J* = 8.5, 1.3 Hz, 1H, H9), 7.11 (td, *J* = 8.2, 0.9 Hz, 1H, H8), 7.06 – 6.96 (m, 2H, H15/H16), 5.73 (s, 1H, H2), 4.26 (s, 2H, H20), 3.07 (q, *J* = 7.2 Hz, 2H, H21), 1.26 (t, *J* = 7.2 Hz, 3H, H22); **^{13}C-NMR (151 MHz, DMSO-*d*$_6$)** δ 152.23, 151.66, 150.51, 145.54, 138.13, 134.88, 131.22, 126.98, 124.85, 124.51, 123.79, 123.03, 120.44, 118.91, 118.54, 117.80, 116.94, 116.33, 87.99, 49.06, 43.14, 11.35; **LC-MS (ESI$^+$):** Purity 98%, (t_R 2.573 min), m/z 460.0 $[M + H]^+$.

1-((5-chloro-3-((ethylamino)methyl)-2-hydroxyphenyl)amino)-3-(trifluoromethyl)benzo[4,5]imidazo[1,2-a]pyridine-4-carbonitrile **(12)**

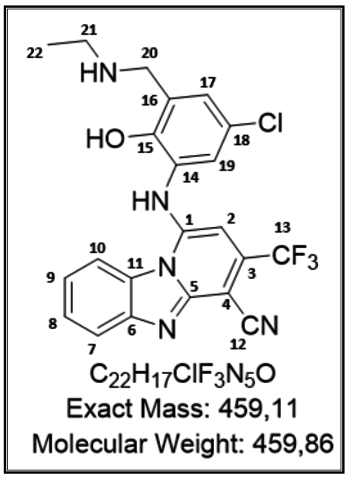

Obtained from **3.3f** (65 mg, 1.2 eq), compound **1.3a** (80 mg, 1.0 eq) and KH_2PO_4 (73 mg, 2 eq) to isolate **12** as a brown powder (21.8 mg, 18%). M.P. 274 – 276 °C, R_f = 0.37 (20% MeOH/DCM); **^{1}H-NMR (600 MHz, DMSO-*d*$_6$)** δ 8.82 (dd, *J* = 8.0, 2.0 Hz, 1H, H10), 7.58 (dd, *J* = 8.0, 1.8 Hz, 1H, H7), 7.35 (td, *J* = 8.3, 1.3 Hz, 1H, H9), 7.11 (td, *J* = 7.4, 1.2 Hz, 1H, H8), 7.10 – 7.09 (m, 1H, H19), 6.99 (d, *J* = 2.6 Hz, 1H, H17), 5.69 (s, 1H, H2), 4.12 (s, 2H, H20), 3.02 (q, *J* = 7.2 Hz, 2H, H21), 1.24 (t, *J* = 7.2 Hz, 3H, H22); **^{13}C-NMR (151 MHz, DMSO-*d*$_6$)** δ 152.21, 151.63, 147.71, 145.53, 140.53, 135.00), 131.22, 125.31, 124.51, 123.70, 123.01, 122.58, 122.29, 120.37, 118.93, 118.49, 117.78, 116.36, 87.86, 45.19, 42.63, 11.39; **LC-MS (ESI$^+$):** Purity 98%, (t_R 2.576 min), m/z 460.1 $[M + H]^+$.

1-((3-((ethylamino)methyl)-2-hydroxy-6-methylphenyl)amino)-3-(trifluoromethyl)benzo[4,5]imidazo[1,2-a]pyridine-4-carbonitrile **(13)**

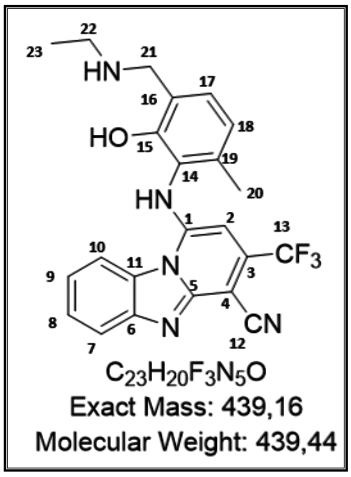

Obtained from **3.3f** (51 mg, 1.2 eq), compound **1.3a** (70 mg, 1.0 eq) and KH_2PO_4 (65 mg, 2 eq) to isolate **13** as a yellow powder (14 mg, 13%). M.P. 244–245 °C, R_f = 0.25 (15% MeOH/DCM); **^{1}H-NMR (400 MHz, DMSO-*d*$_6$)** δ 8.87 (dd, *J* = 8.0, 1.8 Hz, 1H, H10), 7.59 (dd, *J* = 8.0, 1.8 Hz, 1H, H7), 7.36 (td, *J* = 8.4, 1.2 Hz, 1H, H9), 7.14 (td, *J* = 8.5, 1.4 Hz, 1H, H8), 6.95 (d, *J* = 7.7 Hz, 1H, H17), 6.80 (d, *J* = 7.8 Hz, 1H, H18), 5.31 (s, 1H, H2), 4.1 (s, 2H, H21), 2.99 (q, *J* = 7.3 Hz, 2H, H22), 2.03 (s, 3H, H20), 1.23 (t, *J* = 7.2 Hz, 3H, H23); **^{13}C-NMR (101 MHz, DMSO-*d*$_6$)** δ 151.58, 151.29, 147.72, 144.88, 137.11, 134.56, 131.34, 127.96, 126.64, 124.81, 124.47, 122.99, 121.34, 119.12, 118.59, 117.76, 116.13, 115.94, 89.16, 45.73, 42.27, 18.18, 11.29; **LC-MS (ESI$^+$):** Purity 98%, (t_R 2.492 min), m/z 440.1 $[M + H]^+$.

1-((3-((ethylamino)methyl)-2-hydroxy-5-methylphenyl)amino)-3-(trifluoromethyl)benzo[4,5]imidazo[1,2-a]pyridine-4-carbonitrile **(14)**

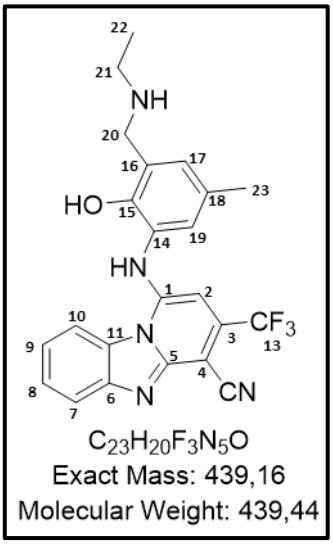

Obtained from **3.3g** (47 mg, 1.2 eq), compound **1.3a** (65 mg, 1.0 eq) and KH_2PO_4 (60 mg, 2 eq) to isolate **14** as a red powder (31 mg, 32%). M.P. 266–268 °C, R_f = 0.33 (15% MeOH/DCM); **^{1}H-NMR (600 MHz, DMSO-*d*$_6$)** δ 8.84 (dd, *J* = 8.1, 2.2 Hz, 1H, H10), 77.57 (dd, *J* = 8.2, 1.7 Hz, 1H, H7), 7.34 (td, *J* = 8.3, 1.3 Hz, 1H, H9), 7.10 (td, *J* = 8.1, 1.0 Hz, 1H, H8), 6.84 (d, *J* = 2.1 Hz, 1H, H17), 6.80 (d, *J* = 2.0 Hz, 1H, H19), 5.73 (s, 1H, H2), 4.09 (s, 2H, H20), 3.01 (q, *J* = 7.2 Hz, 2H, H21), 2.24 (s, 3H, H23), 1.24 (t, *J* = 7.2 Hz, 3H, H22); **^{13}C-NMR (151 MHz, DMSO-*d*$_6$)** δ 151.82, 146.10, 145.27, 138.50, 134.80, 134.49, 131.26, 128.49, 125.36, 125.15, 124.40, 123.63, 122.64, 118.87, 118.69, 118.39, 117.64, 116.13, 88.62, 45.73, 42.47, 20.76, 11.32; **LC-MS (ESI$^+$):** Purity 99%, (t_R 2.511min), m/z 440.1 $[M + H]^+$.

1-((3-((ethylamino)methyl)-2-hydroxyphenyl)amino)-3-(trifluoromethyl)benzo[4,5]imidazo[1,2-a]pyridine-4-carbonitrile **(15)**

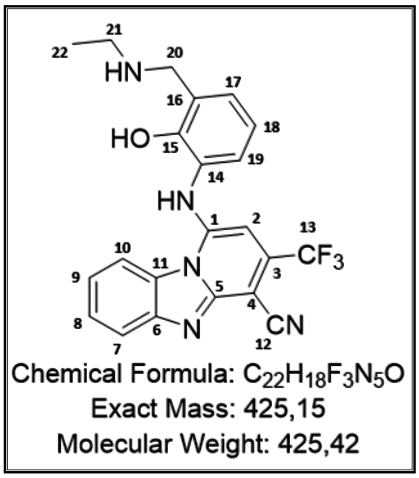

Obtained from **3.3c** (71 mg, 1.2 eq), compound **1.3a** (86 mg, 1.0 eq) and KH_2PO_4 (79 mg, 2 eq) to isolate **15** as a yellow solid (31.8 mg, 26%). M.P. 275–277 °C, R_f = 0.31 (15% MeOH/DCM); **^{1}H-NMR (600 MHz, DMSO-*d*$_6$)** δ 8.83 (dd, *J* = 8.1, 1.8 Hz, 1H, H10), 7.56 (dd, *J* = 8.1, 1.8 Hz, 1H, H7), 7.34 (td, *J* = 8.2, 1.3 Hz, 1H, H9), 7.11 (td, *J* = 8.2, 1.2 Hz, 1H, H8), 7.01 (dd, *J* = 7.6, 1.6 Hz, 1H, H17), 6.97 (dd, *J* = 7.7, 1.6 Hz, 1H, H19), 6.85 (t, *J* = 7.7 Hz, 1H, H18), 5.76 (s, 1H, H2), 4.11 (s, 2H, H20), 3.00 (q, *J* = 7.2 Hz, 2H, H21), 1.22 (t, *J* = 7.3 Hz, 3H, H22); **^{13}C-NMR (151 MHz, DMSO-*d*$_6$)** δ 151.59, 148.52, 144.33, 138.30, 134.68, 131.00, 125.09, 124.73, 123.15, 122.93, 120.52, 119.94, 119.29, 118.82, 118.32, 117.77, 117.30, 115.88, 114.35, 45.66, 42.51, 11.31; **LC-MS (ESI$^+$):** Purity 97%, (t_R 2.460 min), m/z 426.2 $[M + H]^+$.

General synthetic procedure and characterization of target compounds 16-28

The appropriate amine/Mannich base (1.5 eq) was dissolved in EtOH (2 mL) and added to the appropriate chlorinated PBI intermediate **1.3a-1.3d** (1.0 eq) and KH_2PO_4 (2.0 eq). The reaction mixture was allowed to stir at 23 °C for 12 h. The reaction mixture was diluted in EtOH (5 mL) and reduced *in vacuo*. The resulting residue was purified using column chromatography (DCM/MeOH) and reduced *in vacuo*. The residue was then triturated using pentane or diethyl ether to isolate final compounds **16-28.**

1-((3-((diethylamino)methyl)-2-hydroxy-5-methylphenyl)amino)-3-(trifluoromethyl)benzo[4,5]imidazo[1,2-a]pyridine-4-carbonitrile **(16)**

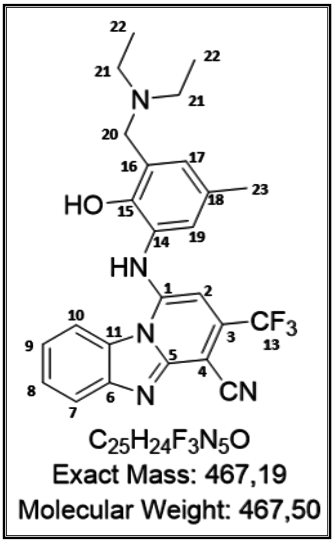

Obtained from **3.3g** (106 mg, 1.5 eq), compound **1.3a** (100 mg, 1.0 eq) and KH_2PO_4 (92 mg, 2 eq) to isolate **16** as a yellow solid (41.3 mg, 26%). M.P. 268–269 °C R_f = 0.54 (9% MeOH/DCM); **^{1}H-NMR (600 MHz, DMSO-*d*$_6$)** δ 8.85 (d, *J* = 8.2 Hz, 1H, H10), 7.63 (d, *J* = 8.0 Hz, 1H, H7), 7.46 (t, *J* = 7.7 Hz, 1H, H9), 7.25 (t, *J* = 7.7 Hz, 1H, H8), 7.00 (d, *J* = 2.1 Hz, 1H, H19), 6.88 (d, *J* = 2.1 Hz, 1H, H17), 5.80 (s, 1H, H2), 4.24 (s, 2H, H20), 3.12 (q, *J* = 7.2 Hz, 4H, H21), 2.26 (s, 3H, H23), 1.27 (t, *J* = 7.2 Hz, 6H, H22); **^{13}C-NMR (151 MHz, DMSO-*d*$_6$)** δ 151.08, 149.99, 146.68, 139.24, 135.94, 135.56, 133.67, 133.54, 130.37, 127.99, 126.67, 125.21, 123.58, 121.41, 118.84, 117.78, 117.65, 114.64, 92.29, 51.24, 46.42 (2C), 19.21, 10.29 (2C); **LC-MS (ESI$^+$):** Purity 98%, (t_R 2.151 min), m/z 468.2 $[M + H]^+$.

1-((3-((ethylamino)methyl)-4-hydroxyphenyl)amino)-3-methylbenzo[4,5]imidazo[1,2-a]pyridine-4-carbonitrile **(17)**

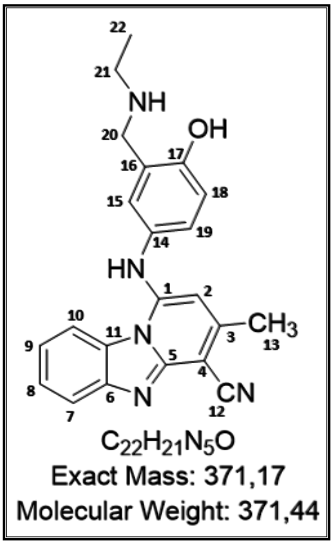

Obtained from **3.3a** (85 mg, 1.5 eq), compound **1.3b** (100 mg, 1.0 eq) and KH_2PO_4 (92 mg, 2 eq) to isolate **17** as a yellow solid (42 mg, 33%). M.P. 227–228 °C, R_f = 0.09 (10% MeOH/DCM); **^{1}H-NMR (600 MHz, DMSO-*d*$_6$)** δ 8.47 (d, *J* = 8.3 Hz, 1H, H10), 7.72 (d, *J* = 8.3 Hz, 1H, H7), 7.47 (t, *J* = 7.7 Hz, 1H, H9), 7.30 (s, 1H, H15), 7.25 (t, *J* = 8.4 Hz, 1H, H8), 7.17 (d, *J* = 8.1 Hz, 3H, H19), 7.01 (d, *J* = 8.5 Hz, 1H, H18), 5.95 (s, 1H, H2), 4.02 (s, 2H, H20), 2.91 (q, *J* = 7.3 Hz, 2H, H21), 2.38 (s, 3H, H13), 1.19 (t, *J* = 7.2 Hz, 3H, H22); **^{13}C-NMR (151 MHz, DMSO-*d*$_6$)** δ 153.84, 150.20, 149.40, 149.09, 129.00, 128.79, 127.22, 126.38, 125.99 (2C), 120.40, 119.80, 117.43, 116.82 (2C), 116.66, 116.37, 95.65, 45.10, 42.21, 21.02, 11.36; **LC-MS (ESI$^+$):** Purity 98%, (t_R 2.208 min), m/z 372.1 $[M + H]^+$.

1-((3-((diethylamino)methyl)-4-hydroxyphenyl)amino)-3-methylbenzo[4,5]imidazo[1,2-a]pyridine-4-carbonitrile **(18)**

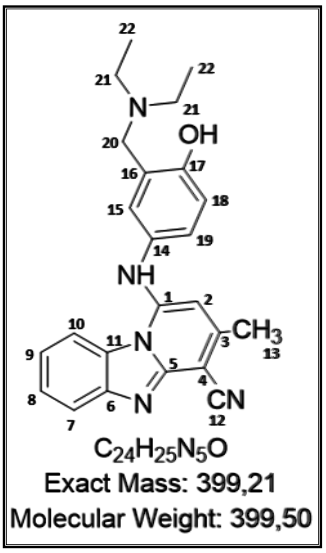

Obtained from **3.3i** (98 mg, 1.5 eq), compound **1.3b** (100mg, 1.0 eq) and KH_2PO_4 (92 mg, 2 eq) to isolate **18** as a yellow solid (46 mg, 34%). M.P. 243–244 °C, R_f = 0.48 (9% MeOH/DCM); **^{1}H-NMR (600 MHz, DMSO-*d*$_6$)** δ 10.10 (s, 1H, O**H**), 8.52 (d, *J* = 8.4 Hz, 1H, H10), 7.78 (d, *J* = 8.3 Hz, 1H, H7), 7.59 (t, *J* = 7.8 Hz, 1H, H9), 7.49 (d, *J* = 2.7 Hz, 1H, H15), 7.38 (t, *J* = 7.9 Hz, 1H, H8), 7.28 (dd, *J* = 8.6, 2.7 Hz, 1H, H19), 7.13 (d, *J* = 8.6 Hz, 1H, H18), 6.27 (s, 1H, H2), 4.17 (d, *J* = 5.2 Hz, 2H, H20), 3.11 – 2.97 (m, 3H, H21), 2.46 (s, 3H, H13), 1.23 (t, *J* = 7.2 Hz, 6H, H22); **^{13}C-NMR (151 MHz, DMSO-*d*$_6$)** δ 155.26, 152.62, 148.87, 147.75, 130.64, 129.09, 128.00, 127.53, 127.39, 121.81, 119.88, 117.91, 117.32 (2C), 116.86, 116.40, 115.98, 98.52, 49.82, 46.72 (2C), 21.09, 8.96 (2C); **LC-MS (ESI$^+$):** Purity 98%, (t_R 2.071 min), m/z 400.3 $[M + H]^+$.

1-((3-((ethylamino)methyl)-2-hydroxy-5-methylphenyl)amino)-3-methylbenzo[4,5]imidazo[1,2-a]pyridine-4-carbonitrile **(19)**

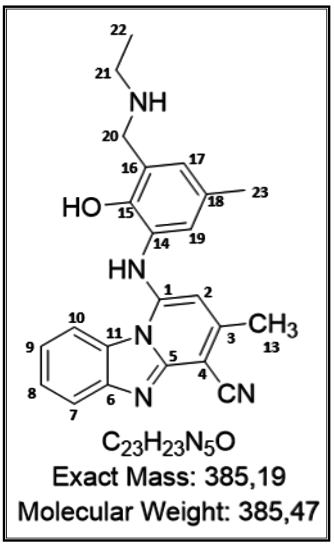

Obtained from **3.3g** (92 mg, 1.5 eq), compound **1.3b** (100mg, 1.0 eq) and KH_2PO_4 (92 mg, 2 eq) to isolate **19** as a yellow solid (33 mg, 25%). M.P. 217–218 °C, R_f = 0.1 (10% MeOH/DCM), **^{1}H-NMR (400 MHz, DMSO-*d*$_6$)** δ 8.52 (d, *J* = 8.1 Hz, 1H, H10), 7.57 – 7.49 (m, 2H, H7 / H19), 7.48 (t, *J* = 7.6 Hz, 1H, H9), 7.37 – 7.27 (m, 2H, H8 / H17), 5.86 (s, 1H, H2), 4.16 (s, 1H, H20), 3.06 (q, *J* = 7.2 Hz, 2H, H21), 2.34 (s, 3H, H13), 1.27 (t, *J* = 7.2 Hz, 3H, H22); **^{13}C-NMR (101 MHz, DMSO-*d*$_6$)** δ 159.24, 151.58, 149.35, 148.97, 133.95, 129.00, 128.48, 126.65, 126.25, 122.39, 122.25, 120.85, 119.36, 117.30, 116.77, 116.41, 112.51, 104.11, 42.97, 42.72, 20.79, 19.56, 11.28; **LC-MS (ESI$^+$):** Purity 98% (t_R 2.326 min), m/z 386.1 $[M + H]^+$.

1-((3-((diethylamino)methyl)-2-hydroxy-5-methylphenyl)amino)-3-methylbenzo[4,5]imidazo[1,2-a]pyridine-4-carbonitrile **(20)**

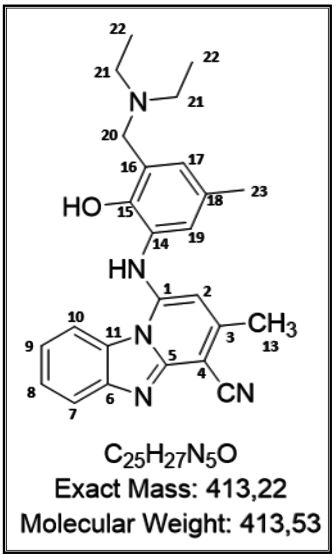

Obtained from **3.3j** (106 mg, 1.5 eq), compound **1.3b** (100mg, 1.0 eq) and KH_2PO_4 (92 mg, 2 eq) to isolate **20** as a yellow solid (55 mg, 39%). M.P. 234–235 °C, R_f = 0.48 (10% MeOH/DCM); **^{1}H-NMR (600 MHz, DMSO-*d*$_6$)** δ 10.12 (s, 1H, OH), 8.68 (d, *J* = 8.4 Hz, 1H, H10), 7.76 (d, *J* = 8.2 Hz, 1H, H7), 7.59 (t, *J* = 7.7 Hz, 1H, H9), 7.38 (t, *J* = 7.8 Hz, 1H, H8), 7.36 (s, 1H, H19), 7.13 (s, 1H, H17), 4.25 (s, 2H, H20), 3.10 – 3.02 (m, 4H, H21), 2.40 (s, 3H, H13), 2.24 (s, 3H, H23), 1.26 (t, *J* = 7.2 Hz, 6H, H22); **^{13}C-NMR (151 MHz, DMSO-*d*$_6$)** δ 151.75, 149.25, 148.99, 147.61, 145.83, 131.99, 129.59, 129.21, 128.30, 127.23, 123.85, 121.79, 119.47, 118.97, 117.31, 116.17, 115.86, 97.79, 50.18, 46.64 (2C), 21.03, 20.49, 8.94 (2C); **LC-MS (ESI$^+$):** Purity 98%, (t_R 2.393 min), m/z 414.2 $[M + H]^+$.

1-((3-((ethylamino)methyl)-4-hydroxyphenyl)amino)-7,8-difluoro-3-methylbenzo[4,5]imidazo[1,2-a]pyridine-4-carbonitrile **(21)**

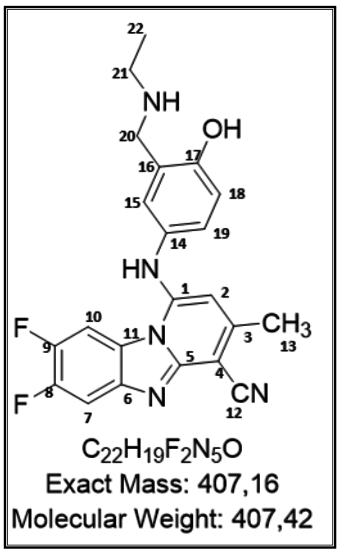

Obtained from **3.3a** (90 mg, 1.5 eq), compound **1.3d** (100mg, 1.0 eq) and KH_2PO_4 (92 mg, 2 eq) to isolate **21** as a yellow solid (33 mg, 22%). M.P. 269–270 °C, R_f = 0.12 (10 % MeOH/DCM); **^{1}H-NMR (600 MHz, DMSO-*d*$_6$)** δ 8.58 (dd, *J* = 11.6, 7.6 Hz, 1H, H10), 7.70 (dd, *J* = 11.2, 7.7 Hz, 1H, H7), 7.23 (d, *J* = 2.6 Hz, 1H, H15), 7.13 (dd, *J* = 8.7, 2.6 Hz, 1H, H19), 6.98 (d, *J* = 8.6 Hz, 1H, H18), 5.84 (s, 1H, H2), 4.03 (s, 2H, H20), 2.93 (q, *J* = 7.3 Hz, 2H, H21), 2.33 (s, 3H, H13), 1.19 (t, *J* = 7.2 Hz, 3H, H22); **^{13}C-NMR (151 MHz, DMSO-*d*$_6$)** δ 153.46, 151.65, 149.51, 149.14, 147.91, 147.81, 145.12, 143.55, 141.19, 127.27, 126.48, 124.40, 119.57, 117.81, 116.73, 104.97, 104.81, 95.13, 45.10, 42.27, 21.05, 11.29; **^{19}F NMR (377 MHz, DMSO-*d*$_6$) δ** -140.10, -146.56; **LC-MS (ESI$^+$):** Purity 98%, (t_R 2.263 min), m/z 408.2 $[M + H]^+$.

1-((3-((diethylamino)methyl)-4-hydroxyphenyl)amino)-7,8-difluoro-3-methylbenzo[4,5]imidazo[1,2-a]pyridine-4-carbonitrile **(22)**

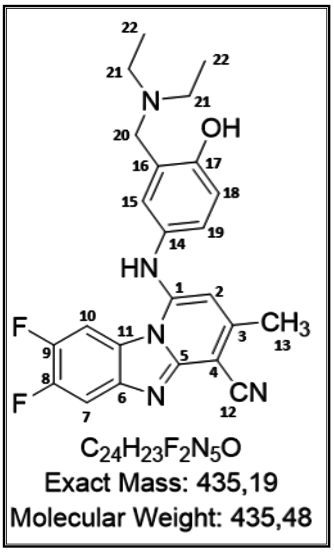

Obtained from **3.3i** (100 mg, 1.2 eq), compound **1.3d** (100mg, 1.0 eq) and KH_2PO_4 (92 mg, 2 eq) to isolate **22** as a yellow solid (45 mg, 29%). M.P. 289–290 °C, R_f = 0.44 (10% MeOH/DCM); **^{1}H-NMR (600 MHz, DMSO-*d*$_6$)** δ 8.55 (dd, *J* = 11.4, 7.3 Hz, 1H, H10), 7.82 (dd, *J* = 11.0, 7.6 Hz, 1H, H7), 7.43 (d, *J* = 2.7 Hz, 1H, H15), 7.28 (dd, *J* = 7.7, 2.6 Hz, 1H, H19), 7.08 (d, *J* = 8.6 Hz, 1H, H18), 6.03 (s, 1H, H2), 4.18 (s, 2H, H20), 3.06 (q, *J* = 7.24 Hz, 4H, H21), 2.41 (s, 3H, H13), 1.23 (t, *J* = 7.2 Hz, 6H, H22); **^{13}C-NMR (151 MHz, DMSO-*d*$_6$)** δ 155.05, 151.43, 150.63, 149.93, 148.14, 145.66, 144.18, 129.11, 127.71, 123.73, 123.66, 117.95, 117.15, 116.59, 105.61, 105.15, 104.98, 96.44, 50.15, 46.92 (2C), 21.03, 9.00 (2C); **LC-MS (ESI$^+$):** Purity 98%, (t_R 2.322 min), m/z 436.2 $[M + H]^+$.

1-((3-((ethylamino)methyl)-2-hydroxy-5-methylphenyl)amino)-7,8-difluoro-3-methylbenzo[4,5]imidazo[1,2-a]pyridine-4-carbonitrile **(23)**

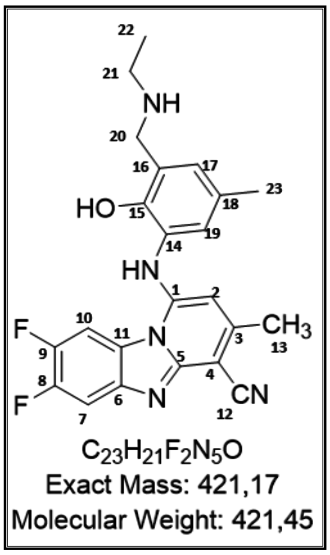

Obtained from **3.3g** (98 mg, 1.5 eq), compound **1.3d** (100mg, 1.0 eq) and KH_2PO_4 (92 mg, 2 eq) to isolate **23** as a yellow solid (45 mg, 29%). M.P. 257–258 °C, R_f = 0.47 (10% MeOH/DCM); **^{1}H-NMR (400 MHz, DMSO-*d*$_6$)** δ 8.77 (dd, *J* = 11.8, 7.4 Hz, 1H, H10), 7.88 – 7.79 (m, 1H, H7), 7.23 (d, *J* = 2.3 Hz, 1H, H19), 6.89 (d, *J* = 2.4 Hz, 1H, H17), 5.60 (s, 1H, H2), 4.15 (s, 2H, H20), 3.05 (q, *J* = 7.2 Hz, 2H, H21), 2.44 (s, 3H, H13), 2.39 (s, 3H, H23), 1.27 (t, *J* = 7.3 Hz, 3H, H22); **^{13}C-NMR (101 MHz, DMSO-*d*$_6$)** δ 152.21, 150.71, 150.16, 148.48, 147.87, 146.02, 143.81, 143.67, 138.81, 129.13, 124.14, 124.03, 122.49, 119.87, 116.80, 105.64, 105.39, 94.81, 42.88, 42.44, 21.05, 19.78, 11.29; **^{19}F NMR (377 MHz, DMSO-*d*$_6$)** δ -139.04 (d, *J* = 22.1 Hz), -145.75 (d, *J* = 22.6 Hz); **LC-MS (ESI$^+$):** Purity 98%, (t_R 2.406 min), m/z 422.2 $[M + H]^+$.

1-((3-((diethylamino)methyl)-2-hydroxy-5-methylphenyl)amino)-7,8-difluoro-3-methylbenzo[4,5]imidazo[1,2-a]pyridine-4-carbonitrile **(24)**

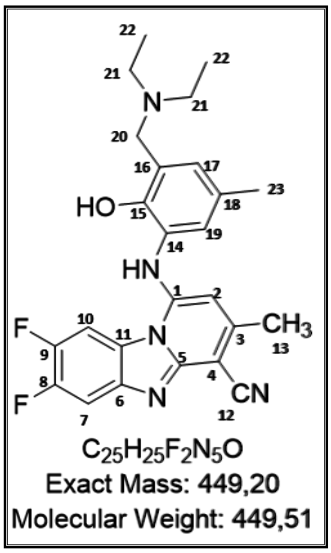

Obtained from **3.3j** (105 mg, 1.2 eq), compound **1.3d** (100mg, 1.0 eq) and KH_2PO_4 (92 mg, 2 eq) to isolate **24** as a yellow solid (41 mg, 25%). M.P. 205–206 °C, R_f = 0.47 (10% MeOH/DCM); **^{1}H-NMR (600 MHz, DMSO-*d*$_6$)** δ 8.69 (dd, *J* = 11.6, 7.3 Hz, 1H, H10), 7.79 (dd, *J* = 11.6, 7.3 Hz, 1H, H7), 7.27 (s, 1H, H19), 7.14 (s, 1H, H17), 5.59 (s, 1H, H2), 4.23 (s, 2H, H20), 3.08 (q, *J* = 7.2 Hz, 4H, H21), 2.35 (s, 3H, H13), 2.24 (s, 3H, H23), 1.24 (t, *J* = 7.2 Hz, 6H, H22); **^{13}C-NMR (151 MHz, DMSO-*d*$_6$)** δ 150.99, 150.57, 149.88, 149.65, 148.05, 145.73, 144.17, 131.97, 129.76, 129.53, 124.04, 123.97, 119.29, 116.76, 105.51, 105.34, 105.08, 95.30, 50.57, 46.90 (2C), 21.00, 20.43, 9.01 (2C); **LC-MS (ESI$^+$):** Purity 98%, (t_R 2.461 min), m/z 450.2 $[M + H]^+$.

1-((3-((ethylamino)methyl)-4-hydroxyphenyl)amino)-7,8-difluoro-3-(trifluoromethyl)benzo[4,5]imidazo[1,2-a]pyridine-4-carbonitrile **(25)**

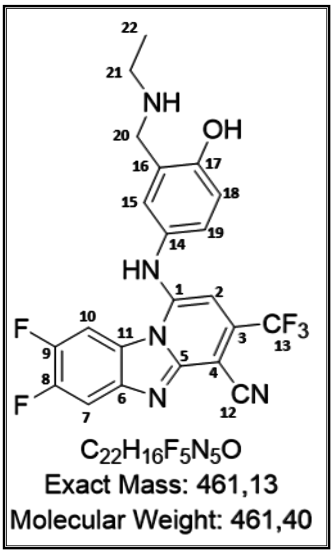

Obtained from **3.3a** (75 mg, 1.5 eq), compound **1.3c** (100mg, 1.0 eq) and KH_2PO_4 (92 mg, 2 eq) to isolate **25** as a yellow solid (25 mg, 18%). M.P. 265–266 °C, R_f = 0.13 (10% MeOH/DCM); **^{1}H-NMR (400 MHz, DMSO-*d*$_6$)** δ 8.80 (dd, *J* = 11.5, 7.7 Hz, 1H, H10), 7.79 (dd, *J* = 10.9, 7.4 Hz, 1H, H7), 7.24 (d, *J* = 2.6 Hz, 1H, H15), 7.14 (dd, *J* = 8.6, 2.6 Hz, 1H, H19), 7.04 (d, *J* = 8.5 Hz, 1H, H18), 6.04 (s, 1H, H2), 4.10 (s, 2H, H20), 3.15 – 3.04 (m, 2H, H21), 1.23 (t, *J* = 7.3 Hz, 3H, H22); **^{13}C-NMR (101 MHz, DMSO-*d*$_6$)** δ 164.70, 153.68, 151.17, 149.67, 143.98, 139.51, 135.53, 127.99, 127.05, 126.06, 124.61, 121.65, 119.70, 116.89, 115.87, 105.53, 105.27, 46.17, 45.12, 42.32, 11.24, 9.04; **^{19}F NMR (377 MHz, DMSO-*d*$_6$)** δ -62.33, -138.74, -144.74; **LC-MS (ESI$^+$):** Purity 98%, (t_R 2.402 min), m/z 462.1 $[M + H]^+$.

1-((3-((diethylamino)methyl)-4-hydroxyphenyl)amino)-7,8-difluoro-3-(trifluoromethyl)benzo[4,5]imidazo[1,2-a]pyridine-4-carbonitrile **(26)**

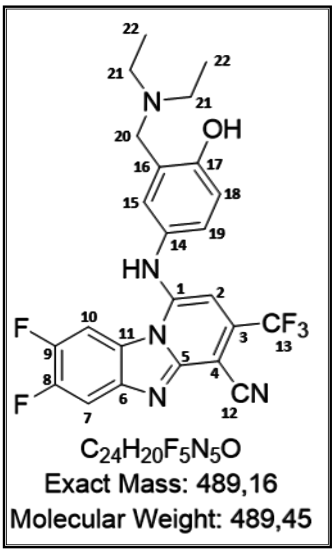

Obtained from **3.3i** (44 mg, 1.2 eq), compound **1.3c** (50mg, 1.0 eq) and KH_2PO_4 (46 mg, 2 eq) to isolate **26** as a yellow solid (8.7 mg, 12%). M.P. 150–151 °C, R_f = 0.49 (10% MeOH/DCM); **^{1}H-NMR (600 MHz, DMSO-*d*$_6$)** δ 8.70 (dd, *J* = 11.5, 8.2 Hz, 1H, H10), 7.51 (dd, *J* = 11.4, 7.5 Hz, 1H, H7), 7.01 (d, *J* = 2.5 Hz, 1H, H15), 6.93 (d, *J* = 8.5 Hz, 1H, H18), 6.89 (dd, *J* = 8.5, 2.5 Hz, 1H, H19), 5.70 (s, 1H, H2), 4.17 (s, 2H, H20), 3.08 (q, *J* = 7.2 Hz, 4H, H21), 1.21 (t, *J* = 7.2 Hz, 6H, H22); **^{13}C-NMR (151 MHz, DMSO-*d*$_6$)** δ 153.48, 152.12, 150.44, 147.20, 142.41, 141.60, 134.86, 134.66, 126.12, 125.95, 124.72, 122.91, 118.33, 117.73, 116.95, 104.90, 103.25, 88.59, 70.22, 50.91, 47.08 (2C), 8.99 (2C); **LC-MS (ESI$^+$):** Purity 98%, (t_R 2.445 min), m/z 490.2 $[M + H]^+$.

1-((3-((ethylamino)methyl)-2-hydroxy-5-methylphenyl)amino)-7,8-difluoro-3-(trifluoromethyl)benzo[4,5]imidazo[1,2-a]pyridine-4-carbonitrile **(27)**

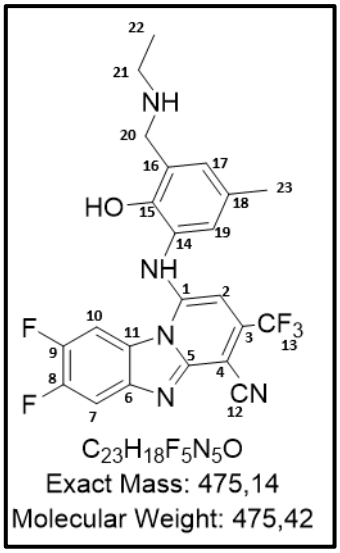

Obtained from **3.3g** (82 mg, 1.5 eq), compound **1.3c** (100 mg, 1.0 eq) and KH_2PO_4 (92 mg, 2 eq) to isolate **27** as a yellow solid (17 mg, 12%). M.P. >300 °C, R_f = 0.41 (10% MeOH/DCM); **^{1}H-NMR (600 MHz, DMSO-*d*$_6$)** δ 8.75 (dd, *J* = 11.6, 8.1 Hz, 1H, H10), 7.54 (dd, *J* = 11.1, 7.4 Hz, 1H, H7), 6.84 (s, 1H, H19), 6.79 (s, 1H, H17), 5.69 (s, 1H, H2), 4.06 (s, 2H, H20), 3.00 – 2.96 (m, 2H, H21), 2.20 (s, 3H, H23), 1.20 (t, *J* = 7.3 Hz, 3H, H22); **^{13}C-NMR (151 MHz, DMSO-*d*$_6$)** δ 152.86, 151.06, 149.06, 146.33, 144.72, 135.00, 134.80, 128.59, 126.00, 124.57, 124.19, 122.75, 118.88, 117.82, 105.83, 105.66, 103.19, 89.22, 46.27, 45.69, 42.49, 20.66, 11.29; **^{19}F NMR (377 MHz, DMSO-*d*$_6$)** δ -62.34, -141.54, -147.82; **LC-MS (ESI$^+$):** Purity 98%, (t_R 2.607 min), m/z 476.1 $[M + H]^+$.

1-((3-((diethylamino)methyl)-2-hydroxy-5-methylphenyl)amino)-7,8-difluoro-3-(trifluoromethyl)benzo[4,5]imidazo[1,2-a]pyridine-4-carbonitrile **(28)**

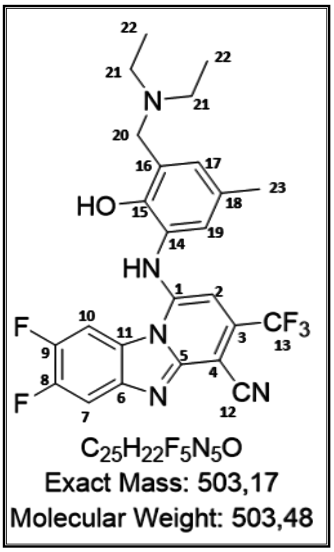

Obtained from **3.3j** (47 mg, 1.2 eq), compound **1.3c** (50 mg, 1.0 eq) and KH_2PO_4 (92 mg, 2 eq) to isolate **28** as a yellow solid (19 mg, 25%). M.P. 235–236 °C, R_f = 0.41 (10% MeOH/DCM); **^{1}H-NMR (600 MHz, DMSO-*d*$_6$)** δ 8.72 (dd, *J* = 11.5, 8.1 Hz, 1H, H10), 7.51 (dd, *J* = 11.4, 7.4 Hz, 1H, H7), 6.86 (s, 1H, H19), 6.80 (s, 1H, H17), 5.63 (s, 1H, H2), 4.20 (s, 2H, H20), 3.10 (q, *J* = 7.2 Hz, 4H, H21), 2.20 (s, 3H, H23), 1.23 (t, *J* = 7.2 Hz, 6H, H22); **^{13}C-NMR (151 MHz, DMSO-*d*$_6$)** δ 153.02, 151.19, 148.99, 147.40, 146.82, 144.63, 143.08, 140.97, 134.96, 128.86, 126.93, 126.07, 124.76, 122.79, 117.99, 117.29, 105.61, 103.02, 89.08, 51.17, 47.14 (2C), 20.64, 8.97 (2C); **LC-MS (ESI$^+$):** Purity 98%, (t_R 2.635 min), m/z 504.2 $[M + H]^+$.

CHAPTER 6: References

1. WHO. *World Malaria Report. Colombia*. WHO; **2019**.

2. Ridley RG. Medical need, scientific opportunity and the drive for antimalarial drugs. *Nature*. **2002**; 415, 686-693.

3. World Health Organisation (WHO). *World Malaria Report*. Geneva, Switzerland; **2017**.

4. Hemingway J, Ranson H, Magill A, et al. Averting a malaria disaster: Will insecticide resistance derail malaria control? *Lancet*. **2016**; 387, 1785-1788.

5. Ashley EA, Dhorda M, Fairhurst RM, et al. Spread of artemisinin resistance in Plasmodium falciparum malaria. *N Engl J Med*. **2014**, 371, 411-423.

6. Neafsey DE, Juraska M, Bedford T, et al. Genetic diversity and protective efficacy of the RTS,S/AS01 malaria vaccine. *N Engl J Med*. **2015**; 373, 2025-2037.

7. Singh K, Okombo J, Brunschwig C, et al. Antimalarial Pyrido[1,2-a]benzimidazoles: Lead Optimization, Parasite Life Cycle Stage Profile, Mechanistic Evaluation, Killing Kinetics, and in Vivo Oral Efficacy in a Mouse Model. *J Med Chem*. **2017**; 60, 1432-1448.

8. Thota S, Yerra R. Drug Discovery and Development of Antimalarial Agents : Recent Advances. *Curr Protein Pept Sci Bras*. **2016**; 17, 275-279.

9. Thota S, Yerra R. Drug discovery and development of antimalarial agents: Recent advances. *Curr Protein Pept Sci*. **2016**; 17, 275-279.

10. Battle KE, Guerra CA, Golding N, et al. Global database of matched Plasmodium falciparum and P. vivax incidence and prevalence records from 1985-2013. *Sci Data*. **2015**; 2, 1-12.

11. Tsuji M, Kain KC. Malaria. In: *Medical Parasitology*; **2009**.

12. Moreira CK, Templeton TJ, Lavazec C, et al. The Plasmodium TRAP/MIC2

family member, TRAP-Like Protein (TLP), is involved in tissue traversal by sporozoites. *Cell Microbiol*. **2008**; 10, 1505-1516.

13. Cowman AF, Healer J, Marapana D, Marsh K. Malaria: Biology and Disease. *Cell*. **2016**; 167, 610-624.

14. Tavares J, Formaglio P, Thiberge S, et al. Role of host cell traversal by the malaria sporozoite during liver infection. *J Exp Med*. **2013**; 210, 905-915.

15. Galinski MR, Meyer EVS, Barnwell JW. *Plasmodium Vivax. Modern Strategies to Study a Persistent Parasite's Life Cycle*. Elsevier; **2013**; 81, 1-26.

16. Sturm A, Amino R, Van De Sand C, et al. Manipulation of host hepatocytes by the malaria parasite for delivery into liver sinusoids. *Science.* **2006**; 313, 1287-1290.

17. Amino R, Giovannini D, Thiberge S, et al. Host Cell Traversal Is Important for Progression of the Malaria Parasite through the Dermis to the Liver. *Cell Host Microbe*. **2008**; 3, 88-96.

18. Tuteja R. Malaria - An overview. *FEBS J*. **2007**; 274, 4670-4679.

19. Weiss GE, Gilson PR, Taechalertpaisarn T, et al. Revealing the Sequence and Resulting Cellular Morphology of Receptor-Ligand Interactions during Plasmodium falciparum Invasion of Erythrocytes. *PLoS Pathog*. **2015**; 11(2).

20. Lin CS, Uboldi AD, Epp C, et al. Multiple plasmodium falciparum merozoite surface protein 1 complexes mediate merozoite binding to human erythrocytes. *J Biol Chem*. **2016**; 291, 7703-7715

21. Das S, Hertrich N, Perrin AJ, et al. Processing of Plasmodium falciparum Merozoite Surface Protein MSP1 Activates a Spectrin-Binding Function Enabling Parasite Egress from RBCs. *Cell Host Microbe*. **2015**; 18, 433-444.

22. Tham WH, Healer J, Cowman AF. Erythrocyte and reticulocyte binding-like proteins of Plasmodium falciparum. *Trends Parasitol*. **2012**; 28, 23-30.

23. Volz JC, Yap A, Sisquella X, et al. Essential Role of the PfRh5/PfRipr/CyRPA

Complex during Plasmodium falciparum Invasion of Erythrocytes. *Cell Host Microbe*. **2016**; 20, 60-71.

24. Riglar DT, Richard D, Wilson DW, et al. Super-resolution dissection of coordinated events during malaria parasite invasion of the human erythrocyte. *Cell Host Microbe*. **2011**; 9, 9-20.

25. Njoroge M, Njuguna NM, Mutai P, Ongarora DSB, et al. Recent Approaches to Chemical Discovery and Development Against Malaria and the Neglected Tropical Diseases Human African Trypanosomiasis and Schistosomiasis. *Chem Rev*. **2014**; 114, 11138-11163.

26. Reininger L, Billker O, Tewari R, et al. A NIMA-related protein kinase is essential for completion of the sexual cycle of malaria parasites. *J Biol Chem*. **2005**; 280, 31957-31964.

27. Cowman AF, Healer J, Marapana D, et al. Malaria: Biology and Disease. *Cell*. **2016**; 167, 610-624.

28. Mantel PY, Hoang AN, Goldowitz I, et al. Malaria-infected erythrocyte-derived microvesicles mediate cellular communication within the parasite population and with the host immune system. *Cell Host Microbe*. **2013**; 13, 521-534.

29. Lasonder E, Rijpma SR, Van Schaijk BCL, et al. Integrated transcriptomic and proteomic analyses of P. Falciparum gametocytes: Molecular insight into sex-specific processes and translational repression. *Nucleic Acids Res*. **2016**; 44, 6087-6101.

30. Galinski MR, Meyer EVS, Barnwell JW. Plasmodium vivax. Modern Strategies to Study a Persistent Parasite's Life Cycle. *Adv Parasitol*. **2013**; 81, 1-26.

31. Okombo J, Chibale K. Recent updates in the discovery and development of novel antimalarial drug candidates. *Medchemcomm*. **2018**; 9, 437-453.

32. Wells TNC, Van Huijsduijnen RH, Van Voorhis WC. Malaria medicines: A glass half full? *Nat Rev Drug Discov*. **2015**; 14, 424-442.

33. Pluess B, Tanser FC, Lengeler C, et al. Indoor residual spraying for preventing

malaria. *Cochrane Database Syst Rev*. **2010**.

34. Partnership SCT. Efficacy and safety of RTS,S/AS01 malaria vaccine with or without a booster dose in infants and children in Africa: Final results of a phase 3, individually randomised, controlled trial. *Lancet*. **2015**; 386, 31-45.

35. Greenwood B. Progress with the PfSPZ Vaccine for malaria. *Lancet Infect Dis*. **2017**; 17, 463-464.

36. Burrows JN, Hooft Van Huijsduijnen R, Möhrle JJ, Oeuvray C, et al. Designing the next generation of medicines for malaria control and eradication. *Malar J*. **2013**; 12, 187.

37. WHO. Antimalarial Drug Combination Therapy: Report of a WHO Technical Consultation. **2001.**

38. Wilson DW, Langer C, Goodman CD, et al. Defining the timing of action of antimalarial drugs against Plasmodium falciparum. *Antimicrob Agents Chemother*. **2013**; 57, 1455-1467.

39. Nzila A. The past, present and future of antifolates in the treatment of Plasmodium falciparum infection. *J Antimicrob Chemother*. **2006**; 57, 1043-1054.

40. Wesche D. Mechanism of cardiotoxicity of halofantrine. *Clin Pharmacol Ther*. **2000**; 67, 521-529.

41. Baird JK, Hoffman SL. Primaquine therapy for malaria. *Clin Infect Dis*. **2004**; 39, 1336-1345.

42. Llanos-Cuentas A, Lacerda M V., Rueangweerayut R, et al. Tafenoquine plus chloroquine for the treatment and relapse prevention of Plasmodium vivax malaria (DETECTIVE): A multicentre, double-blind, randomised, phase 2b dose-selection study. *Lancet*. **2014**; 383, 1049-1058.

43. Lacerda MVG, Llanos-Cuentas A, Krudsood S, et al. Single-dose tafenoquine to prevent relapse of plasmodium vivax malaria. *N Engl J Med*. **2019**; 380, 215-228.

44. Ashley EA, Mcgready R, Hutagalung R, et al. A Randomized , Controlled Study of a Simple , Once- Daily Regimen of Dihydroartemisinin-Piperaquine for the Treatment of Uncomplicated , Multidrug- Resistant Falciparum Malaria. *Clin Infect Dis*. **2005**; 41, 425-432.

45. Llanos-Cuentas A, Lacerda MVG, Hien TT, et al. Tafenoquine versus primaquine to prevent relapse of plasmodium vivax malaria. *N Engl J Med*. **2019**; 380, 229-241.

46. Burrows JN, Duparc S, Gutteridge WE, et al. New developments in anti-malarial target candidate and product profiles. *Malar J*. **2017**; 16.

47. Abbat S, Jain V, Bharatam P V. Origins of the specificity of inhibitor P218 toward wild-type and mutant PfDHFR: A molecular dynamics analysis. *J Biomol Struct Dyn*. **2015**; 33, 1913-1928.

48. Ashley EA, Phyo AP. Drugs in Development for Malaria. *Drugs*. 2018.

49. Tse EG, Korsik M, Todd MH. The past, present and future of anti-malarial medicines. *Malar J*. **2019**; 18, 1-21.

50. Koller R, Mombo-Ngoma G, Grobusch MP. The early preclinical and clinical development of ganaplacide (KAF156), a novel antimalarial compound. *Expert Opin Investig Drugs*. **2018**; 27, 803-810.

51. Tran TH, White NJ, Nguyen TTN, et al. Estimation of the in vivo MIC of cipargamin in uncomplicated plasmodium falciparum malaria. *Antimicrob Agents Chemother*. **2017;** 61.

52. Margaret A P, Lotharius J, Marsh K, et al. A long-duration dihydroorotate dehydrogenase inhibitor (DSM265) for prevention and treatment of malaria. *Sci Transl Med*. **2015**; 7.

53. White J, Dhingra SK, Deng X, et al. Identification and Mechanistic Understanding of Dihydroorotate Dehydrogenase Point Mutations in Plasmodium falciparum that Confer in Vitro Resistance to the Clinical Candidate DSM265. *ACS Infect Dis*. **2019**; 5, 90-101.

54. McCarthy JS, Rückle T, Elliott S, et al. A Single-Dose Combination Study with the Experimental Antimalarials Artefenomel and DSM265 To Determine Safety and Antimalarial Activity against Blood-Stage Plasmodium falciparum in Healthy Volunteers. *Am Soc Microbiol*. **2020**; 64, 1-10.

55. Sevene E, Banda CG, Mukaka M, et al. Efficacy and safety of dihydroartemisinin-piperaquine for treatment of Plasmodium falciparum uncomplicated malaria in adult patients on antiretroviral therapy in Malawi and Mozambique: An open label non-randomized interventional trial. *Malar J*. **2019**; 18, 1-13.

56. Amaratunga C, Lim P, Suon S, et al. Dihydroartemisinin-piperaquine resistance in Plasmodium falciparum malaria in Cambodia: A multisite prospective cohort study. *Lancet Infect Dis*. **2016**; 16, 357-365.

57. van der Pluijm RW, Imwong M, Chau NH, et al. Determinants of dihydroartemisinin-piperaquine treatment failure in Plasmodium falciparum malaria in Cambodia, Thailand, and Vietnam: a prospective clinical, pharmacological, and genetic study. *Lancet Infect Dis*. **2019**; 19, 952-961.

58. Rajapakse S, Rodrigo C, Fernando SD. Tafenoquine for preventing relapse in people with Plasmodium vivax malaria. *Cochrane Database Syst Rev*. **2015**.

59. Rueangweerayut R, Bancone G, Harrell EJ, et al. Hemolytic potential of tafenoquine in female volunteers heterozygous for Glucose-6-Phosphate Dehydrogenase (G6PD) Deficiency (G6PD Mahidol Variant) versus G6PD-Normal volunteers. *Am J Trop Med Hyg*. **2017**; 97, 702-711.

60. Goldberg DE, Slater AF, Beavis R, et al. Hemoglobin degradation in the human malaria pathogen Plasmodium falciparum: a catabolic pathway initiated by a specific aspartic protease. *J Exp Med*. **1991**; 173, 961-969.

61. O'Neill PM, Shone AE, Stanford D, et al. Synthesis, antimalarial activity, and preclinical pharmacology of a novel series of 4'-fluoro and 4'-chloro analogues of amodiaquine. identification of a suitable "back-up" compound for N-tert-butyl isoquine. *J Med Chem*. **2009**; 52, 1828-1844.

62. Deshpande S, Kuppast B. 4-aminoquinolines: An Overview of Antimalarial Chemotherapy. *Med Chem (Los Angeles)*. **2016**; 6, 1-11.

63. Wunderlich J, Rohrbach P, P. Dalton J. The Malaria Digestive Vacuole. *Front Biosci.* **2012**; 4, 1424-1448.

64. Pisciotta JM, Scholl PF, Shuman JL, et al. Quantitative characterization of hemozoin in Plasmodium berghei and vivax. *Int J Parasitol Drugs Drug Resist*. **2017**; 7, 110-119.

65. Ginsburg H, Famin O, Zhang J, Krugliak M. Inhibition of glutathione-dependent degradation of heme by chloroquine and amodiaquine as a possible basis for their antimalarial mode of action. *Biochem Pharmacol*. **1998**; 56, 1305-1313.

66. Pyrido A, Ndakala AJ, Gessner RK, et al. Antimalarial pyrido[1,2-*a*]benzimidazoles. *J Med Chem*. **2011**; 54, 4581-4589.

67. Li C, Liu B, Chang J, et al. A modern in vivo pharmacokinetic paradigm: Combining snapshot, rapid and full PK approaches to optimize and expedite early drug discovery. *Drug Discov Today*. **2013**; 18, 71-78.

68. Markovsky E, Baabur-Cohen H, Eldar-Boock A, et al. Administration, distribution, metabolism and elimination of polymer therapeutics. *J Control Release*. **2012**; 161, 446-460.

69. Alavijeh MS, Palmer AM. The pivotal role of drug metabolism and pharmacokinetics in the discovery and development of new medicines. *IDrugs*. **2004**; 7, 755-763.

70. Palmer AM. New horizons in drug metabolism, pharmacokinetics and drug discovery. *Drug News Perspect*. **2003**; 16: 57-62.

71. Lin JH, Lu AY. Role of pharmacokinetics and metabolism in drug discovery and development. *Pharmacol Rev*. **1997**; 49, 403-449.

72. Varma M V., Steyn SJ, Allerton C, El-Kattan AF. Predicting Clearance Mechanism in Drug Discovery: Extended Clearance Classification System (ECCS). *Pharm Res*. **2015**; 32, 3785-3802.

73. Walsh JS, Miwa GT. Bioactivation of Drugs: Risk and Drug Design. *Annu Rev Pharmacol Toxicol*. **2011**; 51, 145-167.

74. Sallustio BC, Sabordo L, Nation AME et al. Hepatic Disposition of Electrophilic Acyl Glucuronide Conjugates. *Curr Drug Metab*. **2000**; 1, 163-180.

75. Deprem T, Yıldız S, Sari E, et al. Distribution of glutathione peroxidase 1 in liver tissues of healthy and diabetic rats treated with capsaisin. *Biotech Histochem*. **2015**; 90, 1-7.

76. Davies M, Hawkins C, Pattison D, Rees M. Mammalian Heme Peroxidases: From Molecular Mechanisms to Health Implications. *Antioxid Redox Sigal*.; **2008**, 10, 1199-1234.

77. Kiang TKL, Ensom MHH, Chang TKH. UDP-glucuronosyltransferases and clinical drug-drug interactions. *Pharmacol Ther*. **2005**; 106, 97-132.

78. Langguth HS, Benet LZ. Acyl Glucuronides Revisited: Is the Glucuronidation Proces a Toxification as Well as a Detoxification Mechanism? *Drug Metab Rev*. **1992**; 24, 5-47.

79. Luis PB, Gordon ON, Nakashima F, et al. Oxidative metabolism of curcumin-glucuronide by peroxidases and isolated human leukocytes. *Biochem Pharmacol*. **2017**; 132, 143-149.

80. Kalgutkar AS, Gardner I, Obach RS, et al. A Comprehensive Listing of Bioactivation Pathways of Organic Functional Groups. *Curr Drug Metab*. **2005**; 6, 161-225.

81. Olliaro P, Nevill C, LeBras J, et al. Systematic review of amodiaquine treatment in uncomplicated malaria. *Lancet*. **1996**; 348, 1196-1201.

82. Hawley SR, Bray PG, O'Neill PM, et al. Manipulation of the N-alkyl substituent in amodiaquine to overcome the verapamil-sensitive chloroquine resistance component. *Antimicrob Agents Chemother*. **1996**; 40, 2345-2349.

83. Sinou V, Malaika LTM, Taudon N, et al. Pharmacokinetics and pharmacodynamics of a new ACT formulation: Artesunate/Amodiaquine

(TRIMALACT) following oral administration in African malaria patients. *Eur J Drug Metab Pharmacokinet*. **2009**; 34, 133-142.

84. Desta Z, Kerbusch T, Soukhova N, Richard E, et al. Identification and Characterization of Human Cytochrome P450 Isoforms Interacting with Pimozide. *J Pharmacol Exp Ther.* **1998**; 285, 428-437.

85. Amodiaquine. In: Meyler's side effects of drugs: The international encyclopedia of adverse drug reactions and interactions. Elsevier; **2015**:16, 302-304.

86. Zhang Y, Vermeulen NPE, Commandeur JNM. Characterization of human cytochrome P450 mediated bioactivation of amodiaquine and its major metabolite N-desethylamodiaquine. *Br J Clin Pharmacol*. **2017**; 83, 572-583.

87. Tafazoli S, O'Brien PJ. Amodiaquine-induced oxidative stress in a hepatocyte inflammation model. *Toxicology*. 2009; 256, 101-109.

88. Horton DA, Bourne GT, Smythe ML. The Combinatorial Synthesis of Bicyclic Privileged Structures or Privileged Substructures. *Chem Rev*. **2003**; 103, 893-930.

89. Kotovskaya SK, Baskakova ZM, Charushin VN, et al. Synthesis And Antiviral Activity of Fluorinated pyrido[1,2-*a*]benzimidazoles. *Pharm Chem J*. **2005**; 39, 574-578.

90. Badawey E, Kappe T. Benzimidazole condensed ring system. IX. Potential antineoplastics. New synthesis of some pyrido[1,2-α]benzimidazoles and related derivative. *Eur J Med Chem*. **1995**; 30, 327-332.

91. Wirth CC, Glushakova S, Scheuermayer M, et al. Perforin-like protein PPLP2 permeabilizes the red blood cell membrane during egress of Plasmodium falciparum gametocytes. *Cell Microbiol*. **2014**; 16, 709-733.

92. Okombo J, Brunschwig C, Singh K, et al. Antimalarial Pyrido[1,2-a]benzimidazole Derivatives with Mannich Base Side Chains: Synthesis, Pharmacological Evaluation, and Reactive Metabolite Trapping Studies. *ACS Infect Dis*. **2019**; 5, 372-384.

93. Jewell H, Maggs JL, Harrison AC,et al. Role of hepatic metabolism in the bioactivation and detoxication of amodiaquine. *Xenobiotica*. **1995**; 25, 199-217.

94. Abdel-Magid AF, Carson KG, Harris BD, et al. Reductive amination of aldehydes and ketones with sodium triacetoxyborohydride. Studies on direct and indirect reductive amination procedures. *J Org Chem*. **1996**; 61, 3849-3862.

95. Reader J, Botha M, Theron A, et al. Nowhere to hide: Interrogating different metabolic parameters of Plasmodium falciparum gametocytes in a transmission blocking drug discovery pipeline towards malaria elimination. *Malar J*. **2015**; 14.

96. Jeffries B, Wang Z, Graton J, et al. Reducing the Lipophilicity of Perfluoroalkyl Groups by CF_2-F/CF_2-Me or CF_3/CH_3 Exchange. *J Med Chem*. **2018**; 61, 10602-10618.

97. Trager W, Jensen JB. Continuous culture of Plasmodium falciparum: Its impact on malaria research. *Int J Parasitol*. **1997**; 27, 989-1006.

98. Mosmann T. Rapid colorimetric assay for cellular growth and survival: Application to proliferation and cytotoxicity assays. *J Immunol Methods*. **1983**; 65, 55-63.

99. Verlinden BK, Niemand J, Snyman J, et al. Discovery of novel alkylated (bis)urea and (bis)thiourea polyamine analogues with potent antimalarial activities. *J Med Chem*. **2011**; 54, 6624-6633.